Pertanika Journal of

SCIENCE & TECHNOLOGY

JST

VOL. 32 (S1) 2024

A Special Issue Devoted to
Energy Industry and Industrial Design
(Innovations in Energy Utilization and Equipment Design)

Guest Editors
S. Venkatesh, S. Vijayan & M. M. Matheswaran

PERTANIKA JOURNALS

A scientific journal published by Universiti Putra Malaysia Press

Pertanika Journal of Science & Technology
Pertanika Journal of Science & Technology

Pertanika Journal of Science & Technology

About the Journal

Overview

Pertanika Journal of Science & Technology (JST) is the official journal of Universiti Putra Malaysia published by UPM Press. It is an open-access online scientific journal which is free of charge. It publishes the scientific outputs. It neither accepts nor commissions third party content.

Recognized internationally as the leading peer-reviewed interdisciplinary journal devoted to the publication of original papers, it serves as a forum for practical approaches to improving quality in issues pertaining to science and engineering and its related fields.

JST is currently published 6 issues a year, periodically in January, March, April, July, August, and October. It is considered for publication of original articles according to its scope. The journal publishes in **English** and it is open to authors around the world regardless of the nationality.

The Journal is available world-wide.

Aims and scope

Pertanika Journal of Science and Technology aims to provide a forum for high quality research related to science and engineering research. Areas relevant to the scope of the journal include: bioinformatics, bioscience, biotechnology and bio-molecular sciences, chemistry, computer science, ecology, engineering, engineering design, environmental control and management, mathematics and statistics, medicine and health sciences, nanotechnology, physics, safety and emergency management, and related fields of study.

History

Pertanika was founded in 1978. A decision was made in 1992 to streamline *Pertanika* into three journals as Pertanika Journal of Tropical Agricultural Science, Pertanika Journal of Science & Technology, and Pertanika Journal of Social Sciences & Humanities to meet the need for specialised journals in areas of study aligned with the interdisciplinary strengths of the university.

After almost 28 years, as an interdisciplinary Journal of Science & Technology, the journal now focuses on research in science and engineering and its related fields.

Goal of *Pertanika*

Our goal is to bring the highest quality research to the widest possible audience.

Quality

We aim for excellence, sustained by a responsible and professional approach to journal publishing. Submissions are guaranteed to receive a decision within 14 weeks. The elapsed time from submission to publication for the articles averages 5-6 months.

Abstracting and indexing of *Pertanika*

The journal is indexed in SCOPUS (Elsevier), Clarivate-Emerging Sources Citation Index [ESCI (Web of Science)], BIOSIS, National Agricultural Science (NAL), Google Scholar, MyCite and ISC.

Future vision

We are continuously improving access to our journal archives, content, and research services. We have the drive to realise exciting new horizons that will benefit not only the academic community, but society itself.

Citing journal articles

The abbreviation for Pertanika Journal of Science & Technology is *Pertanika J. Sci. Technol.*

Publication policy

Pertanika policy prohibits an author from submitting the same manuscript for concurrent consideration by two or more publications. It prohibits as well publication of any manuscript that has already been published either in whole or substantial part elsewhere. It also does not permit publication of manuscript that has been published in full in Proceedings.

Code of Ethics

The *Pertanika* Journals and Universiti Putra Malaysia takes seriously the responsibility of all of its journal publications to reflect the highest in publication ethics. Thus all journals and journal editors are expected to abide by the Journal's codes of ethics. Refer to *Pertanika*'s **Code of Ethics** for full details, or visit the Journal's web link at http://www.pertanika.upm.edu.my/code_of_ethics.php

International Standard Serial Number (ISSN)

An ISSN is an 8-digit code used to identify periodicals such as journals of all kinds and on all media–print and electronic. All *Pertanika* journals have ISSN as well as an e-ISSN.

Pertanika Journal of Science & Technology: ISSN 0128-7680 (*Print*); ISSN 2231-8526 (*Online*).

Lag time

A decision on acceptance or rejection of a manuscript is reached in 3 to 4 months (average 14 weeks). The elapsed time from submission to publication for the articles averages 5-6 months.

Authorship

Authors are not permitted to add or remove any names from the authorship provided at the time of initial submission without the consent of the Journal's Chief Executive Editor.

Manuscript preparation

Refer to *Pertanika*'s **Instructions to Authors** through the official website.

Editorial process

Authors are notified with an acknowledgement containing a *Manuscript ID* on receipt of a manuscript, and upon the editorial decision regarding publication.

Pertanika follows a **double-blind peer-review** process. Manuscripts deemed suitable for publication are usually sent to reviewers. Authors are encouraged to suggest names of at least three potential reviewers at the time of submission of their manuscript to *Pertanika*, but the editors will make the final choice. The editors are not, however, bound by these suggestions.

Notification of the editorial decision is usually provided within ten to fourteen weeks from the receipt of manuscript. Publication of solicited manuscripts is not guaranteed. In most cases, manuscripts are accepted conditionally, pending an author's revision of the material.

The Journal's peer-review

In the peer-review process, three referees independently evaluate the scientific quality of the submitted manuscripts.

Peer reviewers are experts chosen by journal editors to provide written assessment of the **strengths** and **weaknesses** of written research, with the aim of improving the reporting of research and identifying the most appropriate and highest quality material for the journal.

Pertanika Journal of Science & Technology
Pertanika Journal of Science & Technology

Pertanika Journal of Science & Technology
Pertanika Journal of Science & Technology

Operating and review process

What happens to a manuscript once it is submitted to *Pertanika*? Typically, there are seven steps to the editorial review process:

1. The Journal's Chief Executive Editor (CEE) and the Editorial Board Members (EBMs) examine the paper to determine whether it is appropriate for the journal and should be reviewed. If not appropriate, the manuscript is rejected outright and the author is informed.

2. The CEE sends the article-identifying information having been removed, to 2 or 3 reviewers who are specialists in the subject matter represented by the article. The CEE requests them to complete the review within 3 weeks.

   Comments to authors are about the appropriateness and adequacy of the theoretical or conceptual framework, literature review, method, results and discussion, and conclusions. Reviewers often include suggestions for strengthening of the manuscript. Comments to the editor are in the nature of the significance of the work and its potential contribution to the research field.

3. The Editor-in-Chief (EiC) examines the review reports and decides whether to accept or reject the manuscript, invites the author(s) to revise and resubmit the manuscript, or seek additional review reports. Final acceptance or rejection rests with the CEE and EiC, who reserve the right to refuse any material for publication. In rare instances, the manuscript is accepted with almost no revision. Almost without exception, reviewers' comments (to the author) are forwarded to the author. If a revision is indicated, the editor provides guidelines to the authors for attending to the reviewers' suggestions and perhaps additional advice about revising the manuscript.

4. The authors decide whether and how to address the reviewers' comments and criticisms and the editor's concerns. The authors return a revised version of the paper to the CEE along with specific information describing how they have answered' the concerns of the reviewers and the editor, usually in a tabular form. The author(s) may also submit a rebuttal if there is a need especially when the authors disagree with certain comments provided by reviewer(s).

5. The CEE sends the revised paper out for re-review. Typically, at least 1 of the original reviewers will be asked to examine the article.

6. When the reviewers have completed their work, the EiC examines their comments and decides whether the paper is ready to be published, needs another round of revisions, or should be rejected. If the decision is to accept, the CEE is notified.

7. The CEE reserves the final right to accept or reject any material for publication, if the processing of a particular manuscript is deemed not to be in compliance with the S.O.P. of *Pertanika*. An acceptance letter is sent to all authors.

   The editorial office ensures that the manuscript adheres to the correct style (in-text citations, the reference list, and tables are typical areas of concern, clarity, and grammar). The authors are asked to respond to any minor queries by the editorial office. Following these corrections, page proofs are mailed to the corresponding authors for their final approval. At this point, **only essential changes are accepted**. Finally, the manuscript appears in the pages of the journal and is posted online.

Pertanika Journal of

SCIENCE & TECNOLOGY

A Special Issue Devoted to

Energy Industry and Industrial Design
(Innovations in Energy Utilization and Equipment Design)

VOL. 32 (S1) 2024

(Special Issue)

Guest Editors

S. Venkatesh, S. Vijayan & M. M. Matheswaran

PERTANIKA JOURNALS

A scientific journal published by Universiti Putra Malaysia Press

PJST
Pertanika Journal of Science & Technology
AN INTERNATIONAL PEER-REVIEWED JOURNAL

EDITORIAL OFFICE
JOURNAL DIVISION
Putra Science Park
1st Floor, IDEA Tower II
UPM-MTDC Technology Centre
Universiti Putra Malaysia
43400 Serdang, Selangor Malaysia.

Gen Enquiry
Tel. No: +603 9769 1622 | 1616
E-mail:
executive_editor.pertanika@upm.edu.my
URL: www.journals-jd.upm.edu.my

PUBLISHER
UPM Press
Universiti Putra Malaysia
43400 UPM, Serdang, Selangor, Malaysia.
Tel: +603 9769 8851
E-mail: penerbit@putra.upm.edu.my
URL: http://penerbit.upm.edu.my

ABSTRACTING AND INDEXING OF PERTANIKA JOURNALS

The journal is indexed in SCOPUS (Elsevier), Clarivate-Emerging Sources Citation Index (ESCI), BIOSIS, National Agricultural Science (NAL), Google Scholar, MyCite, ISC. In addition, Pertanika JSSH is recipient of "CREAM" Award conferred by Ministry of Higher Education (MoHE), Malaysia.

Pertanika Journal of Science & Technology
Vol. 32 (S1) 2024

Contents

Preface

We are delighted to present this Special Issue on ‘Innovations in Energy Utilization and Equipment Design’. In the ever-evolving landscape of industrial processes, addressing energy utilization and emission control has emerged as a pivotal strategy across diverse sectors, including chemical, textile, mechanical, pharmaceutical, and powder metallurgy industries. As we confront the complex challenges of climate change, resource scarcity, and the growing demand for sustainable solutions, the significance of advancements in energy technology becomes increasingly important to establish a sustainable and clean environment.

This compilation is a testament to the unwavering commitment to progress in energy utilization and equipment design. The papers selected for this Special Issue focus on innovations and technological improvements in designing energy-efficient equipment, vital in minimizing energy consumption and operational costs. Researchers are actively contributing through experimental, theoretical, and numerical methods, with a recent surge in the application of computational simulation tools. This approach expedites analysis and proves cost-effective, aligning with the growing need for sustainable practices in the industry.

This Special Issue is a platform for original research and review articles showcasing cutting-edge emission and energy utilization innovations. The presented papers shed light on the ongoing efforts to strike a delicate balance between the modification of design parameters in processing equipment and the increasing energy requirements. Stricter emission norms and climate change concerns act as catalysts, urging researchers to pioneer innovations in energy-related operations within plants.

Each paper explores distinct aspects of technology, from the aerodynamic design of Unmanned Aerial Vehicles (UAVs) for agriculture and surveying applications to the assessment of energy conservation potentials in industries. The first paper details the meticulous design of UAVs for surveillance and agriculture, highlighting the superior aerodynamic efficiency of high-wing UAV configurations through flow analyses and validation. The second paper explores ground effects on UAVs, revealing disparities between simulated data and DATCOM predictions under various conditions. The third paper conducts a comprehensive energy audit of the Ethiopian leather industry, proposing cost-effective energy-saving techniques related to industrial energy consumption. The fourth paper delves into the Ethiopian cement industry’s power consumption and production rates, emphasizing economic impacts. The fifth paper addresses solar energy prediction challenges, employing a Model Predictive Controller for improved accuracy. Finally, a fuzzy logic-based power optimizer for solar PV systems is introduced, exhibiting promising results.

We extend our heartfelt gratitude to all the contributors whose work collectively contributes to the ongoing dialogue surrounding energy efficiency and environmental sustainability in industrial processes. May this Special Issue inspire further advancements, collaborative efforts, and a shared commitment to shaping a greener, more efficient future for industrial operations.

Guest Editors

S. Venkatesh *(Assoc. Prof. Dr.)*
S. Vijayan *(Dr.)*
M. M. Matheswaran *(Dr.)*

Pertanika J. Sci. & Technol. 32 (S1): 1 - 19 (2024)

PERTANIKA JOURNALS

SCIENCE & TECHNOLOGY

Journal homepage: http://www.pertanika.upm.edu.my/

Design and Analysis of UAV Profile for Agriculture and Surveying Application

Mukesh Raju[1]*, Theerthamalai Pakkiri[2], Praveenkumar Marankumar[1], Prashanth Marankumar[1] and Inamul Hasan[3]

[1]*Department of Aerospace Engineering, ACS College of Engineering, Bangalore 560074, India*
[2]*Department of Aerospace & Aeronautical Engineering, ACS College of Engineering, Bangalore 560074, India*
[3]*Department of Aeronautical Engineering, ACS College of Engineering, Bangalore 560074, India*

ABSTRACT

This study represents the aerodynamic design of an Unmanned aerial vehicle intended forsurveillance or agriculture with a maximum take weight of 125 kg. Weight estimation and constraint analysis were done based on the Mission profile. Design of Computer-Aided Design (CAD) models were generated for three different configurations using CATIA V5R20 as a high wing, mid-wing, and low wing. Flow analysis was done for the above configurations at various angles of attack. ANSYS 15 wasused for the flow Analysis. A Tetrahedron element meshed the model with the minimum required orthogonal quality. Five microns were given to the initial layer height of the prism mesh. Spalart Allmaras model is used as the Turbulence model in the solver. The aerodynamic characteristics of the above configuration obtained from Computational Fluid Dynamics (CFD) results were comparedwith the DATCOM program and validated with the wind tunnel experimental test data. The open-circuited suction-type Subsonic wind tunnel was employed for the test. The aerodynamic properties for the angle of attack in the range of -2° to 14° angle of attack are calculated using a six-component balance. The study aims to find the Unmanned Aerial Vehicle (UAV) configuration based on the aerodynamic characteristics obtained from the CFD and DATCOM results. High-wing UAVs have better aerodynamic efficiency than the other two configurations.

Keywords: Aerodynamic efficiency, CFD analysis, DATCOM, UAV, wind tunnel testing

ARTICLE INFO

Article history:
Received: 27 July 2023
Accepted: 17 October 2023
Published: 19 January 2024

DOI: https://doi.org/10.47836/pjst.32.S1.01

E-mail addresses:
vsmprm@gmail.com (Mukesh Raju)
ptmalai@gmail.com (Theerthamalai Pakkiri)
praveenkumarm5195@gmail.com (Praveenkumar Marankumar)
prashanthm1896@gmail.com (Prashanth Marankumar)
aero.inamulhasan@gmail.com (Inamul Hasan)
*Corresponding author

ISSN: 0128-7680
e-ISSN: 2231-8526

INTRODUCTION

An unmanned aerial vehicle is an aircraft without a pilot or passengers, generally calleda drone. The flight path of UAVs is controlled and operated either with dynamic automation systems or autonomously using preprogrammed flight paths or by remote control from a pilot. Pilot control may be controlled either from the ground or from another vehicle.

Three important parts are required for a UAV to have a successful flight. First is the aerial platform, which contains the navigation system, the airframe, the payload, and the power system. Second is the Ground Control Station (GCS), which helps provide human control remotely. Finally, the communication system helps transfer communication between the ground and the vehicle.

UAVs are nowadays used in various applications. In intelligence and reconnaissance missions, in the operation of stealth-type like micro or mini-UAVs, insect-type small structures, such as flapping-wing ornithopters, make surveillance and targets easy. Also, it isvery helpful in aerial photography, LiDAR platforms, and filmmaking in urban and rural areas with less space and in rescue and surveillance activities such as the search for missing persons and firefighting. UAVs are used in many applications where aircraft or helicopters cannot be used due to the size and shape of the vehicle. Some other applications are remote sensing, forest fire, and transportation of goods.

The advantages of UAVs are mainly environmental safety, cost-cutting technology, better quality of aerial photography, programmed precisely to a specific location, easily controllable or deployable, reduced danger and health risks, and flexibility for quick inspections and reaching hazardous areas with easy navigation. Some limitations of UAVs are that they may trespass in an individual private place and fall prey to manipulation. Somerestrictions from the government and the local city will make it difficult to fly UAVs in a restricted area, causing legal action. Sometimes, the installed software issues or malfunctions will lead to failure in the respective mission.

The conceptual design of agricultural aircraft optimized for aerodynamic performance is represented by Bravo-Mosquera et al. (2018). The authors designed six configurations by changing the cant angles of the winglet in UAV to obtain the best aerodynamic characteristics through CFD analysis. The overall aerodynamic performance obtained from CFD for the baseline concept withoptimal multi-winglet design has been compared. The survey of UAVs used in disaster research and management concept with imagery acquisition was studied by Adams et al. (2013). To improve the performance of UAVs in pressurized structures-based technologies by examining how to construct the UAV with a considerable weight percentage that should be supported by an inflatable structure containing air and concluded that the pressurized structures-based technologies reduce the energy required to keep the UAV aloft (Edge et al., 2010). The procedure for constructing a UAV by Laghari et al. (2023) has designed a UAV that actsas a path glider in normal situations and as a fire

extinguisher in emergencies. The conceptual design of an agricultural aircraft intended for agricultural industry needs was summarized. The proposed design suits the requirements of variable load and low-altitude flight (Sharma & Manna, 2017). The design and aerodynamic performance analysis for a UAV with a payload of 60 kg by increasing the span efficiency. The author compared various wingtip geometries for better performance and an effective aerodynamic improvement by reducing complicated algorithms and time (Turanoguz & Alemdaroglu, 2015).

The optimized design of the drone can be obtained by reducing the weight and maintainingthe strength along with reducing the deformation at a higher temperature with the selected AL-7075 T6 for reducing the weight of drone (Hasan et al., 2022a; Khamsi, 2019). The aerodynamic characteristics of Hawkeye UAVs with the help of flow analysis using Reynolds-averaged Navier-Stokes equations for numerical methods and the Spalart-Allmaras Turbulence model are used for simulation. The authors concluded that both the moment and lift co-efficient of Hawkeye UAV were lesser than TERES-02 aircraft due to improper wing design (Johari et al., 2021). The conceptual design of a fixed-wing UAV using a Conventional aircraft design approach and estimated the take-off weight using CFD analysis for optimized design for aerodynamic efficiency by Sharif (2021). The design and analysis of UAV with solar energy as a power source for long endurance at low altitudes concluded that the Solar UAV is an alternative to the conventional UAV for long endurance flight, which can beused for surveillance (Sri et al., 2016).

The design of a trim distributed electric propulsion-based blended wing body configuration by CFD simulation and Wind tunnel testing toevaluate the design quality and obtained the lift-to-drag ratio of 22.31 at an angle of attack of 4°. The cruise condition's pitching moment and static margin met the required design requirements (Wang & Zhou, 2022). The design of agricultural use of unmanned aerial vehiclesconcluded that the UAVs did not require a separate navigation station andairport since they could be landed on the edge of the agricultural land. UAVs also reduce the no-land flight rate due to lower labor intensity and lower operational costs (del Cerro et al., 2021). The applications of UAV in physiological and biophysical assessments, spraying of phytosanitary, monitoring the biological targets, and topographic surveys were studied by Amaral etal. (2020). The author concluded that the UAV could replace human activities in agriculture,like crop monitoring phytosanitary and spraying pesticides. The usage of UAVs in the agricultural field was studied, and it concluded that UAVs could improve field management and productivity can also be increased. Also, UAVs cannot address every issue in the field, but they can help with some specific agricultural difficulties (Norasma et al., 2019). The preliminary design of UAVs used for surveillance during fire and rescue using CFD concluded that the CFD results matchthe experimental and real-time conditions (Casas et al., 2008).

The design of UAVs with mathematical models for small UAVs step-by-step used USAF Digital DATCOM to estimate the aerodynamic coefficients. It also concluded that DATCOM offers less precision than CFD and wind tunnel tests, but it operates significantly more effectively by cutting down on significant processing time and design costs. Also, the coefficients of state-space matrices can be calculated using stability and control coefficients and derivatives acquired from DATCOM (Elharouny et al., 2012). The CFD simulation to calculate the unmanned aerial vehicle's (Khau) aerodynamic coefficients using the DATCOM and compared them with the wind tunnel test data proved that the N-S computational method had a better agreement with the test data. However, there is a discrepancy with the DATCOM in the prediction of the moments, but there is a good agreement with the lift coefficient in the DATCOM data (Shafer et al., 2014). The aerodynamic coefficients of unmanned aerial vehicles using Favre-Averaged Navier Stokes in CFD and compared the data with the wind tunnel data using thin and hybrid boundary layer approach to calculate the aerodynamic performance. This study concluded that the thin boundary layer approach has discrepancies in high angles of attack but reduced the computational time.

In contrast, the hybrid boundary layer approach could only increase lift prediction compared to the thin boundary layer approach. Still, it did offer improvements in computational time and convergence of the solution at high angles of attack (Shah et al., 2018). The 3-D simulation for the NACA airfoil and Pioneer RQ-2A piloted vehicle was performed using the three-dimensional, transient, and incompressible formulation for the Reynolds number ranging from 5×10^4 to 2.88×10^6 for different angles of attack and validated with wind tunnel test data. The author concluded that the prediction had a better agreement with the wind tunnel data; the vortex shedding and the streamline and vortex structure highlighted wing tip vortices at high angles of attack (Liu et al., 2020). The procedure for predicting the aerodynamic coefficients for Boeing 747 from the geometrical parameters using the software XFLR and DATCOM was conducted and concluded that the XFLR and DATACOM data had very good longitudinal stability and control data with the derivatives and they are reliable, but XFLR is a better tool than the DATCOM due to some of the inherent limitations in DATCOM (Ahmad et al., 2021).

MATERIALS AND METHODS

The flow of the project starts with mission requirements wherein particular launch altitude, cruise altitude, payload capacity, range, and endurance have been considered. Initial weight estimation has been done. The primary and secondary sub-systems were selected using this initial mass estimation. Considering the initial mass estimation, the initial layout configuration was started, and six types of UAV configurations were designed to satisfy the mission requirement. Then, the selected six design configurations were imported to

the CFD analysis tool for the post-processingwork, i.e., calculating lift, drag, and moment coefficients. Then, using the DATCOM program, the co-efficient of lift, drag, and moment were tabulated for the six design configurations.The values obtained from CFD analysis were compared with DATCOM program values to selectthe UAV configuration with better aerodynamic performance for the mission requirements considered. The flow chart of the research work is shown in Figure 1.

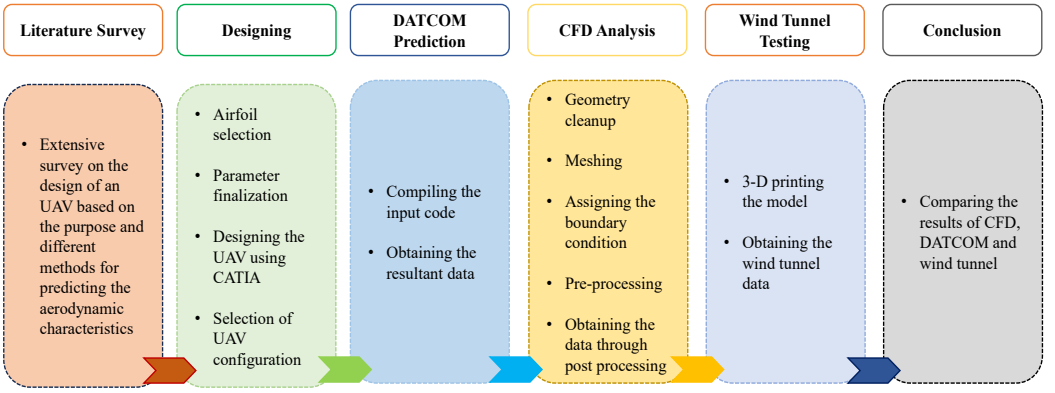

Figure 1. Flowchart of the project

Modeling and Analysis

As mentioned above in the abstract, the design was made using the CATIA V5R20 software. A generative shape design tool was used for designing the UAV components. From the Microsoft Excel file, General Station Description (GSD) Point Spline Loft file was used to generate the airfoil shape with NACA 241-212, NACA 2412, and NACA 0012 using CATIA software for the wing, horizontal, and vertical tail.

The dimension of the fuselage is 3.25 m x 0.3 m, the ogival nose length is 0.6m, boat tail length is 0.3 m. It has been selected for the design and designed per the mentioned dimensions. The aspect ratio value of 5 and taper ratio value of 0.5 were selected for the wing, horizontal, and verticaltail design. The dimensions of the wings have the following data. The wingspan is 2.2678 m, the wing area is 1.0286 m^2, and the wing incidence angle of 1° has been selected for the design. The dimensions of a horizontal tail have the following data. A span of 0.9328 m and a tail area of 0.1740 m^2 were selected for the design. The dimensions of the vertical tail are a semi-span of 0.5597 m and a tail area of 0.1740 m^2 was selected. In generative shape design, the design fuselagerevolve option is used after the completion of the sketch. Similarly, multi-section surface and fill options were used for the wing, horizontal, and vertical tail.

UAV Design Layout

Using the above UAV components design, the assembly was made. The assembly design tool wasused in CATIA software for the assembly. The offset constraint optionwas used to assemble all the UAV components in the assembly design tool. The complete UAV assembled section is shown in Figure 2, and the model's detail is shown in Tables 1(a) and 1(b).

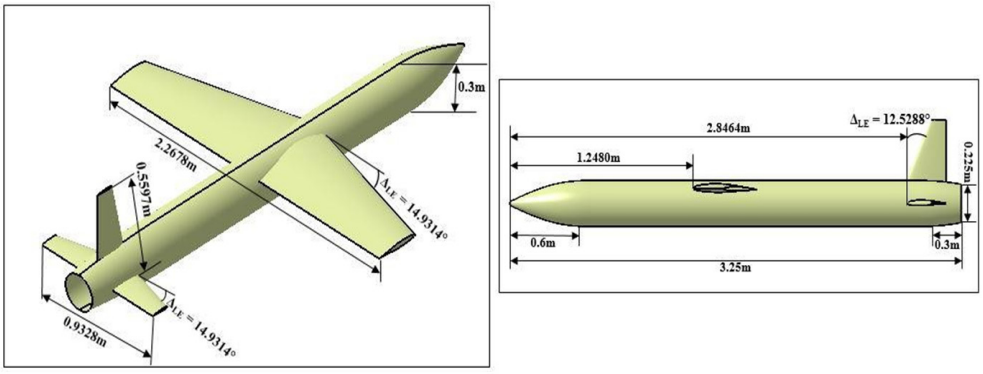

Figure 2. Conventional type-high wing UAV configuration

Table 1(a)
Details of the fuselage

Fuselage Parameter	Dimension
Fuselage Length	3.25 m
Fuselage Diameter	0.3 m
Fuselage Base Diameter	0.225 m
Fuselage Nose Length	0.6 m
Fuselage Base Length	0.3 m

Pre-Processing Work

The ANSYS software was used for pre-processing, including domain creation, application of boundary conditions, meshing, and aerodynamic analysis. Creating domain, meshing, and analysis was done using ANSYS software. The designed model was imported to the ICEM CFD tool in ANSYS software, and the spherical domain was created with a radius of 100m. The imported model and the spherical domain created for the model are shownin Figure 3.

Table 1(b)
Details of the wing, horizontal tail, and vertical tail

Parameters	Wing	Horizontal Tail	Vertical Tail
Airfoil	NACA 641-212	NACA 2412	NACA 0012
Root Chord	0.6047	0.2488	0.2488
Tip Chord	0.3024	0.1244	0.1244
MAC	0.4704	0.1935	0.1935
Leading Edge Sweep	14.93	14.93	12.53
Incidence Angle	1°	-	-
Span	2.2678	0.9328	0.5597
Aspect Ratio	5	5	5
Planform Area	1.0286	0.174	0.174
Leading Edge Position from the Nose	1.248	2.8464	2.8464

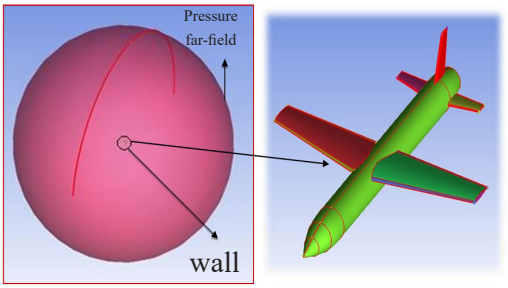

Figure 3. Domain created for the UAV model

The mesh parameters, such as size and type, were selected, and the element size was specified in the setup. Then, the mesh was generated. The robust Octree method was used for creating the surface mesh, and Quick Delaunay was used for creating the volume mesh. A prism layer of 15 numbers was created around the modelwith an initial height of 5 microns. 91,80,225 elements were generated with 24,58,615 nodes. The Grid independent study was carried out to get accurate results. The grid-independent study was carried out for 66,92,668 elements, 83,78,783 elements, 87,86,592 elements, 91,80,225 elements, and 1,24,67,408 elements. The results obtained for the third, fourth, and fifth have almost the sameaerodynamic coefficient value; hence, the fifth mesh set is selected. Then, the Boundary Conditionwas assigned to the model and the domain. The surface mesh was generated to the domain, and the details of the mesh parameters are shown in Table 2. Then, the meshed domain and the models are shown in Figure 4.

Table 2
Meshing parameter

Parameter	Specifications
Topology Tolerance	0.1 mm
Element Scale Factor	1
Max. Element Size	10000
Type of Shell Mesh	All-Tri
Meshing Method	Patch-Dependent
Type of Volume Mesh	Mixed/Tetra
Meshing Method	Robust (Octree), Quick Delaunay
Tetra Size Ratio	1.2
Prism Height Limit Factor	0.33
No. Prism Layer	15
Prism Initial Height	4 microns

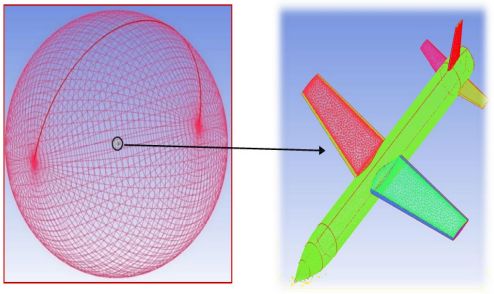

Figure 4. Surface mesh at the model and the domain

After surface meshing, volume mesh was generated to the surface meshed domain and theUAV model. Then, the prism layer was generated on the surface of the UAV. The cross-sectional view of the volume mesh for the domain and the model is shown in Figure 5, the prism layer on the surfaces of the UAV is shown in Figure 6, and the solver parameters are shown in Table 3.

The generated mesh was imported to fluent, and then the SA model and the properties of the air were assigned. The velocity magnitude and direction were given in the boundary condition, andthe reference values were given. The analysis was done for the Mach number of 0.31, and the data was saved in the case and data format. The results were post-processed for the analyzed data. Pressure contours and velocitystreamlines were taken during post-processing. The CL, CD, and CM data obtained are based on the governing equations mentioned in section 3.2.1, and the data obtained are discussed in the result section.

Table 3
Solver parameters

Parameter	Specifications
Solver Type	Pressure based
Viscous Model	Spalart Allmaras
Energy Equation	On
Density	Ideal Gas
Viscosity	Sutherland
Operating Pressure	0
Gauge Pressure	37601.7 N/m^2
Mach Number	0.31
Temperature	238.619 K
Reference Area	1.0286
Reference Length	0.4074

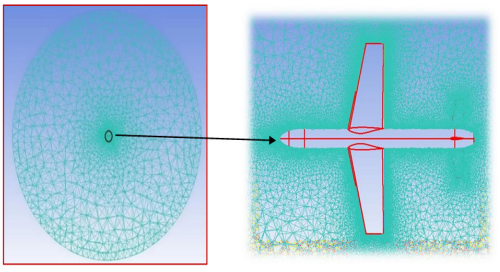

Figure 5. Cross-sectional view of volume mesh

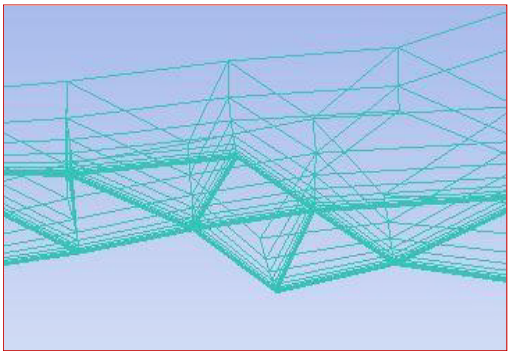

Figure 6. Prism layer on the surface of the UAV

Governing Equations

Basic governing equations are conservation of mass, momentum, and energy under steady-state conditions in 3D form for incompressible and compressible fluid are given below (Hasan et al., 2022b). The fluid that we have used in this study is air. Neglecting the body forces the general form of the continuity, momentum, and energy equations can be written in a Cartesian tensor form as follows:

Continuity Equation. The continuity equation is obtained from conservation laws, which can be derived from Gauss's and Ampere's laws. The concept of mass flow and mass flux is important. Mass can neither becreated nor destroyed, and the continuity equation is mentioned in Equation 1.

$$\frac{\partial u}{\partial x}+\frac{\partial v}{\partial x}+\frac{\partial w}{\partial x}=0 \quad (1)$$

Momentum Equation. Under steady-state conditions and the fluid properties such as density and dynamic viscosity are considered constant, then body force in all directions is negligible. The Navier-Stokes equation iswritten in x, y, and z components for 3-D flow, which is mentioned in Equations 2, 3, and 4.

X-momentum:

$$U\left[\frac{\partial u}{\partial x}\right]+V\left[\frac{\partial u}{\partial y}\right]+W\left[\frac{\partial u}{\partial z}\right]=-\frac{1}{\rho}\left[\frac{\partial p}{\partial x}\right]+V\left[\frac{\partial^2 u}{\partial x^2}+\frac{\partial^2 u}{\partial y^2}+\frac{\partial^2 u}{\partial z^2}\right] \quad (2)$$

Y-momentum:

$$U\left[\frac{\partial v}{\partial x}\right]+V\left[\frac{\partial v}{\partial y}\right]+W\left[\frac{\partial v}{\partial z}\right]=-\frac{1}{\rho}\left[\frac{\partial p}{\partial y}\right]+V\left[\frac{\partial^2 v}{\partial x^2}+\frac{\partial^2 v}{\partial y^2}+\frac{\partial^2 v}{\partial z^2}\right] \quad (3)$$

Z-momentum:

$$U\left[\frac{\partial w}{\partial x}\right]+V\left[\frac{\partial w}{\partial y}\right]+W\left[\frac{\partial w}{\partial z}\right]=-\frac{1}{\rho}\left[\frac{\partial p}{\partial z}\right]+V\left[\frac{\partial^2 w}{\partial x^2}+\frac{\partial^2 w}{\partial y^2}+\frac{\partial^2 w}{\partial z^2}\right] \quad (4)$$

Energy Equation. For an incompressible fluid, keeping thermal conductivity constant, no viscosity dissipation,and no heat generation under steady-state conditions. Then, the energy equation reduces, as shown in Equation 5.

$$U\frac{\partial T}{\partial x}+V\frac{\partial T}{\partial y}+W\frac{\partial T}{\partial z}=\alpha\left[\frac{\partial^2 T}{\partial x^2}+\frac{\partial^2 T}{\partial y^2}+\frac{\partial^2 T}{\partial z^2}\right] \quad (5)$$

Where, $\alpha=\frac{k}{\rho C_p}$

Flow Contours

After obtaining the results from the analysis, contour plots of pressure, velocity, temperature, and Mach number contours can be obtained from a fluent solver. This research plotted pressure contours, velocity contours, and velocity streamline contours.

Pressure Contours

The pressure contour of the UAV has been plotted for 2° AOA (Figure 7). The maximum and minimum pressure values have been obtained by plotting the contours. The pressure contoursof the complete UAV, wing, horizontal and vertical tail are shown in Figures 7(a) to 7(d), respectively.

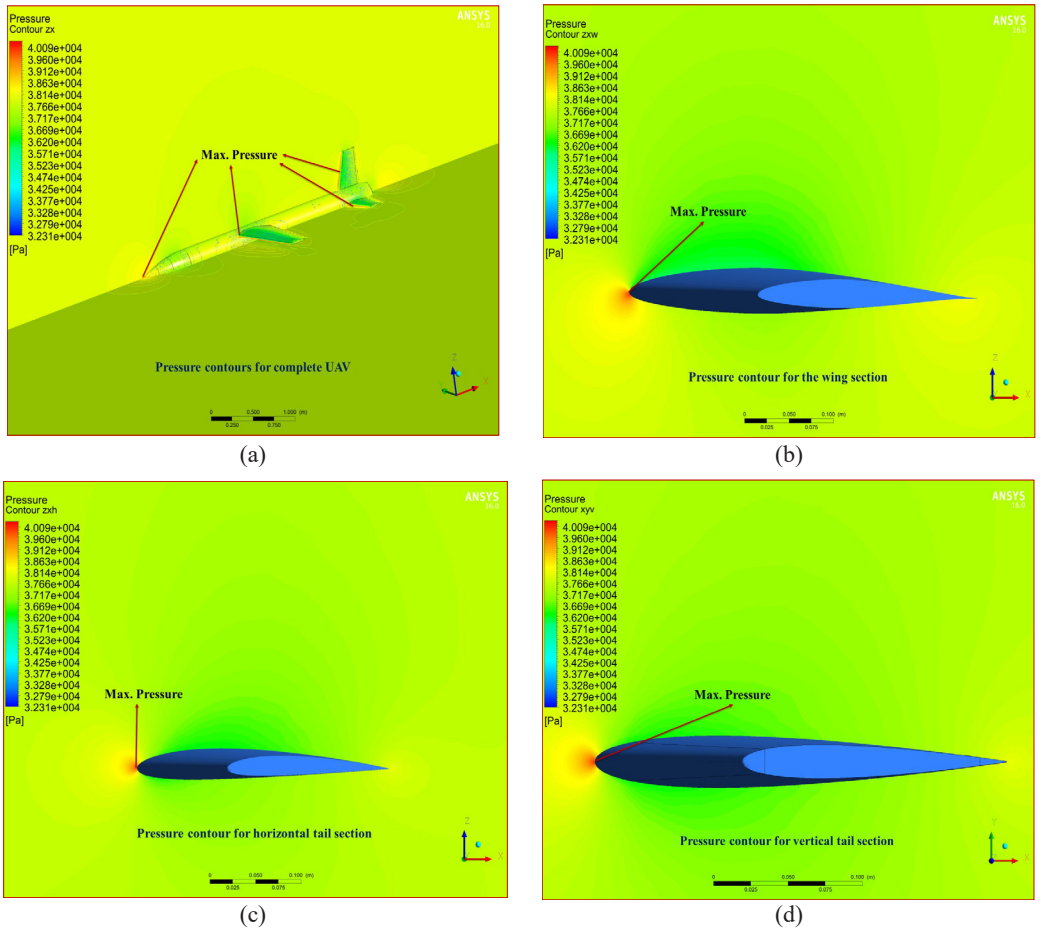

Figure 7. Pressure contours of UAV at 2° AOA (a) Pressure contours for complete UAV (b) Pressure contour for the wing section (c) Pressure contour for horizontal tail section (d) Pressure contour for vertical tail section

Velocity Contours

The velocity contour of the UAV has been plotted for 2° AOA and is shown in Figure 8. The maximum and minimum velocity values have been obtained by plotting the contours. Velocitycontours of the complete UAV, wing, horizontal tail, and vertical tail have been shown in Figures 8(a) to 8(d), respectively.

Velocity Streamline Contours

The Velocity Streamline Contour (VSC) of the UAV has been plotted for 2° AOA (Figure 9). Velocity streamline contours represent the fluid flow direction around the UAV's surface.The maximum and minimum velocity streamline values were obtained by plotting the contours. Velocity streamline contours of complete UAV, wing and HT, wing, horizontal tail, and the vertical tail have been shown in Figures 9(a) to 9(e), respectively.

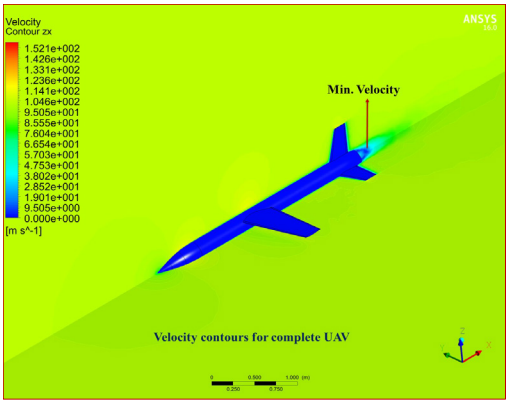

(a)

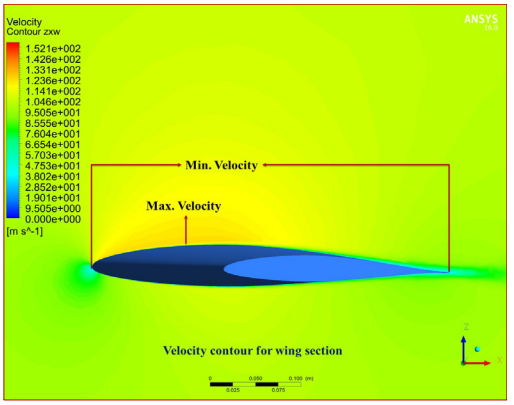

(b)

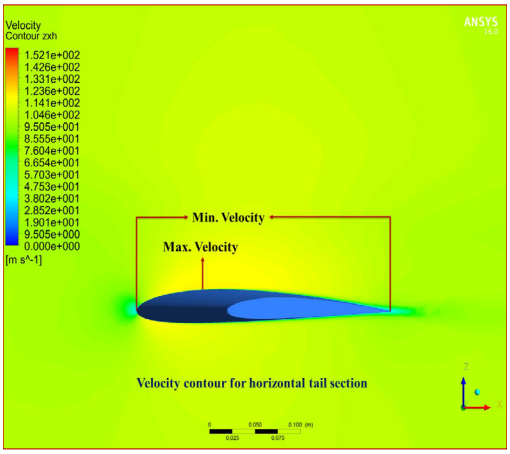

(c)

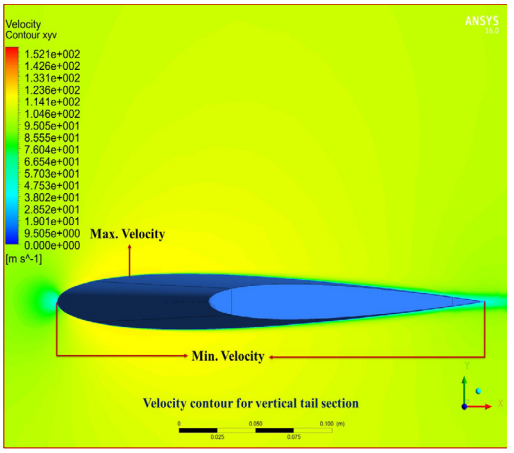

(d)

Figure 8. Velocity contours of UAV at 2° AOA (a) Velocity contours for complete UAV (b) Velocity contour for wing section (c) Velocity contour for horizontal tail section (d) Velocity contour for vertical tail section

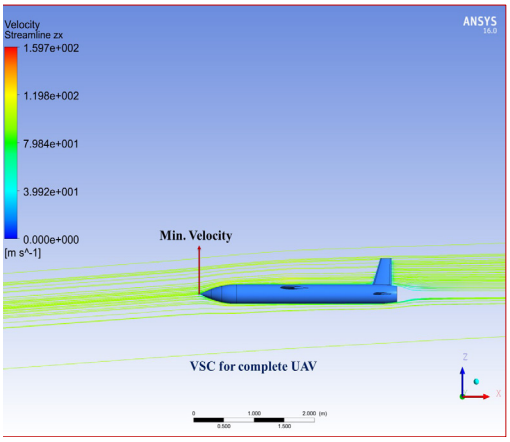

(a)

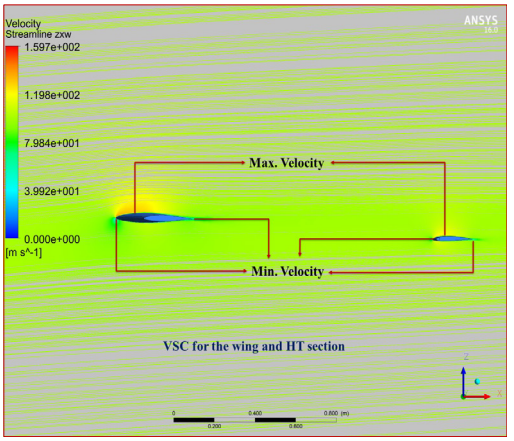

(b)

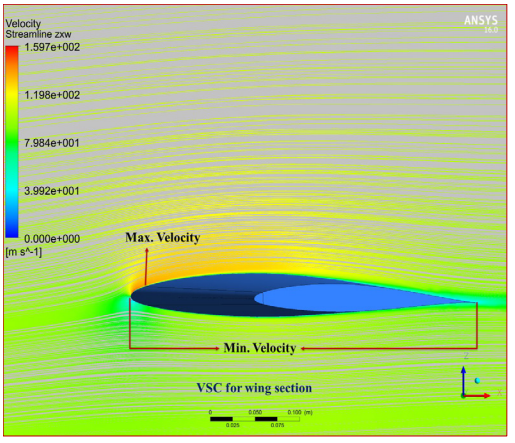

(c)

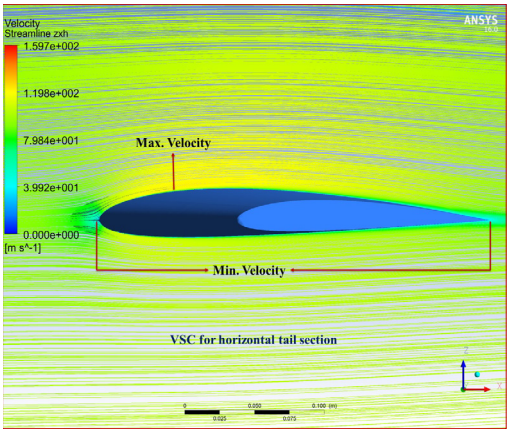

(d)

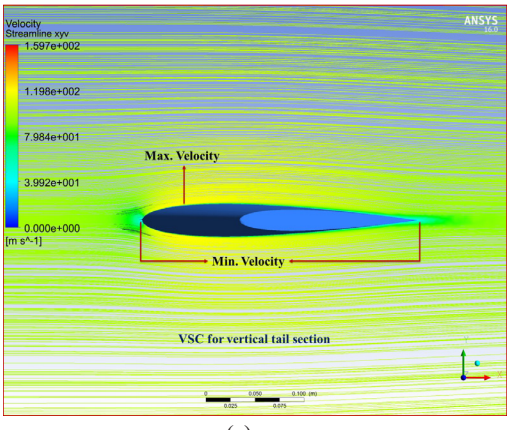

(e)

Figure 9. Velocity Streamline contours of UAV at 2° AOA (a) VSC for complete UAV (b) VSC for the wing and HT section (c) VSC for wing section (d) VSC for horizontal tail section (e) VSC for vertical tail section

RESULTS AND DISCUSSION

CFD Results

The results are obtained from ANSYS FLUENT by giving the input values like velocity, pressure value, and temperature in the boundary condition. As an output, we get the results like liftcoefficient, drag coefficient, and moment coefficient for different angles of attack. The difference between pressure created above and below the body's surface when the body moves aroundin space and measuring this factor is known as the Lift coefficient. The drag coefficient is usedto denote the rearward force that disturbs the airflow of an airfoil and is a dimensionless quantity.The moment ratio to the product of dynamic pressure and the wing's surface area is known as the Moment coefficient. The results were obtained for 11 different AOA, i.e., from -6° to 14° with an increment of 2° by changing the X and Y component values in the input values in the software. The values of the coefficient of lift, drag, and moment for different angles of attack are mentioned in Table 1. As per the result mentioned in Table 4, a stall occurs at a 14° AOA, and the maximum lift occurs at a 12° AOA (Piedra et al., 2018; Ramji et al., 2016).

Table 4
CFD result for UAV configuration

SI. No	AOA (α)	C_L	C_D	C_M	C_L / C_D
1	-6°	-0.3287	0.0381	-0.0362	-8.6266
2	-4°	-0.1636	0.0301	-0.0440	-5.4265
3	-2°	0.0028	0.0281	-0.0529	0.1007
4	0°	0.1694	0.0298	-0.0638	5.6886
5	2°	0.3367	0.0353	-0.0798	9.5311
6	4°	0.5057	0.0459	-0.1017	11.0274
7	6°	0.6756	0.0596	-0.1290	11.3299
8	8°	0.8434	0.0777	-0.1595	10.8573
9	10°	1.0074	0.1012	-0.2078	9.9524
10	12°	1.1514	0.1300	-0.2626	8.8557
11	14°	1.0095	0.2311	-0.3826	4.3681

DATCOM Result

The results are obtained from the DATCOM program. In the DATCOM program, some of the parameters of the UAV were given as input values, and input parameters are shown in the Tables 5(a) to 5(e). The parameters like Mach number, Reynolds number, angle of attack, reference area, CG values along the x-axis and z-axis, MAC, the position of the wing, vertical tail, horizontal tail, root chord, tip chord of wing, span, and semi-span of the wing, will be given as inputs and the output file will execute in another file in .out format.

Table 5(a)
General input parameters for the program

General Parameter	Input Values
Mach No	0.31
Alpha sweep	-6° to 14°
Reynolds Number	1.8E+06
Reference Area	1.0286 m^2
Reference Length	0.4074 m
Moment Reference Point	1.5 m

Table 5(b)
Fuselage input parameters for the program

Fuselage Parameter	Input Values
Fuselage Length	3.25 m
Fuselage Diameter	0.3 m
Fuselage Base Diameter	0.225 m
Fuselage Nose Length	0.6 m
Fuselage Base Length	0.3 m

Table 5(c)
Wing input parameters for the program

Wing Parameter	Input Values
Wing Airfoil Type	NACA 641-212
Wingspan	2.316 m
Root Chord	0.617 m
Tip Chord	0.308 m

Table 5(c) *(continue)*

Wing Parameter	Input Values
Semi Span	1.158 m
Exposed Semi-span	1.009 m
Sweep Angle	14.93°
Wing Incidence Angle	1°
Wing Location from Nose Tip	1.2426 m

Table 5(d)
Horizontal tail input parameters for the program

Horizontal Tail Parameter	Input Values
HT Airfoil Type	NACA 2412
Root Chord	0.1778 m
Tip Chord	0.0889 m
Semi Span	0.3335 m
Exposed Semi-span	0.1864 m
Sweep Angle	14.93°
HT Location from Nose Tip	2.8759 m

Table 5(e)
Vertical tail input parameters for the program

Vertical Tail Parameter	Input Values
VT Airfoil Type	NACA 0012
Root Chord	0.1778 m
Tip Chord	0.0889 m
Semi Span	0.4001 m
Exposed Semi-span	0.2531 m
Sweep Angle	12.53°
VT Location from Nose Tip	2.8759 m

In the output file, the lift coefficient, drag coefficient, pitching moment coefficient, vehicle axial force, vehicle normal force, and side force coefficient will be executed. The results were obtained for the same AOA mentioned in the CFD result. The obtained results are mentioned in Table 6 (Paul et al.,2021; Wu et al., 2019).

Table 6
DATCOM result for UAV configuration

SI. No	AOA (α)	C_L	C_D	C_M	C_L / C_D
1	-6°	-0.3090	0.0370	0.0543	-8.3514
2	-4°	-0.1650	0.0280	0.0151	-5.8929
3	-2°	-0.0280	0.0250	-0.0227	-1.1200
4	0°	0.1070	0.0270	-0.0583	3.9630
5	2°	0.2500	0.0330	-0.0910	7.5758
6	4°	0.4020	0.0460	-0.1218	8.7391
7	6°	0.5610	0.0650	-0.1540	8.6308
8	8°	0.7260	0.0910	-0.1956	7.9780
9	10°	0.8950	0.1250	-0.2384	7.1600
10	12°	1.0680	0.1680	-0.2718	6.3571
11	14°	1.2370	0.2160	-0.3095	5.7296

Wind Tunnel Testing

The wind tunnel model of the UAV was 3D printed utilizing the Fused Deposition Modeling (FDM) method using Polylactic acid (PLA) material with a resolution of 100 microns. To fit inside the wind tunnel test section, the printed model has a scale ratio of 1:6.5, and the 3D-printed UAV model is shown in Figure 10. The experiment was conducted in a subsonic-type wind tunnel with free stream velocities from 5 m/s to 80 m/s and less than 0.5% free stream turbulence intensity. The wind tunnel is shown in Figure 11 and 12 show the model fitted inside the test section. The open-circuited suction type windtunnel is the type of wind tunnel used for the experimental data analysis. The wind tunnel test section

has the specification of length of 2 m, Width of 0.6 m, and 0.6 m height. Six component balance,the equipment used to determine aerodynamic characteristics, has an AOA range of +20° to -20° for the test trial. The model was tested at 30 m/s while the AOA was changed from -2° to 14°, witha 2° increment in between. The wind tunnel test data obtained are shown in Table 7 (Peng et al., 2022).

Figure 10. Image of the 3D printed model placed in 6 component balance

Figure 11. Image of the wind tunnel

Figure 12. 3D printed model in the test section

Table 7
Experimental results obtained from wind tunnel for the UAV configuration

SI. No	AOA (α)	C_L	C_D	C_M	C_L / C_D
1	-2°	0.2491	0.0623	0.0043	3.9984
2	0°	0.3389	0.0578	-0.0278	5.8633
3	2°	0.3967	0.0630	-0.0662	6.2968
4	4°	0.5168	0.0608	-0.1329	8.5000
5	6°	0.6043	0.0734	-0.1480	8.2330
6	8°	0.6748	0.0927	-0.2047	7.2794
7	10°	0.7534	0.1127	-0.2380	6.6850
8	12°	0.7593	0.2180	-0.2430	3.4830
9	14°	0.7215	0.2358	-0.2094	3.0598

Comparison of DATCOM Values, CFD Values, and Wind Tunnel Experimental Values

The CFD, DATCOM program, and experimental wind tunnel results are compared, like the lift, drag, and pitching moment coefficient. The compared results of CFD, DATCOM, and wind tunnel were plotted in the graphs. Graphs were plotted in four types as a

for C_L/C_D versus angle of attack, which is shown in Figure 16. The values from all three approaches had minor variances when the resultswere compared. In the coefficient of lift section, stall angles in CFD and experimental results occurat 14° of the angles of attack. However, in DATCOM data, stall angles occur between 16° and 18° of the angle of attack. The calculated values used as input to the program and cause differences in DATCOM results could contain a small proportion of errors.

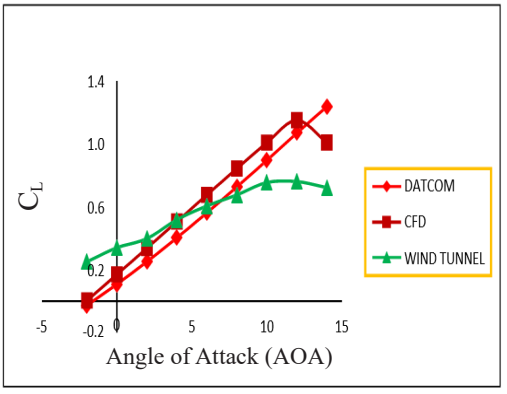

Figure 13. Comparison of DATCOM, CFD, and Wind Tunnel results for C_L vs. AOA

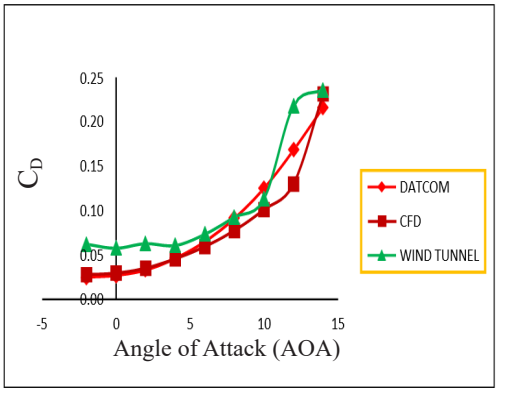

Figure 14. Comparison of DATCOM, CFD, and Wind Tunnel results for C_D vs. AOA

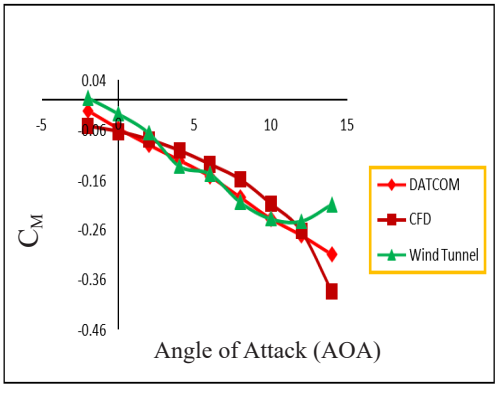

Figure 15. Comparison of DATCOM, CFD, and Wind Tunnel results for C_M vs. AOA

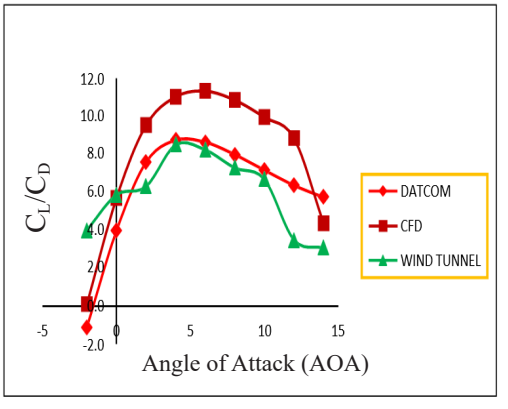

Figure 16. Comparison of DATCOM, CFD, and Wind Tunnel results for C_L / C_D vs. AOA

CONCLUSION

In this work, the aerodynamic performance of a UAV used for agricultural or surveying applications were compared. Initially, three types of UAV configurations were selected. Then, comparing the analysis results, one configuration was selected for better performance. Theconfigurations selected were conventional type-high-wing, conventional type mid-wing, and conventional type low-wing configurations. Analysis was done for differentangles of

attack varied from -6° to 14° with an increment of 2°. The aerodynamic performance values like the coefficient of lift, coefficient of drag, and pitching moment coefficient for all three types of configurations were noted down.

Input values were given to the DATCOM program to verify that the obtained CFD result was correct. Once the results from the DATCOM program were obtained, both results were compared.The compared results varied by ±2.8%. Then, tests in a wind tunnel were conducted for validation.The experimental data from wind tunnel testing has more closely aligned values, and windtunnel data agreed well with the CFD and DATCOM results.

Then, from the CFD, DATCOM, and wind tunnel test result data, we can conclude that theconventional type-high wing configuration has better efficiency than the other two configurations. So, the conventional type-high-wing UAV configuration from the design suggested in this researchcan be used for agricultural or surveying purposes.

ACKNOWLEDGEMENT

The Part of this work is funded by Aeronautical Development Establishment (Defence Research & Development Organization), Bangalore, India. Project grant No: ADE/PPA/14923/CARS/21-22/01.

REFERENCES

Adams, S. M., Levitan, M. L., & Friedland, C. J. (2013). High resolution imagery collection utilizing unmanned aerial vehicles (UAVs) for post-disaster studies. *Advances in Hurricane Engineering* (pp. 777-793). https://doi.org/10.1061/9780784412626.067

Ahmad, M., Hussain, Z. L., Shah, S. I. A., & Shams, T. A. (2021). Estimation of stability parameters for wide body aircraft using computational techniques. *Applied Sciences*, *11*(5), 2087. https://doi.org/10.3390/app11052087

Amaral, L. R. D, Zerbato, C., Freitas, R. G. D., Barbosa Júnior, M. R., & Simões, I. O. P. D. S. (2020). UAV applications in Agriculture 4.0. *Revista Ciência Agronômica*, *51*(5). https://doi.org/10.5935/1806-6690.20200091

Bravo-Mosquera, P. D., Cerón-Muñoz, H. D., Díaz-Vázquez, G., & Catalano, F. M. (2018). Conceptual design and CFD analysis of a new prototype of agricultural aircraft. *Aerospace Science and Technology*, *80*, 156–176. https://doi.org/10.1016/j.ast.2018.07.014

Casas, L. E., Hall, J. M., Montgomery, S. A., Patel, H. G., Samra, S. S., Si Tou, J., Quijano, O., Mourtos, N. J., & Papadopoulos, P. P. (2008). Preliminary design and CFD analysis of a fire surveillance unmanned aerial vehicle. In *Proceedings, Thermal-Fluids Analysis Workshop* (p. 50).

del Cerro, J., Cruz Ulloa, C., Barrientos, A., & de León Rivas, J. (2021). Unmanned aerial aehicles in Agriculture: A survey. *Agronomy*, *11*(2), 203. https://doi.org/10.3390/agronomy11020203

Edge, H., Collins, J., Brown, A., Coatney, M., Roget, B., Slegers, N., & Johnson, A. (2010). Lighter-than-air and Pressurized structures technology for Unmanned Aerial Vehicles (UAVs). *Army Research Laboratory Report ARL-TR-5068, Defense Technical Information Center, Army Research Laboratory, Aberdeen Proving Ground, MD, USA*. https://doi.org/10.21236/ada513823

Elharouny, A. S., Youssef, A. M., Zakaria, M. Y., & Abdel-Hameed, M. M. (2012, May). Procedures for mathematical modeling of small unmanned aerial vehicles. In *The International Conference on Applied Mechanics and Mechanical Engineering* (Vol. 15, pp. 1-12). Military Technical College.

Hasan, I., Mukesh, R., Krishnan, P. R., Srinath, R., Babu, D. P., & Gurmu, N. L. (2022). Wind tunnel testing and validation of helicopter rotor blades using additive manufacturing. *Advances in Materials Science and Engineering*, *2022*, 1–13. https://doi.org/10.1155/2022/4052208

Hasan, I., Mukesh, R., Radha Krishnan, P., Srinath, R., & B. Dhanya Prakash, R. (2022). Forward flight performance analysis of supercritical airfoil in helicopter main rotor. *Intelligent Automation & Soft Computing*, *33*(1), 567–584. https://doi.org/10.32604/iasc.2022.023252

Johari, M. S., Ali, Z. M., Wisnoe, W., Ismail, N., & Ishak, I. S. (2021). Computational aerodynamic analysis of UiTM's hawkeye UAV aircraft, *Journal of Aeronautics, Astronautics and Aviation*, *53*(2), 295-302. https://doi.org/10.6125/JoAAA.202106_53(2).23

Khamsi, M. (2019). Design and analysis of an unmanned aerial vehicle capable of carrying the camera. *Universal Journal of Mechanical Engineering*, *7*(3), 87–96. https://doi.org/10.13189/ujme.2019.070302

Laghari, A. A., Jumani, A. K., Laghari, R. A., & Nawaz, H. (2023). Unmanned aerial vehicles: A review. *Cognitive Robotics*, *3*, 8–22. https://doi.org/10.1016/j.cogr.2022.12.004

Liu, I.-H., Torelli, R., Prabhakar, N., & Karbowski, D. (2020). CFD modeling of unmanned aerial systems with cut-cell grids and adaptive mesh refinement. In *AIAA Scitech 2020 Forum* (p. 0538). https://doi.org/10.2514/6.2020-0538

Norasma, C. Y. N., Fadzilah, M. A., Roslin, N. A., Zanariah, Z. W. N., Tarmidi, Z., & Candra, F. S. (2019). Unmanned aerial vehicle applications in agriculture. In *IOP Conference Series: Materials Science and Engineering* (Vol. 506, p. 012063). IOP Publishing. https://doi.org/10.1088/1757-899x/506/1/012063

Paul, J. L., Vasile, J. D., & DeSpirito, J. (2021). Comparison of aeroprediction methods for guided munitions. In *AIAA Scitech 2021 Forum (p. 0024).* https://doi.org/10.2514/6.2021-0024

Peng, X., Zhu, H., Xu, D., Xiao, M., Wang, W., & Cai, G. (2022). Aerodynamic performance uncertainty analysis and optimization of a conventional axisymmetric vehicle based on parallel polynomial chaos expansions. *Aerospace*, *9*(8), 396. https://doi.org/10.3390/aerospace9080396

Piedra, S., Martinez, E., Escalante-Velazquez, C. A., & Jimenez, S. M. A. (2018). Computational aerodynamics analysis of a light sport aircraft: Compliance study for stall speed and longitudinal stability certification requirements. *Aerospace Science and Technology*, *82–83*, 234–242. https://doi.org/10.1016/j.ast.2018.09.016

Ramji, V., Mukesh, R., & Hasan, I. (2016). Design and numerical simulation of convergent divergent nozzle. *Applied Mechanics and Materials*, *852*, 617–624. https://doi.org/10.4028/www.scientific.net/amm.852.617

Shafer, T., Viken, S., Favaregh, N. M., Zeune, C. H., Williams, N., & Dansie, J. (2014). Comparison of computational approaches for rapid aerodynamic assessment of small UAVs. In *52nd Aerospace Sciences Meeting (p. 0039).* AIAA. https://doi.org/10.2514/6.2014-0039

Shah, H., Pampala, R. B., & Olivares, G. (2018). CFD analysis and experimental validation of an unmanned aerial vehicle. In *2018 Applied Aerodynamics Conference.* AIAA. https://doi.org/10.2514/6.2018-4216

Sharma, N. & Manna, K. T. (2017), Conceptual design approach of agricultural aircrafts. In *International Conference Proceeding ICCCT* (pp. 122-133). IJCRT.

Sharif, A. (2021). Conceptual design and analysis of a fixed wing mini unmanned aerial vehicle for humanitarian assistance operations. In *AIAA SCITECH 2022 Forum* (p. 1504). https://doi.org/10.2514/6.2022-1504

Sri, K. R. B., Aneesh, P., Bhanu, K., & Natarajan, M. (2016). Design Aaalysis of solar-powered unmanned aerial vehicle. *Journal of Aerospace Technology and Management*, *8*(4), 397–407. https://doi.org/10.5028/jatm.v8i4.666

Turanoguz, E. & Alemdaroglu, N. (2015, June, 9-12). Design of a medium range tactical UAV and improvement of its performance by using Winglets. In *2015 International Conference on Unmanned Aircraft Systems (ICUAS)* (pp. 1074-1083). IEEE. http://doi.org/10.1109/ICUAS.2015.7152399

Wang, K., & Zhou, Z. (2022). Aerodynamic design, analysis and validation of a small blended-wing-body unmanned aerial vehicle. *Aerospace*, *9*(1), 36. https://doi.org/10.3390/aerospace9010036

Wu, H., Gao, M., Song, W., Jie, Z., & Wang, Y. (2019). Accuracy analysis of aerodynamic calculation of twodimensional ballistic correction projectile based on missile datcom. *IOP Conference Series: Materials Science and Engineering*, *612*(3), 032096. https://doi.org/10.1088/1757-899x/612/3/032096

Pertanika J. Sci. & Technol. 32 (S1): 21 - 32 (2024)

PERTANIKA JOURNALS

SCIENCE & TECHNOLOGY

Journal homepage: http://www.pertanika.upm.edu.my/

Performance Evaluation of UAV Airfoil Under Various Ground Conditions

Dhanya Prakash R Babu[1,2]*, Madhesh Devasenan[2], Ganeshan Pushpanathan[3] and Mukesh Raju[4]

[1]Department of Aeronautical Engineering, ACS College of Engineering, Bangalore 560074, India
[2]Department of Mechanical Engineering, Academy of Maritime Education and Training (AMET) Deemed to be University, Chennai 603112, India
[3]Centre for Augmented Intelligence and Design, Department of Mechanical Engineering, Sri Eshwar College of Engineering, Coimbatore 641202, India
[4]Department of Aerospace Engineering, ACS College of Engineering, Bangalore 560074, India

ABSTRACT

Investigation of ground effects on Unmanned Aerial Vehicle (UAV) are limited. The UAV's ground effect on the water surface and irregular surfaces has not been studied well. The principal objective of this research is to apply numerical solutions to investigate the flow physics and aerodynamic characteristics of selected NACA4412 airfoil for different h/c and surface roughness conditions in the ground effect scenario. The k-ω turbulence model and compressible RANS equations are solved using the Finite Volume Method (FVM). The simulated data is authenticated with the reference data and compared with the DATCOM data. The results express that the lift coefficient variations for various surface roughness are affected by the h/c proportion. The drag coefficient for various roughness has the same pattern for different ratios and almost has the same difference from high to lower values. The result shows that the DATCOM code cannot predict the aerodynamic characteristics with ground effects.

Keywords: Aerodynamic characteristics, DATCOM, ground effects, h/c ratio, roughness

ARTICLE INFO

Article history:
Received: 27 July 2023
Accepted: 17 October 2023
Published: 19 January 2024

DOI: https://doi.org/10.47836/pjst.32.S1.02

E-mail addresses:
dhanyaprakashr@gmail.com (Dhanya Prakash R Babu)
madhesh.d@ametuniv.ac.in (Madhesh Devasenan)
ganeshan.p@sece.ac.in (Ganeshan Pushpanathan)
vsmprm@gmail.com (Mukesh Raja)
*Corresponding author

INTRODUCTION

The term "ground effect" denotes the favorable influence on an aircraft wing's horizontal surfaces' lifting property when the aircraft's wing is available near the ground (Figure 1). This outcome comes from the ground's nearness changing the airflow below the surfaces. Ground Effect's ability to increase lift is primarily due to a

ISSN: 0128-7680
e-ISSN: 2231-8526

decrease in drag produced, which raises lift to drag ratio. In maximum cases, a direct rise in lift produced by the wing supplements this enhanced lift. The wing tip is where induced drag decreases, depending on wing lift. The shape of the wing tip vortex, created as an airfoil passes through the air due to the pressure underneath a wing being greater than the pressure above it, is altered when it is created near the ground. When the airflow is forced outward, vortices close to the ground become elliptical instead of circular. It raises the wing's effective aspect ratio over its geometric aspect ratio and lowers generated drag. Power, lift, and airspeed are enhanced for any specific engine.

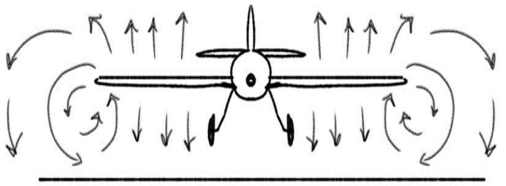

Figure 1. Ground effect

There are two types of ground effects: in-ground and out-ground. In the air downside, the airfoil can react with the ground, whereas in the out-ground effects, the air is not able to react with the ground. In the case of ground effect, less angle of attack (AOA) is needed for a given amount of lift before a wing stalls. The degree of this reduction in stalling AOA will depend on the type of airfoil used, although it may be some degree. Any decrease in a specific wing's maximum coefficient of lift in ground effect relative to that coefficient in free air will likewise influence the differential. Figure 2 illustrates the variation of stalling AOA in and out of the effect caused by the ground. It follows that for a given AOA, the wing will produce maximum lift at a lower AOA than in free air because carrying a wing into the ground improves lift. Figure 3 illustrates the pressure distribution on the wing due to ground effect.

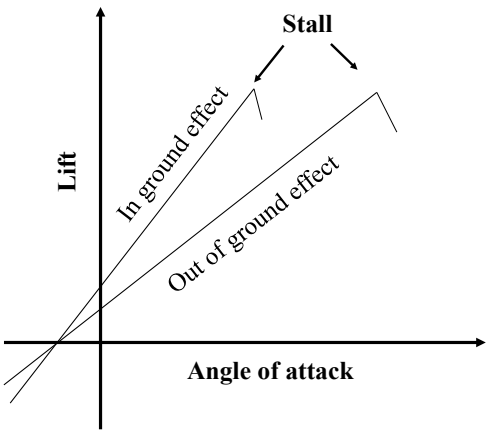

Figure 2. Ground effect in lift

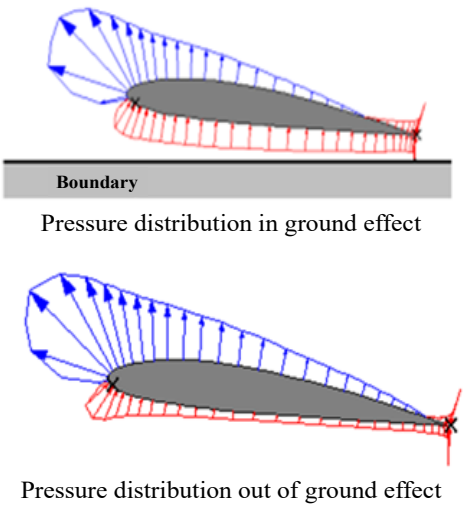

Figure 3. Pressure distribution due to ground effect

DATCOM was created in FORTRAN in 1979 and retitled by USAF. DATCOM is intended to be used for the preliminary design of an aircraft. It considers the conventional body-wing-tail configurations, which include control effectiveness for various high-lift control devices. It is the computer program to speed up the process of analyzing the existing or new design. Based on the configuration details of the design and the flight condition, it can immediately give the aerodynamic derivative of the aircraft. DATCOM calculates the static stability, high lift and control devices, and dynamic derivatives features. It also provides a trim option for determining the control deflections at subsonic Mach numbers. It has been created modularly, and the modular approach is used because it simplifies the program development.

De Divitiis (2005) proposed the analytical formulation for the force and moment calculation in the existence of ground and at an altitude. The study investigated the aerodynamic characteristics of a vehicle at an altitude and in the existence of ground effect and discussed the stability and performance characteristics of the vehicle. Then, the study validated the obtained results with the literature results and concluded that the coefficient of lift increases when h/c (ratio of height above ground to the airfoil chord) diminishes in the effect of the ground. Jamei et al. (2012) investigated the aerodynamic behavior of compound wings in ground effects. They selected NACA 6409 airfoil for the compound wing. The aerodynamic coefficients of the wing are associated with the rectangular wing for various ground clearances. They concluded that the compound wing had a high lift coefficient and a lower drag coefficient than the rectangular wing for the small ground gap.

Using CFD Simulation, Qu et al. (2014a) studied the NACA 4412 airfoil aerodynamic characteristics in dynamic ground effects. They concluded that the dynamic ground effect lift is less than the static ground effect when h/c is less than one. It is nearly equal to the static effect when h/c is between 0.5 and one and is greater than the static effect when h/c is greater than one. Using ANSYS Fluent, Qu et al. (2014b) simulated the flow around a wing in ground effects flying at an angle of attack 3° and 9° over the wavy and flat ground. They concluded that the lift, drag, and pitching moments are periodic when the wing is in the wavy ground, the aerodynamic forces are in the same pattern for the flat and wavy ground, and the aerodynamic forces increase for both angles of attack as the flight height decreases. However, the lift-to-drag ratio increases for the angle of attack of 3° while the lift-to-drag ratio rises first and then decreases for the AOA of 9°.

Roozitalab and Kharati-Koopaee (2021) investigated the Gurney flap's effect on the aerodynamic characteristics of the NACA 4412 airfoil in mutational ground effect during the launch and landing process. They concluded that during those times, the lift coefficients decrease, and the decrease in lift and increase in drag is more favorable in the landing process than the takeoff process. Gao et al. (2018) experimented with the RAE2822 airfoil's flow mechanics and aerodynamics by altering the ground clearance from the ground at

alpha sweeps of 0 to 12 degrees and Mach numbers of 0.5 to 0.8 in ground effect. The experiment concluded that in the high ground gap, lift increases by a small amount and drag increases due to the stagnation point downward movement, which decreases the strength of the shock, and in low ground clearance, the lift decreases, and the drag increases due to the presence of shock on the airfoil at the lower surface.

Page and McGuirk (2009) demonstrated the feasibility of LES CFD Methodology to represent the Harrier aircraft at touch-down. They concluded that the LES method is the appropriate tool for predicting the mean flow and unsteady oscillations, which is difficult in RANS-based CFD. Furthermore, Sharma et al. (2021) simulated the flow of wind Over the Deck and ground effects during the landing and approach of the helicopter on a ship deck and incorporated the static and finite state models. The simulation concluded that the wind over the deck induces high-frequency drifts and oscillations, more control effects are required when the wind over the deck is included for the entire helicopter, and the ground effect of static deck roll inclination causes the change in longitudinal cyclic input.

Zheng et al. (2021) studied the ditching characteristics of BWB aircraft numerically and validated the results with the high-speed ditching experimental results for 3D flat plates. The study concluded that the aircraft's proposed motion steadily diminishes until it glides on water. Further, Papadopoulos et al. (2021) presented a conceptual design of a combined box-wing and blended-wing unmanned aerial platform and studied the effect of flight without the ground effects. They concluded that the Unmanned Ground Effect Vehicle (UGEV) configuration has significant potential as a substitute for ships or seaplanes, based on its capacity to carry a higher cargo than seaplanes and transport it faster than ships.

Abney and McDaniel (2005) compared the aerodynamic results obtained from the missile DATCOM with the wind tunnel data for a high angle of attack at Mach number less than one. The prediction of normal force and longitudinal location of the center of pressure is well suited to the wind tunnel data for the AOA up to 45°. The prediction of axial force had a variance near the 30° AOA. Furthermore, Kefalas and Margaris (2018) simulated the flow field around Sonerai II LS aircraft. They concluded that the slope of the CFD lift curve is higher than that of the DATCOM lift curve. The results of digital DATCOM with those from CFD reveal that the post-stall zone has a lesser lift. The CFD data is steeper than the DATCOM.

In addition, Othman (2017) evaluated the longitudinal characteristics of an aircraft by CFD at the transonic speed and compared the results with the Wind tunnel data and DATCOM, comparing the pitching moment data. He concluded that the normal, axial, and pitching moment coefficient attained by the CFD is consistent with the wind tunnel data, but the DATCOM has a slight variation with the wind tunnel data. Moreover, the Missile DATCOM is a better prediction code for longitudinal aerodynamic coefficients for the lower angle of attack, and DATCOM prediction has nonlinear flow physics for the vortex models.

Paul et al. (2021) evaluated the prediction of aerodynamic data for four guided munitions, and the results were validated with test data. Vinayagar et al. (2022) and Ramshankar et al. (2023) studied the optimization of Crashworthiness Parameters of Thin-Walled Conoidal Structures and hybrid composites in aerospace applications. Thus, the literature review reveals that investigating the ground effect on UAVs is very limited, especially since the 'UAV's ground effect on the water surface and irregular surfaces has not been studied well.

MATERIALS AND METHODS

Methodology

To begin with, a wide literature review was done to understand the previous findings on ground effects. From the literature survey, the airfoil was selected, and the ground effects were investigated. The methodology of this work is bestowed in Figure 4. The geometry of the airfoil and mesh generation were done in ANSYS. With the fine unstructured mesh, analysis was carried out for the aerodynamic characteristics with ground effects. The CFD Analysis was carried out for different h/c ratios and surface roughness at a velocity of 30m/s. Then, the results are validated with the experimental results and compared with DATCOM data.

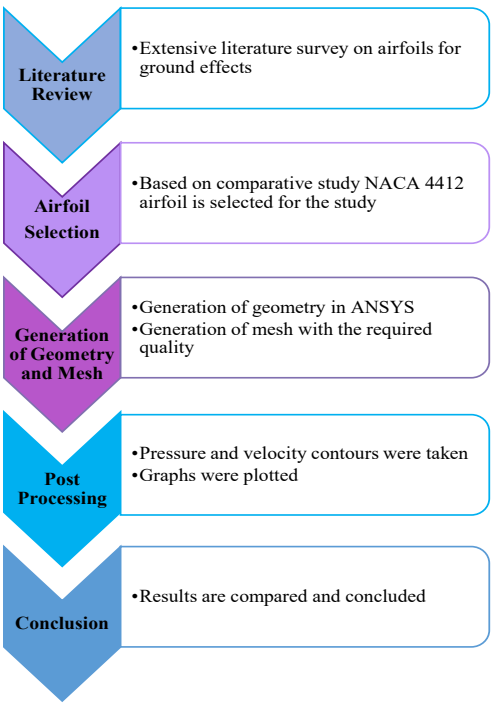

Figure 4. Methodology

Airfoil Selection and Ground Effects Investigation

The selection of the right airfoil geometry is one of the building blocks in the aerodynamic design process. Airfoil selection is based on multiple parameters such as Reynolds number, Thickness to chord ratio, Maximum coefficient of lift, and L/D ratio. Studies and research on the design of UAV wings, a few of the most common airfoils used in UAVs are NASA/Langley LS (1)-0417mod airfoil, Eppler–e 423, Selig S1223, Wortmannfx 74-cl5-140 mod, and NACA4412. Based on a comparative study, NACA4412 has shown promising characteristics that suit the requirement of a UAV wing. For further proceedings, NACA4412 will be selected as our baseline airfoil. When an aircraft glides at or below nearly half the length of the wingspan directly above the water or ground

surface, the ground effect occurs. Modern UAVs must be designed in such a way that they can take off and land on any kind of terrain. Hence, it is essential to investigate the ground effect of the UAV wing/airfoil at various ground conditions. The moving wall (ground) will be included in the simulations. Deploying flaps and spoilers may yield interesting physics when combined with ground effects.

Pre-Processing

The coordinates of NACA 4412 Airfoil are imported in ANSYS, and the domain is created. The global mesh parameters are given, and the surface mesh is generated for the domain with the minimum quality. The unstructured mesh is selected since the quality of the mesh is better than the structured mesh. Figure 5 depicts the mesh of the domain and the boundary condition.

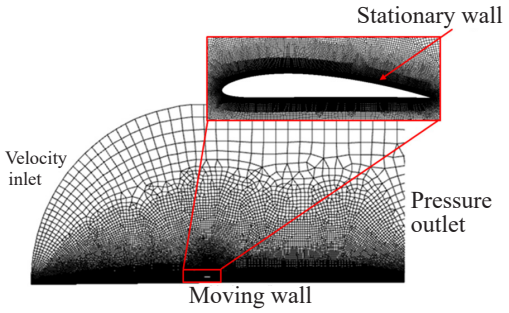

Figure 5. Surface mesh for the domain

The generated mesh has 434000 elements with 340556 nodes and a boundary layer thickness of 1 e^{-5}. The generated mesh was imported to ANSYS Fluent, and then the properties of the air were assigned. The velocity magnitude and direction were given in the boundary condition, and the reference values were given. The k-ω turbulence model equations and compressible RANS equations are used for the simulation. The governing equation for the turbulence kinetic energy is below (Jamei et al., 2012).

$$\frac{\partial(\rho k)}{\partial t} + div(\rho k U) = div\left[\frac{\mu_t}{\sigma_k} grad(k) + 2\mu_t S_{ij} \cdot S_{ij} - \rho\varepsilon\right] \quad (1)$$

$$\frac{\partial(\rho \varepsilon)}{\partial t} + div(\rho \varepsilon U) = div\left[\frac{\mu_t}{\sigma_\varepsilon} grad(\varepsilon)\right] + C_{1\varepsilon}\frac{\varepsilon}{k} 2\mu_t S_{ij} \cdot S_{ij} - C_{2\varepsilon}\rho\frac{\varepsilon^2}{k} \quad (2)$$

Where

k = turbulent kinetic energy
ρ = air density
U = Free stream velocity
S = reference area
ε = turbulent energy dissipation rate
Sij = mean rate of the deformation sensor
μ_t = air turbulent viscosity
μ = air viscosity

The analysis was performed at a speed of 30 m/s along with h/c values of 0.25, 0.5, and 1.0 and surface roughness values of 0.001, 0.005, 0.01, 0.02, 0.03, 0.04 and 0.05. The h/c is the distance ratio between the airfoil and ground to the chord length of the airfoil. The analysis was done, and the data was saved in a case and format. The results were post-processed for the analyzed data. Pressure contours and velocity contours were taken during post-processing. The C_L and C_D data obtained based on the governing equations and the data obtained are discussed later.

Post-Processing

After obtaining the results from the analysis, contour plots of pressure, velocity, temperature, and Mach number contours can be obtained from the fluent solver. In this present work, pressure contours and velocity contours were plotted. Figures 6 and 7 depict the pressure and velocity contour for the airfoil at 30 m/s, with h/c values of 1, 0.5, and 0.25 and roughness values of 0.001, 0.01, and 0.05. In Figure 6, the blue color on the upper surface of the airfoil indicates that the pressure value is low, and near the leading edge of the airfoil is red color, which has the maximum value of pressure. In Figure 7, the velocity on the airfoil's upper surface is maximum, which is red in the velocity magnitude. The velocity is zero on the surface of the airfoil. The velocity gradually increases from the surface of the airfoil to the maximum value, which the color variation can be seen in the images.

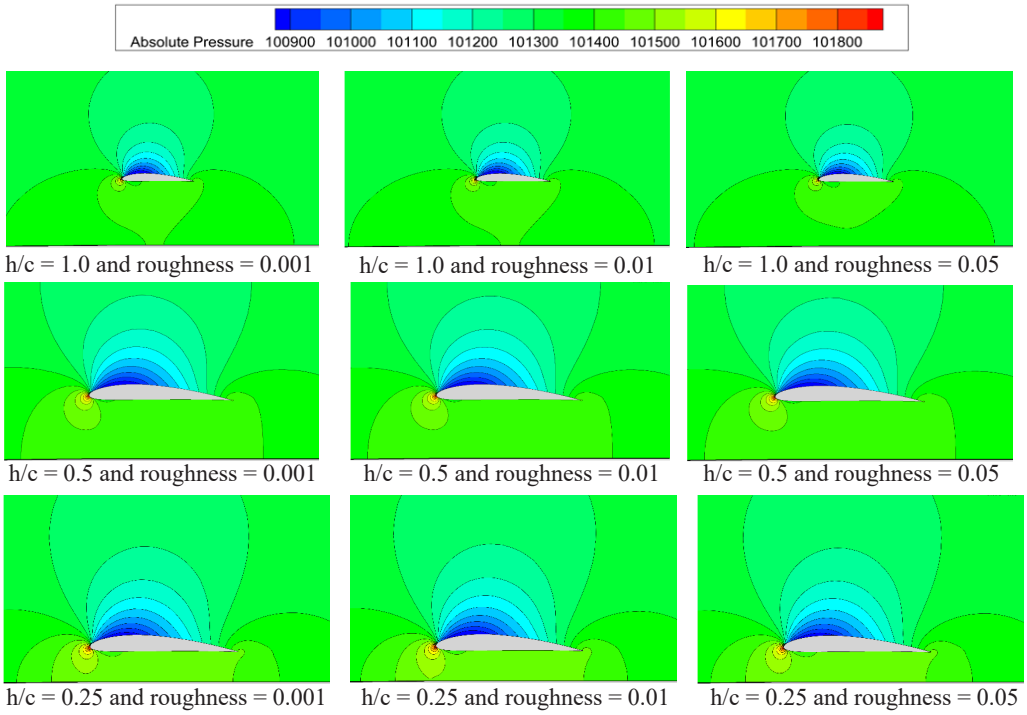

Figure 6. Pressure contour at 30 m/s

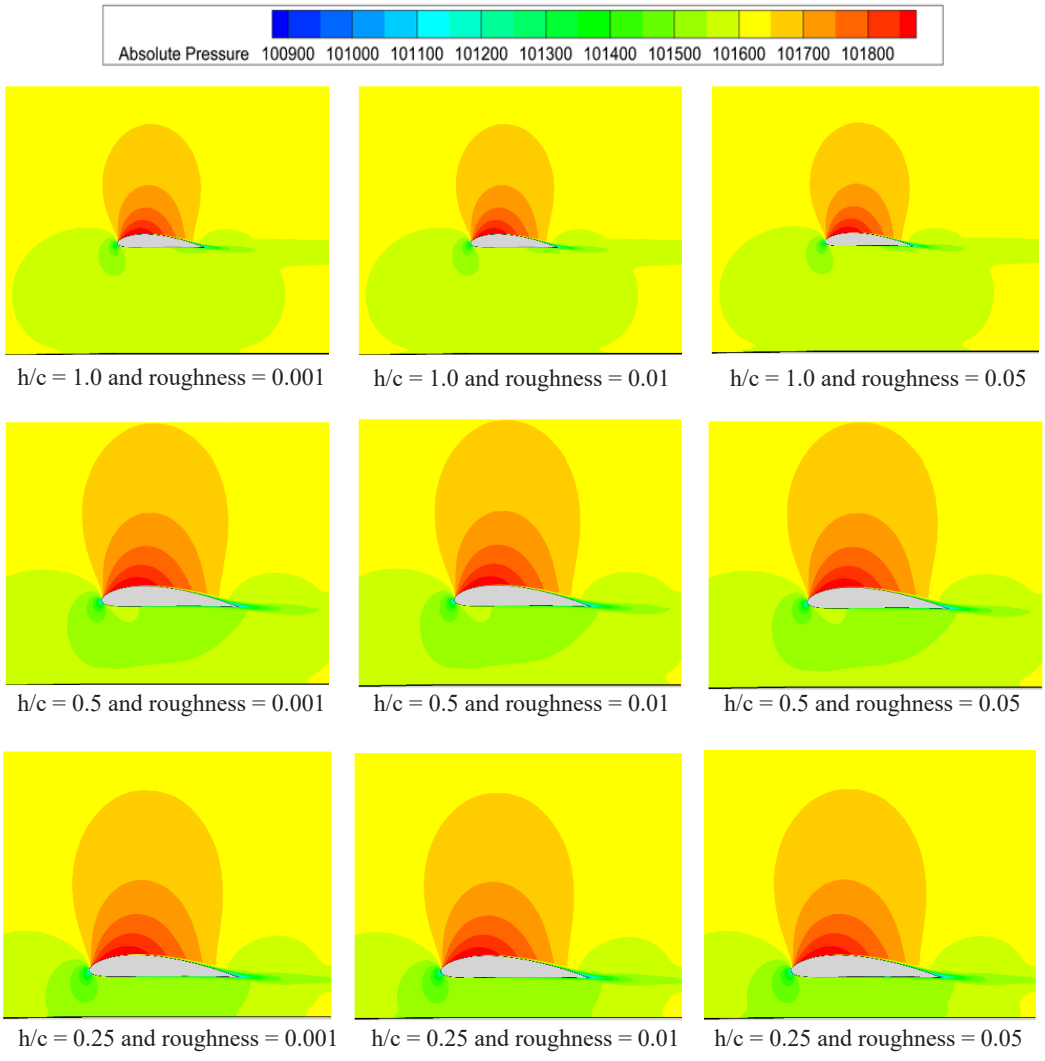

Figure 7. Velocity contour at 30m/s

RESULTS AND DISCUSSION

The results were obtained using the ANSYS package by giving the input values like velocity, surface roughness, and pressure in boundary conditions. As an output, we get the results like lift and drag coefficients for different AOA. The difference between pressure created above and below the body's surface when the body moves around in space and measuring this factor is known as the Lift coefficient. The drag coefficient is used to quantify the rearward force that disturbs the airflow of an airfoil and is a dimensionless quantity. The DATCOM results are obtained by inputting parameters like airfoil type, Reynolds number, Mach number, and angle of attack flight altitude. The CFD results for h/c = 0.4

and Reynolds number 3.2e5 are validated with the experimental results and compared with the DATCOM data. Figure 8 compares the lift coefficient obtained from Experimental, DATCOM, and CFD data. The plot shows that the computational results qualitatively agree with experimental values. However, the DATCOM data has discrepancies with the CFD and Experimental data. The DATCOM cannot predict the aerodynamic behavior of 4412 Airfoil with ground effects due to limitations in the code that the ground roughness cannot be given in the program.

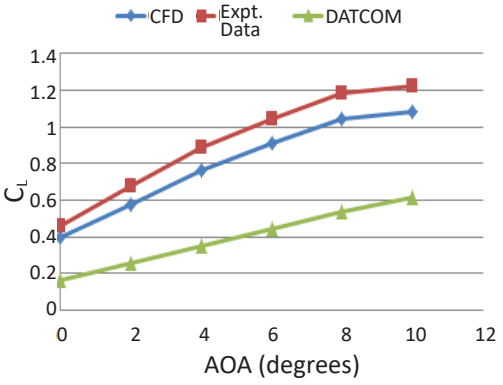

Figure 8. Lift coefficient vs. AOA for h/c = 0.4 and R_e= 3.2x10^5

Figure 9 depicts the NACA 4412 airfoil aerodynamic characteristics with ground effects for different roughness values with h/c as 1. The plot shows that the coefficient values vary from 0.4537 to 0.4571 and reach a maximum value at a roughness of 0.05, whereas the coefficient of drag varies from 0.0042 to 0.0055 and reaches a maximum value at a roughness of 0.001.

Figure 10 depicts the NACA 4412 airfoil aerodynamic characteristics for ground effects having different roughness values with h/c as 0.5. The plot shows that the coefficient values vary from 0.3558 to 0.356 and reach a maximum value at a roughness of 0.05, whereas the coefficient of drag varies from 0.0056 to 0.0196 and reaches a maximum value at a roughness of 0.001.

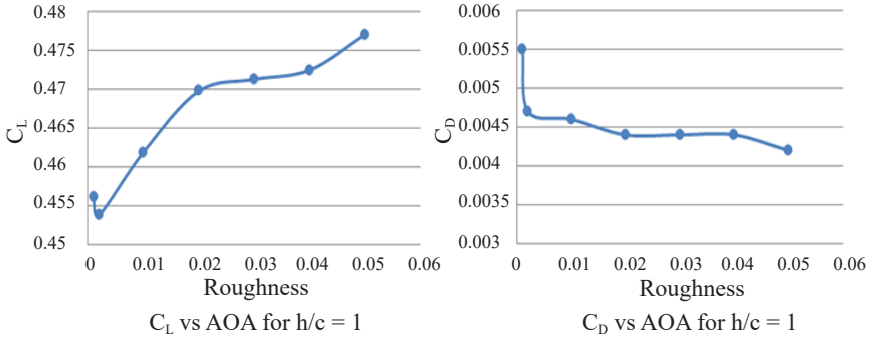

Figure 9. Aerodynamic characteristics for various roughness at h/c = 1

Figure 11 depicts the aerodynamic characteristics of the chosen airfoil with ground effects for different roughness values with h/c as 0.25. The plot shows that the coefficient values vary from 0.3398 to 0.4079 and reach a maximum value at a roughness of 0.05, whereas the coefficient of drag varies from 0.0071 to 0.0212 and reaches a maximum value at a roughness of 0.001.

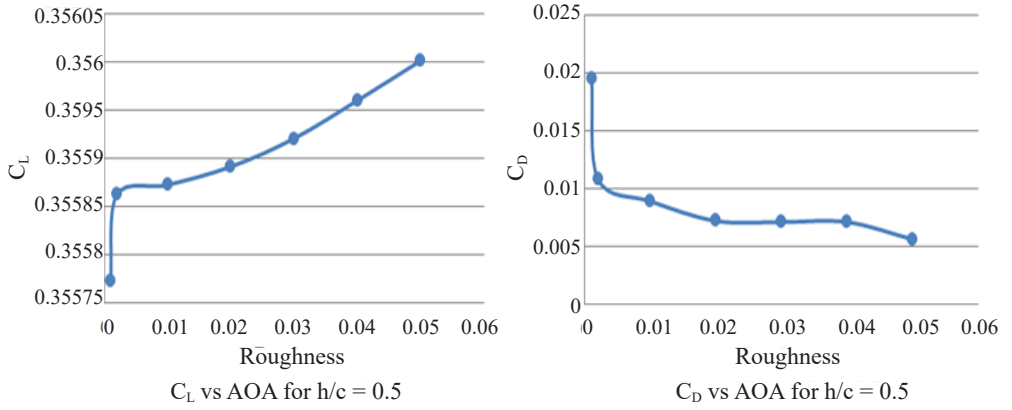

Figure 10. Aerodynamic characteristics for various roughness at h/c = 0.5

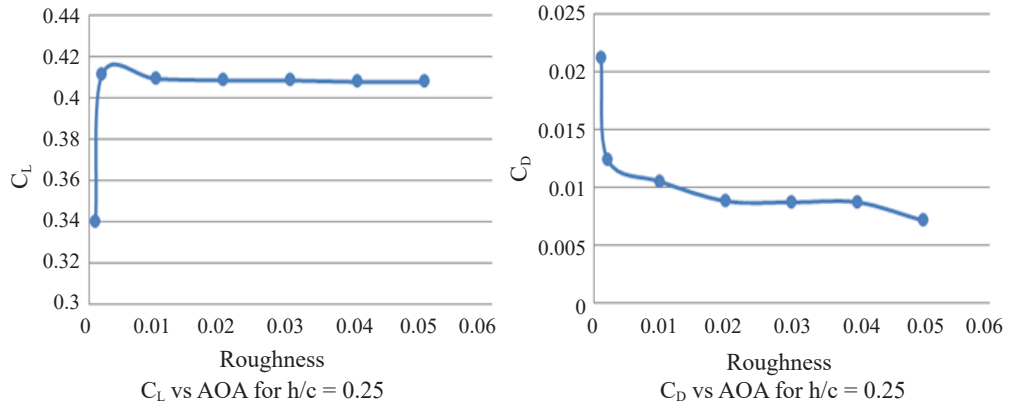

Figure 11. Aerodynamic characteristics for various roughness at h/c = 0.25

CONCLUSION

The present research examined airfoil flow physics and erodynamic characteristics (NACA 4412) by considering the ground effect for different h/c and surface roughness conditions. DATCOM prediction code cannot be used to predict aerodynamic characteristics with ground effects. The results show that the drag coefficient for different h/c ratios varies with a pattern, but the coefficient of lift does not follow any pattern. The coefficient of lift is at its highest value at a roughness of 0.05, while the coefficient of drag is at its lowest value at that same roughness, irrespective of the h/c ratio. In contrast, the coefficient of drag has a maximum value at a roughness of 0.001, whereas the coefficient of lift attains its maximum value at a roughness of 0.001 regardless of the h/c ratio. The difference between the max and min values is almost identical for the drag coefficient for diverse

h/c values. The results show that the roughness method implemented numerically in the present work shows some effects on the aerodynamic coefficients. However, it is not very significant, and the implementation of ground roughness physically is essential. Further future research can be continued by involving the wavy ground effects, which give the aerodynamic performance of the airfoil in real situations.

ACKNOWLEDGEMENT

This work is funded by ACSCE (Bangalore) and Raydynamics (Coimbatore), India.

REFERENCES

Abney, E., & McDaniel, M. (2005). High angle of attack aerodynamic predictions using missile datcom. In *23rd AIAA Applied Aerodynamics Conference* (p. 5086). AIAA. https://doi.org/10.2514/6.2005-5086

de Divitiis, N. (2005). Performance and stability of a winged vehicle in ground effect. *Journal of Aircraft*, *42*(1), 148-157. https://doi.org/10.2514/1.4830

Gao, B., Qu, Q., & Agarwal, R. K. (2018). Aerodynamics of a transonic airfoil in ground effect. *Journal of Aircraft*, *55*(6), *2240-2255.* https://doi.org/10.2514/1.C034998

Jamei., S., Maimun, A., Mansor, S., Azwadi, N., & Priyanto, A. (2012). Numerical investigation on aerodynamic characteristics of a compound wing-in-ground effect. *Journal of Aircraft*, *49*(5), 1297-1305. https://doi.org/10.2514/1.C031627

Kefalas, P., & Margaris, D. P. (2018). Aerodynamic analysis of a light aircraft using computational fluid dynamics. In *8th International Conference from Scientific Computing to Computational Engineering.* LFME.

Othman, N. (2017). Prediction of aerodynamic derivatives using Computational Fluid Dynamics (CFD) at transonic speed. *Journal of Transport System Engineering*, *4*(1), 8-16. https://jtse.utm.my/index.php/jtse/article/view/84

Page, G. J., & McGuirk, J. J. (2009). Large Eddy Simulation of a complete harrier aircraft in ground effect. *The Aeronautical Journal*, *113*(1140), 99-106. https://doi.org/ 10.1017/S0001924000002827

Papadopoulos, C., Mitridis, D., & Yakinthos, K. (2021). Conceptual design of a novel unmanned ground effect vehicle. In *IOP Conference Series, Materials Science and Engineering,* (Vol. 1024, No. 1, p. 012058). IOP Publishing. https://doi.org/10.1088/1757-899X/1024/1/012058

Paul, J. L., Vasile, J. D., & DeSpirito, J. (2021). Comparison of aeroprediction methods for guided munitions. In *AIAA 2021Forum* (p. 0024). AIAA. https://doi.org/10.2514/6.2021-0024

Qu, Q., Jia, X., Wang, W., Liu, P., & Agarwal, A. K. (2014a*).* Numerical simulation of the flowfield of an airfoil in dynamic ground effect. *Journal of Aircraft*, *51*(5), 1659-1662. https://doi.org/10.2514/1.C032452

Qu, Q., Lu, Z., Liu, P., & Agarwal, A. K. (2014b). Numerical study of aerodynamics of a wing-in-ground-effect craft. *Journal of Aircraft*, *51*(3), 913-924. https://doi.org/10.2514/1.C032531

Ramshankar, P., Sashikkumar, M., Ganeshan, P., & Raja, K. (2023). Experimental investigation of hybrid composites using biowastes and *Calotropis gigantea*: An eco-friendly approach. *Global NEST Journal, 25*(4)*,* 70-76. https://doi.org/10.30955/gnj.004620

Roozitalab, E., & Kharati-Koopaee, M. (2021). Effect of Gurney Flap on the aerodynamic behavior of an airfoil in mutational ground effect. *Proceedings of the Institution of Mechanical Engineers, Part G, Journal of Aerospace Engineering*, *235*(3), 339-355. https://doi.org/10.1177/0954410020943754

Sharma, A., Padthe, A., & Friedmann, P. P. (2021). Helicopter shipboard landing simulation including wind, deck motion and dynamic ground effect. *Journal of Aircraft*, *58*(3), 467-486. https://doi.org/10.2514/1.C035973

Vinayagar, K., Ganeshan, P., Raja, P. N., Hussain, M. S. Z., Kumar, P. V., Ramshankar, P., Mohanavel, V, Mathankumar, N., Raja, K., & Bezabih, T. T. (2022). Optimization of crashworthiness parameters of thin-walled conoidal structures. *Advances in Materials Science and Engineering*, *Article ID 4475605*. https://doi.org/10.1155/2022/4475605

Zheng, Y., Qu, Q., Liu, P., Wen, X., & Zhang, Z. (2021). Numerical analysis of the porpoising motion of a blended wing body aircraft during ditching. *Aerospace Science and Technology*, *119,* 107131. https://doi.org/10.1016/j.ast.2021.107131

Pertanika J. Sci. & Technol. 32 (S1): 33 - 54 (2024)

PERTANIKA JOURNALS

SCIENCE & TECHNOLOGY

Journal homepage: http://www.pertanika.upm.edu.my/

Assessment of Detailed Energy Conservation Potentials: The Case of the Ethiopian Leather Industry

Narayanan Kalamegam Millerjothi[1]*, Mulualem G. Gebreslassie[2], Thangavel Nithyanandhan[3] and Barathy Sachuthananthan[4]

[1]Department of Mechanical Engineering, Sri Eshwar College of Engineering, Coimbatore - 641 202, India
[2]Department of Mechanical Engineering, Ethiopian Institute of Technology, Mekelle University, P.O. Box No.231, Ethiopia
[3]Department of Mechanical Engineering, Sri Krishna College of Technology, Coimbatore - 641 042, India
[4]Department of Mechanical Engineering, Sree Vidyanikethan Engineering College, Tirupati - 517102, Andhra Pradesh, India

ABSTRACT

One of the most crucial components in any industrial operation is energy. However, the supply is not limitless. One of the key ingredients in cement production is energy, whose cost share ranges from 8 to 15% of overall production costs in developed nations but is much more in undeveloped nations. Therefore, the objective of this extensive research was to carry out a thorough energy conservation audit at the Sheba leather factory, located in the city of Mekelle, in the north region of Ethiopia. The specific objective of this research was to analyse the patterns of power consumption, identify energy-saving techniques, as well as to propose energy-saving recommendations for their implementation. It was obtained using primary and secondary data from the industry personnel. As a result, a total of 19 recommendations for energy saving were found and were forwarded for consideration. These recommendations have the potential to save a total of about $ 29900 annually, but their implementation would cost close to $ 15900, with a payback period of seven months. These recommendations also cover the utilities of the boiler, motors, blower, air compressors, cooling tower, and lighting. In order to lower their energy use, economic benefits are also considered.

Keywords: Electrical energy, energy audit, energy savings, economics, leather, thermal energy

ARTICLE INFO

Article history:
Received: 27 July 2023
Accepted: 17 October 2023
Published: 19 January 2024

DOI: https://doi.org/10.47836/pjst.32.S1.03

E-mail addresses:
millerjothi.nk@sece.ac.in (Narayanan Kalamegam Millerjothi)
mulualem.gebregiorgis@mu.edu.et (Mulualem G. Gebreslassie)
nithyanandhan.t@skct.edu.in (Thangavel Nithyanandhan)
bsachu7@yahoo.co.in (Barathy Sachuthananthan)
*Corresponding author

INTRODUCTION

Cement production requires significant

ISSN: 0128-7680
e-ISSN: 2231-8526

energy; the global cement industry is estimated to consume 2% of all primary energy used globally (Bhukya & Basak, 2014). Since becoming one of Africa's fastest-growing economies in recent years, Ethiopia has experienced a consistent increase in cement production. Next to the beverage and textile industry, leather is the second largest production in Ethiopia (Ramakrishna, 2014; Tesema & Worrell, 2015). Ethiopia is one of the Sub-Saharan African nations in the continent's eastern region. After Nigeria, Ethiopia has the second-highest population in Africa.

One of the people's primary needs is energy, which is the foundation of global progress and will continue to increase by at least one-third by 2035. Africa has seen enormous economic growth and increasing demand for energy (Fawkes et al., 2016; Gebreslassie et al., 2022). While this is happening, the instability in fuel costs has inspired development in African countries, particularly countries like Ethiopia, to concentrate on energy security and decrease their use of conventional fuels. Energy conservation is a fundamental first step in tackling the energy shortage and environmental degradation. Industrial energy audits aim to lower energy costs by lowering operating costs and raising profits. In Ethiopia, most garments and leather companies do not use energy conservation schemes, mainly because there are no measures in place to ensure that energy-efficiency measures are implemented (Al-Ghandoor et al., 2008; Benhelal et al., 2013; Önüt & Soner, 2007).

Therefore, many developing nations focus on increasing cost benefits by establishing energy efficiency in all process and production industries. In 2010, the United Nations Industrial Development Organization (UNIDO) employed sector-specific performance indicators to assess the energy efficiency potential of various industrial sub-sectors (Mulatu et al., 2018; Singh et al., 2023).

Any country's economic success depends on a number of key factors, including energy. Developing countries like Ethiopia have relatively little scientific data, especially in the major energy-consuming sectors like textile and leather factories, where there is a lack of clear data on the energy efficiency as well as power consumption patterns of the various factory processes. In addition, no research-based data can support further studies on the effective utilisation of both electrical and thermal energy as well as the implementation of renewable energy and waste to energy wherever possible. In view of the economic aspect, once we know or identify the amount of energy loss and where it has happened, it will help to show the decision makers to correct (to reduce the loss) or reuse it by finding another mechanism (Edenhofer et al., 2012; Tesema et al., 2015).

Therefore, the purpose of the existing study was to carry out a thorough, detailed energy audit and analyse the major energy-consuming processes of the Sheba leather industry in this pilot project. The factory is situated 45 kilometres away from Mekelle, the regional capital of Tigray, near the town of Wukro. The region is renowned for being the best source of hides and skins, particularly goatskin.

During the preliminary energy audit in the Sheba factory, the electrical and thermal energy consumption was around 33.14% and 66.86%, respectively, but the cost of thermal and electrical energy was recorded to be about 32.94% and 67.06%, respectively. Therefore, we advised a detailed energy audit to identify the source of the plant's energy issues.

SIGNIFICANT OF THE AUDIT PROCESS

In the audit process, the recommendations are proposed based on field measurement with achievable Energy Conservation (ENCON) proposals under no cost/low cost and cost investment categories. Moreover, the minimisation of present energy costs would be optimised by adjusting and optimising energy usage.

OBJECTIVES OF THE AUDIT

The main objective of this energy assessment was to assess the types of energy resources being extensively utilised, the technologies implemented, and the energy consumption with regard to the energy required by different factory utilisations to implement conservation measures. It has been achieved by:

a) Assessing the present pattern of energy consumption in each plant of the factory
b) Relating energy inputs and production output
c) Identifying potential areas of thermal and electrical energy economy
d) Minimising thermal energy wastages in major areas and optimising thermal energy distribution in end usage
e) Identifying immediate (especially no/low cost) improvements/savings
f) Identifying energy conservation opportunities and proposing possible applications of renewable energy sources

MATERIALS AND METHODS

Methodology

A comprehensive energy audit has been conducted in two stages in the Sheba leather factory: pre-audit phase I and detailed audit phase II. Physical measurement was used for most of the approaches in this investigation in the various processes of the factory (Da Cunha, 2007; IEA, 2020; Sony & Mekoth, 2018). The energy auditing was conducted at the key processes of Tannery Plant and Shoe Plant. In the detailed energy audit, the production process was evaluated through observations, interviews, and a register book of industry personnel and physical measurements of all major utilities using advanced instruments to analyse the energy utilisation of the entire industry.

Data Processing

The following expressions (Equation 1) were used to determine the energy measurements with respect to each utility, as shown below:

Boiler

The following expression can be used to compute the percentage of fuel savings when the boiler's operating pressure is reduced (Berry et al., 2006):

$$\left[\frac{h_{9\,bar} - h_{7.5\,bar}}{h_{9bar}}\right] x100 \quad (1)$$

where "h" is the enthalpy of the corresponding steam pressure

The following heat transfer formula (Equation 2) is used to calculate the amount of heat lost from the bare hot water pipeline:

$$hxAx\Delta T \quad (2)$$

where h = Convection heat transfer coefficient (W/(m^2°C))
A = Surface area of the pipeline (m^2)
ΔT = Temperature difference (°C)

The thermodynamic relation (Equation 3) shown below can be used to calculate the waste heat recovery from the flue gas and the heat content in the hot water of the boiler (Equation 4) (Berry et al., 2006):

$$Q_{fg} = m_{air} x Cp_{air} x (T_{hotair} - T_{ambair}) \quad (3)$$

$$Q_{water} = m_w x Cp_w x (T_{hw} - T_{cw}) \quad (4)$$

Compressors

Equation 5 can be used to calculate anticipated power usage during bandwidth reduction.

$$\left[\frac{P2^{0.36} - 1}{P1^{0.36} - 1}\right] \quad (5)$$

where P_2 and P_1 are cut off and cut in pressure, respectively

In compressed air systems, leaks are the primary source of energy loss. The following method was used during the leakage test, as stated below:
Step 1: The compressor was set up to work under the required operating pressure.
Step 2: All machine valves were shut off, and the required sections were permitted access to compressed air.
Step 3: The time spent loading and unloading compressed air during the flow was measured and registered.

Step 4: The work from step 3 was carried out 3multiple times to obtain average values for a precise output. The percentage of air leakage is estimated by Equation 6.

$$\% \text{ of Air leakage quantity} = \left[\frac{load}{(load+Noload)}\right] x100 \quad (6)$$

Motors, Fans & Blowers

Actual measurements of the voltage, current, and power factor for motors, fans, blowers, and compressors were taken using a power analyser. The Specification of the instruments used in the study is summarised in Table 1.

Economics Analysis

This study employed the simple payback period (SPP) method to analyse energy economics. SPP is a first approximation used in economic analysis to determine the time (in years) needed to recover the initial investment (First Cost), taking into account solely the net annual savings representing the returns on investment. Typically, the basic payback period is determined as follows (Equation 7):

$$Simplepaybackperiod = \frac{Firstcost}{Yearlybenefits - Yearlycosts} \quad (7)$$

Table 1
Specification of the instruments

Instruments Name	Make	Range	Uncertainty
Infrared temperature measuring instrument	TESTO 830-T4	-30 to + 400°C Type K (NiCr-Ni)	± 0.5°C + 0.5% of m.v.
Light intensity measuring instrument	TESTO 540	0 to 99999 Lux	± 3 lux or ± 3% of m.v.
Digital pressure manometer	TESO 510i	-150 to 150 hPa	± 0.05 hPa
For non-contact and mechanical measurement	TESTO 470	+1 to +99999 rpm	± 0.02% of m.v.
Vane anemometer	TESTO 410i	0.4 to 30 m/s	± (0.2 m/s + 2% of m.v.)
Flue gas analyser	TESTO 300 O_2	0 to 21 vol.%	± 0.2 vol.%
	TESTO 300 CO	0 to 4,000 ppm	± 5% of m.v. (400 to 4,000 ppm)
	TESTO 300 NO_x	0 to 3,000 ppm	± 5% of m.v.(100 to 3,000 ppm)
	TESTO 300 CO_2	± 0.2 vol.%	0.1 vol.%
Power analyser	PCE-PA 8000 PF (power factor), kWh, KVAh, kVARH, PF	Voltage: 10–600 Current 0.2–1200	± 0.01% V ± 0.05% A

ENERGY PROFILE OF THE COMPANY

Energy Utilisation Status of the Sheba Industry

Each plant's thermal and electrical energy bills were compiled to assess the factory's present energy consumption status. Transformers with the 1250 kVA and 800 kVA capacity were connected to meet the Tannery plant's electrical load requirements. For the Shoe plant, the 800 kVA transformers were connected to meet the Shoe plant's electrical load requirements. The transformer details are summarised in Table 2.

Table 2
Technical details of transformers

No	Connected plant	Transformer Details (kVA)	Qty	Operation days/week	hrs/day	No. of days/yr	Total hrs/y
1	Tannery plant	1250 (rated voltage HV 15000V/48.11A, LV 400V/1804.2)	1	6	16	317	5075
		800 (rated voltage HV 15000V/30.79A, LV 400V/1154.7)	1	6	16	317	5075
2	Shoe plant	800 (rated voltage HV 15000V/30.79A, LV 400V/1154.7)	1	6	8	317	2535

From May 2019 to April 2020, the Sheba factory used 0.865 million kWh of electricity supplied by the Ethiopian Electricity Utility (EEU). The energy share pattern of the thermal and electricity is given in Table 3 and graphically illustrated in Figure 1. An overall power factor of 0.85 was maintained in the factory.

Table 3
Energy usage pattern

No	Energy Source	Type of Energy	Unit	Annual Consumption	Direct Energy Equivalent 10^6 MJ/y	% Share	
1	EEU	Electrical	kWh	865500	3.1	32.71	33.14
2	DG		kWh	11250	0.04	0.42	
3	Steam Boiler	Thermal (FO)	Lit	155991	6.3	66.48	66.86
4	DG	Thermal (Diesel)	Lit	890	0.036	0.38	

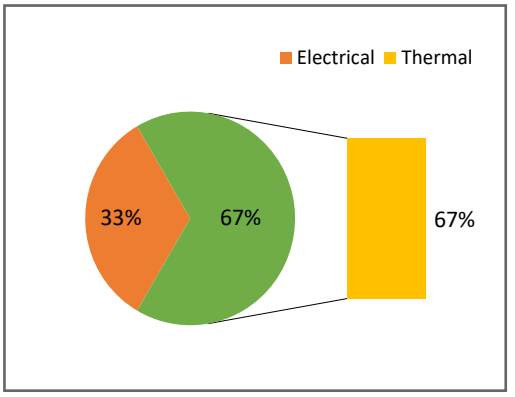

Figure 1. Graphical view of energy consumption pattern (MJ/Annum)

The expenditure incurred annually towards the above-cited energy usage is given in Table 4 and Figure 2. As illustrated in Figure 1, thermal energy is used for steam generation at around 6.3 x 10^3 MJ per annum, which is shared to 67% of total energy consumption. It indicates that thermal energy consumption is high for the dyeing section.

From (the EEU) electricity bill every month, it was noted that the Tannery Plant's power factor penalty and maximum demand penalty were around $ 315 and $ 72, respectively. Similar penalties for power factor and maximum demand for the shoe production plant were around $ 63 and $ 200, respectively. The increase in the unit cost may be due to an excess penalty in the power factor and maximum demand reached.

Table 4
Energy cost pattern

No	Energy Source	Type of Energy	Unit	Annual Consumption	Cost ($)	Total Cost Incurred ($/y)	% Share	
1	EEU	Electrical	kWh	865500	0.041	35485.5	32.51	32.94
2	DG		kWh	11250	0.041	461.25	0.43	
3	Steam Boiler	Thermal (Furnace oil)	Lit	155991	0.471	73471.76	66.64	67.06
4	DG	Thermal (Diesel)	Lit	890	0.528	469.92	0.43	

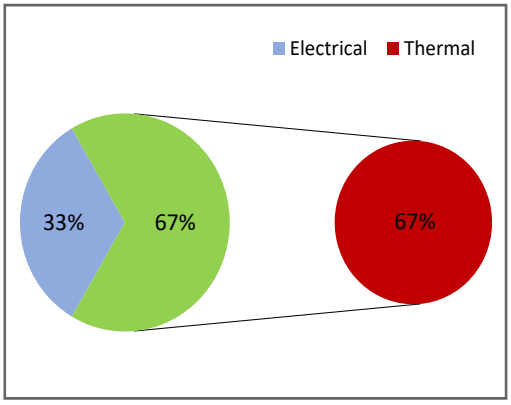

Figure 2. Graphical view of energy cost pattern ($/Annum)

Energy Consumption Distribution

The details of the electricity bill for May 2019 to April 2020 were obtained, and the variance in all parameters was reviewed

month-wise. Figure 3 depicts the electricity consumption distribution pattern for the entire plant. The tannery plant consumed roughly 72%, while the shoe manufacturing factory consumed less, roughly 28%.

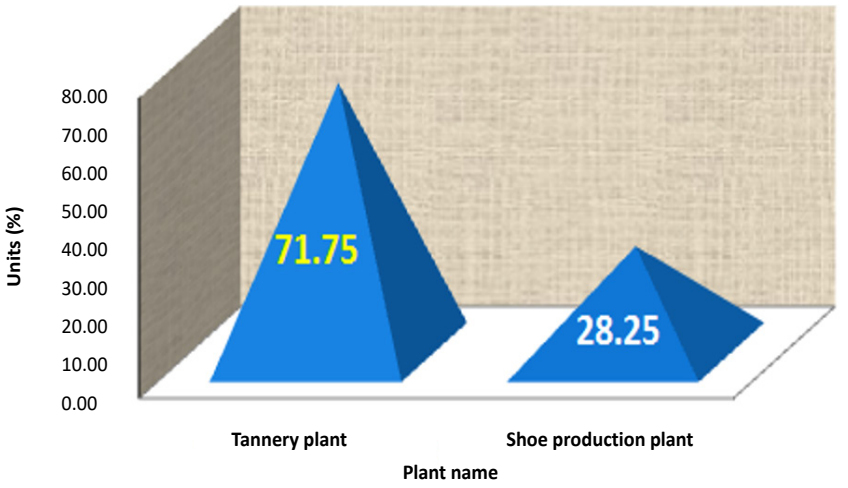

Figure 3. Electricity consumption distribution pattern for the entire plant

The monthly average specific energy consumption for the Tannery plant is shown in Figure 4. It is to be observed that the monthly average specific energy consumption was around 1.02 kWh per square foot of leather.

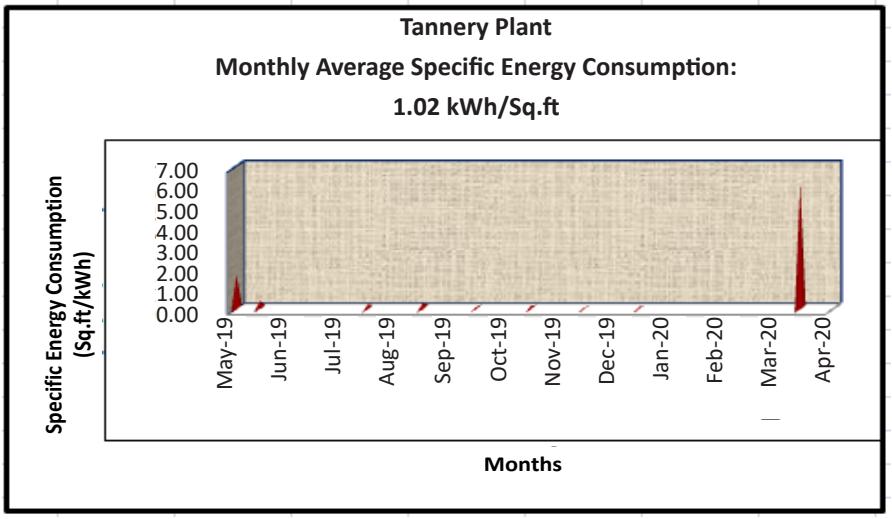

Figure 4. Specific energy consumption for the Tannery plant

The variation in unit cost between May 2019 and April 2020 is depicted in Figure 5. The average monthly unit cost for the Tannery plant was $ 0.04.

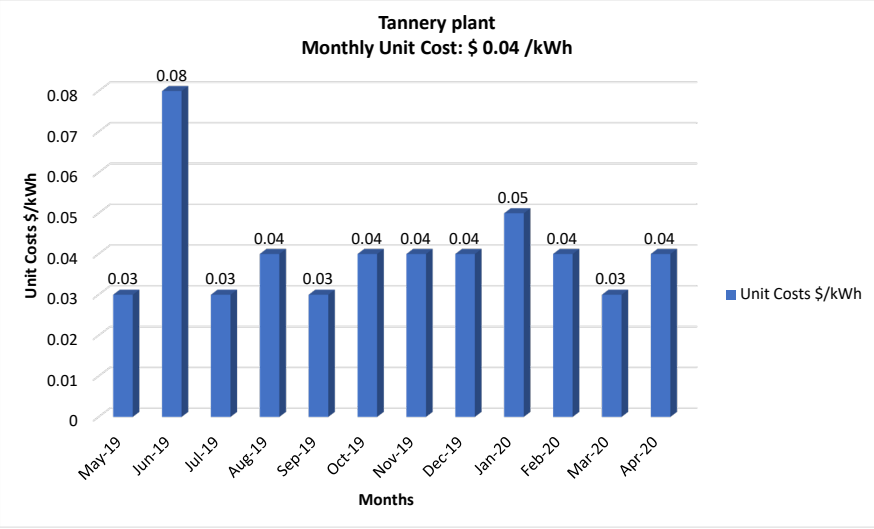

Figure 5. Average unit cost per month for Tannery plant

Figures 6 and 7 show the specific energy consumption and unit cost for the shoe production plant, respectively. The specific energy and unit cost has been computed, and it was observed to be around 4.59 kWh per Shoe pair and $ 0.04 per unit.

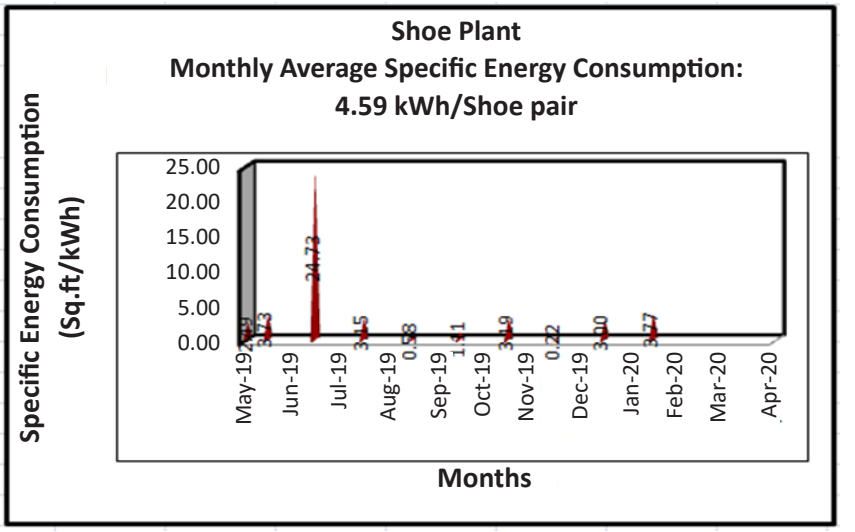

Figure 6. Specific energy consumption for Shoe production plant

From Figure 8, the overall average unit cost for the factory was $ 0.04 per kWh. It is to be observed that the actual calculated unit cost is more than 33% when compared to that of EEU unit cost. The consolidated specific energy consumption is summarised in Table 5.

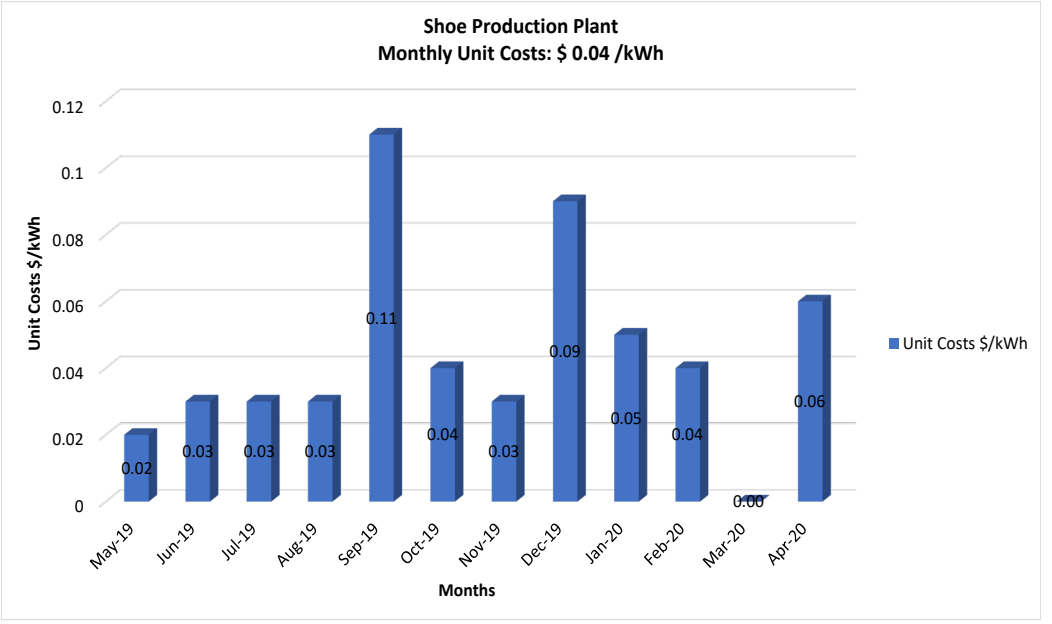

Figure 7. Average Unit cost per month for shoe production plant

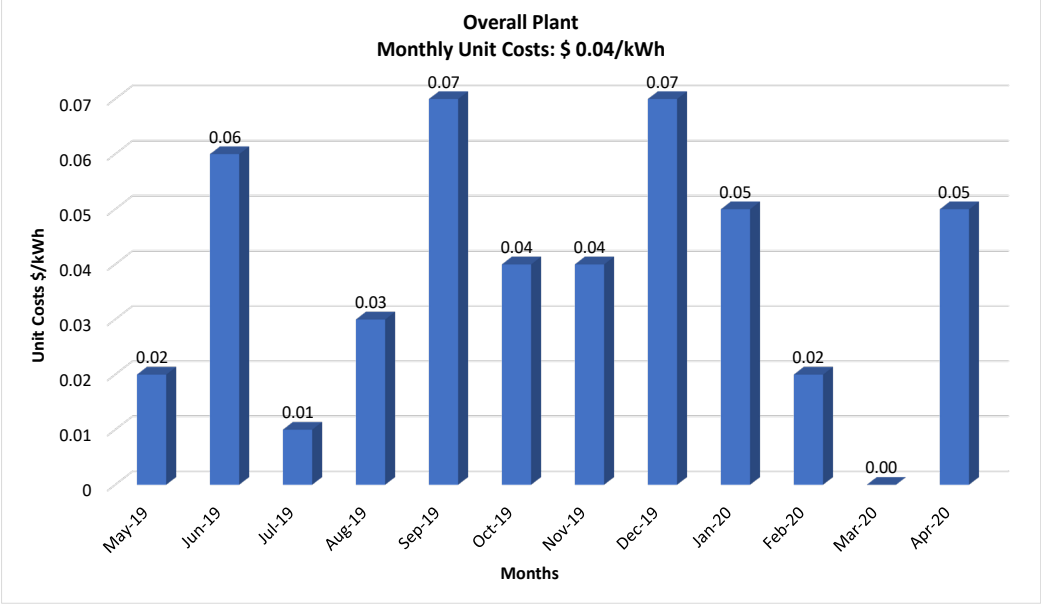

Figure 8. Average unit cost per month for the entire plant

Table 5
Energy efficiency level

No	Plant/Process	Specific energy consumption
1	Tannery	1.02 kWh/sq. ft of leather 0.03 lit of FO/sq. ft of leather
2	Shoe production plant	4.59 kWh/pair of shoes

RESULTS AND DISCUSSIONS

Based on the investment, payback duration, and other benefits, the identified recommendations shall be ranked in a phased manner.

Nil Investment Recommendations

Optimisation of the Operating Steam Pressure. Two furnace oil-fired boilers are installed at the Sheba factory to supply steam at 2.5–10 bar, and one boiler is kept on standby. The boiler was operated between 590 and 760 kg/h against the rated capacity of 2.8 tonnes per hour (27–30% loading), and oil consumption was recorded at around 53 lit/hr (51.8 kg/h). The boiler produces steam to hot water generation for Re tanning drums for the hide and skin section at 35–60°C. During the steam audit, the boiler's current pressure setting ranged from 2.5 to 10 bar (on average, 6.25 bar), but the process only required a maximum steam pressure of 4 to 6 bar. It shows that steam was produced at a higher pressure than was required by the process, which results in increased fuel consumption (20). Therefore, it is advised to run the boiler pressure at the boiler house between 2.5 and 6.5 bar (on average, 4.5 bar). With no additional cost, this would result in significant fuel savings. Making the mentioned changes to the pressure setting will result in an annual savings of more than $ 370.

Operating Pressure Reduction for Screw-type Air Compressors. The compressors at the company are installed in two places to provide the required quantity of air for the Hide and Curst production plant and the Shoe Production plant to perform various process requirements. It was noticed that the air requirement of the whole plant is a maximum of 6 bars for its operation, considering both the tannery and shoe production plant. Thirdly, the compressed air pipe size ranges between 3” and ½” in diameter.

Thus, the pipeline distance and smaller pipe diameter are expected to add to the pressure drop in the pipeline. Therefore, adjusting the compressor's pressure setting bandwidth is advised to lower power usage. Tables 6 and 7 provide the suggested pressure setting and estimated power savings for three compressors.

Table 6
Operating pressure settings for hide and crust production plant air compressor

Identification	Existing pressure bandwidth (bar)		Proposed pressure (bar)		Measured energy consumption (kW)	Expected energy consumption (kW)	Process requirement (bar)
	Cut in	Cut out	Cut in	Cut out			
Comp-1	6.5	7.5	6.2	6.8	16.08	15.03	6 bar only
Comp-2	6.6	7.6	6.2	6.8	16.87	15.76	
Total					32.95	30.79	

Table 7
Proposed pressure settings for shoe production plant air compressor

Identification	Existing pressure bandwidth (bar)		Proposed pressure (bar)		Measured energy consumption (kW)	Expected energy consumption (kW)	Process requirement (bar)
	Cut in	Cut out	Cut in	Cut out			
Comp-3	8	8.5	6.2	6.8	22.49	20.30	6 bar only

With the suggested pressure setting for the three units, the energy usage can be decreased from 164 kW to 147 kW, saving almost $ 3150 annually without any additional investment.

Reduction of Compressed Air Leakages in the System. Two compressors are operating to provide the air supply for the hide and crust production plant, and one compressor is located around the Shoe production plant to fulfil the compressed air demand for various process requirements. Compressors are well known to be important energy consumers. Compressed air must be used optimally and sensibly, only allowing minimum unavoidable leakages. However, 10% of the production of pressurised air is often allowed because more than that would be very difficult to stop. A leakage test was carried out in the Hide and Crust section and shoe production plant to ascertain this. Some of the leakage spots in the pipelines and the quantity of air leakages from the respective plant are shown in Figure 9 and Table 8, respectively.

From the total quantity of compressed air supplied of 14.04 m^3 per minute, 8.64 m^3 per minute was leaked. Therefore, with a permissible 10% leakage, nearly 7.2 m^3 per minute air leakage could be arrested, resulting in a total cost saving of $10,334 per year with zero investment.

Figure 9. Photographic image of leakage points

Reduction of Compressor Air Intake Temperature. Two air compressors used to deliver compressed air for the hide and crust production plant are housed beside the boiler room, where high heat losses are available. All these compressors operate based on Load–No Load mode. During the detailed audit, it was observed that the compressor air suction was kept within the room. The two compressors were kept adjacent to the boiler room. The partition between the boiler shed and the compressor shed is not fully closed; hence, the boiler side radiation was transferred to the compressor house. The temperature within the shed was between 5°C and 6°C higher than the ambient air temperature outside, which was 310°C (Da Cunha, 2007; Rossiter & Jones, 2015).

Table 8
Details of leakage quantity at various plants

Hide and crust plant								
Identification	Trials	I	II	III	Average	Compressor loading (%)	Measured FAD (m^3/min)	Quantity of leakage (m^3/min)
Comp-1	Load	220	210	221	217	60.69	5.88	3.55
	Unload	140	142	135	139			
Comp-2	Load	243	240	245	243	62.87	5.85	3.68
	Unload	142	145	143	143			
Shoe production plant								
Comp-3	Load	100	105	98	101	61.09	2.31	1.41
	Unload	60	65	68	64.5			
						Total	14.04	8.64

It has been established that every 3°C rise in the suction air temperature would increase the compressor power consumption by 1%. Hence, it is suggested to provide ventilation for the suction duct at the hide and crust production plant compressor room. In addition, the partition full partition must be made between the boiler shed and the compressor shed to prevent heat transfer from the boiler shed. Therefore, if ventilation is provided, the motor power usage of 144 kW might be lowered by 2%, saving at least $ 140 annually as a result of the extremely minimal investment, the payback period would be quite low.

Small Investment Recommendations

Proper Insulation of Steam Lines. In the boiler house, during the insulation survey, it was observed that the steam pipelines at certain locations were either improperly insulated or left bare. The average surface temperature of these bare steam pipelines was measured as 105°C. This higher temperature leads to considerable heat loss to the surroundings. The total area of the inefficiently insulated surfaces at the various steam line locations was estimated to be 1.2 m^2. Therefore, it was suggested to insulate the bare hot water pipelines with an investment of $145 and a straightforward payback period of 9 months to reduce convection heat loss and obtain cost savings of $ 200.

Proper Insulation of Hot Water Storage Tank. The factory consumes hot water of around 124,900 litres per day for various processes in the Tannery plant. Raw water at 21°C is heated by saturated steam at 300°C in the heat exchanger between 35°C and 55°C according to hot water demand for each process and stored in the storage tank. It was observed during the study that the entire top portion of the storage tank cover was not insulated and left bare. The entire hot surface of the top portion was simply exposed to the atmosphere. The surface temperature of this top cover varied from 30–45°C. This higher temperature results in considerable heat loss to the surroundings.

It was therefore recommended to appropriately insulate the leftover top portion of the storage tank cover to reduce convection heat loss with an expenditure of $ 150 and a simple payback period of 6 months to reduce convection heat loss and gain cost savings of $ 285.

Utilisation of Exblow Gun for Cleaning Purposes. One of the regular tasks in any industry is using compressed air for cleaning applications. Huge air at low pressure (2.5 ksc) is needed for cleaning applications, whereas compressed air at 6.0 bar is employed for cleaning applications in practically all industries. During the study, compressed air from Compressor No. 1, 2, and 3 was used for all types of cleaning purposes in Tannery and Shoe production plants, respectively. About 18% of compressed air generation is estimated to go for cleaning. It can be reduced to less than 7.5% by optimising the utilisation.

Thus, Exblow Guns were advised to be installed in air cleaning hose pipelines to supply cleaning air at 2.5 bar, which is lower than the 6.5 bar pressure. Depending on the amount of air utilised for cleaning, an air consumption reduction of between 70% and 75% can be achieved (Kingston & Baghzouz, 1994). A $ 185 investment might result in an annual savings of around $ 2150. This results in a maximum payback duration of 1 month.

Replacement of Cast Aluminium Blades with FRP Blades. Cooling tower performance was evaluated for potential energy conservation measures during the detailed energy audit. The industry has 2 cooling towers (CT) for water cooling using a vacuum dryer machine installed in the hide and skin section. The blades of cooling tower fans were found to be made of cast aluminium. Cooling water circulation pump-rated power was recorded as 5.5 kW and 11 kW for skin and hide vacuum dryers, respectively. In order to save energy, it is currently popular to swap out the traditional metal blades on cooling tower fans with blades made of fibre-reinforced plastic (FRP). Therefore, changing the cooling tower fan's present aluminium blades for lighter, properly profiled fibre-reinforced plastic blades is advised. An investment of about $ 300 may result in annual savings of approximately $ 150. A maximum payback duration of 24 months results from this.

Medium Investment Recommendations

Arresting of Steam Leakages. Steam leaking is an obvious indication of waste and needs to be prevented. Latent and sensible energy is lost as a result of steam leaks (Bureau of Energy Efficiency, 2018; Rossiter & Jones, 2015). The employees at the factory would do well to consider the expenses and issues associated with steam loss issues. During the study, steam leakages have been noticed in 5 places, especially in bends, couplings and valves. In a few locations, the steam leaked through the holes on the pipe surface, possibly due to erosion. Hence, replacing the faulty valves and fittings and arresting the Steam Leakages is recommended. Considering the size of leakage points and steam pressure, it was anticipated that about 1.8 kg/h steam would leak from these five identified points. It may be possible to replace bends, T joints, valves, and couplings to save $ 5925 annually with a $ 570 investment and a 1-month payback period.

Installation of Temperature Indicator Cum Controller (TIC) in Cooling Tower. In the Sheba factory, two cooling towers (CT) are operated and powered by 4 kW aluminium blades to supply cooling water to the skin and hide sections. The cooling tower is designed to operate at 9°C and 11°C for skin and hide sections. However, the outlet water temperatures from the cooling tower were observed to be around 20 to 22°C as needed for both sections. It was observed that due to erratic weather variations in the winter season, the outlet water temperatures would go below 10°C. Hence, operating the cooling tower fan only when required is recommended. Hence, operating the cooling tower fan as and only when

required is recommended. It can be achieved by installing a Temperature Indicator Cum Controller (TIC) at the cooling tower water outlet port to sense the temperature continuously and activate the cooling tower fan whenever the water temperature exceeds its set limit (Kingston & Baghzouz, 1994). It would result in appreciable cost savings of $ 385 per year with an investment of $ 430, which gives a payback period of just 14 months.

Installation of Automatic Star-delta-star Starter in the Part-loaded Motor. Power measurements were taken at various locations in the motors. At present, all motors are connected to a star-delta-star starter. Irrespective of the loading of the motor, it goes into Star mode and changes over to Delta-Star mode. The Auto Star-Delta-Star starter is a device with a built-in load sensor which senses the load continuously, and whenever the load goes below 40%, it automatically changes over to Star connection and reverts to Delta mode when the load goes above 40% (Bureau of Energy Efficiency, 2018; Zeitz, 1997).

While the motor operates and loads less than 40%, the iron losses will be more dominant than the current related to copper losses (Ganguly et al., 2016). As a result, the iron losses would be at their lowest since the applied voltage is lower when the motors are linked in star mode. Besides, a considerable power factor improvement would be possible in the star mode connection. Therefore, it is recommended to install Auto Star-Delta-Star Starter for the identified motors since their load varies between 15–40%. A significant amount of kVA would be saved with this technique. With an expenditure of $ 640 and a payback period of about 1 month, this implementation would result in more than $ 2,090 annual savings.

Installation of Servo Stabiliser in the Lighting Feeder. During the lighting audit, the lighting voltage used was 220 V in each lighting feeder located at various sections, and the overall lighting load was 17.06 kW. A reduction in supply voltage by 15% can result in a drop in power consumption by around 15% and an insignificant drop in illumination level by about 3–4% (Bureau of Energy Efficiency, 2018).

By installing a servo stabiliser and keeping the lighting voltage at 205 V, it is possible to optimise the voltage level in the lighting feeder and save significant energy. This technique has been successfully implemented in various companies, and substantial savings have been achieved. The investment required for a 25 kVA servo stabiliser and fitting is nearly $ 715; hence, the cost-saving benefits are around $ 2,980 and a payback period of around 3 months.

Waste Heat Recovery from the Boiler Flue Gas. The Sheba plant has an oil-fired furnace boiler capacity of 2.8 tonnes per hour. It was noticed that an electric heater filament capacity of 5 kW preheated the furnace oil. At a flow rate of 0.324 kg/s, the flue gas exits the boiler from the boiler at a temperature of around 290°C to the atmosphere. If we installed a heat

exchanger to recover this heat, huge savings would be attainable. Hence, it is recommended to install an oil preheater to recover the heat from the flue gas to preheat the furnace oil. If preheated is supplied by waste heat recovery of flue gas, but the combustion would be better, and the energy input requirement would also be lesser as the preheated oil brings in a certain quantum of energy (Ganguly et al., 2016).

Therefore, around 17.2 thousand units can be saved by replacing the 5 kW electrical filament by preheating the inlet air through the outgoing hot flue gas. The approximate $ 1,430 investment for a recuperator with ceramic plates and installation resulted in cost savings of $ 715 in a payback period of less than 24 months.

Large Investment Recommendations

Replacement of Thermodynamic Steam Traps with Floating Ball Steam Traps. In the Sheba leather factory, thermodynamic steam traps (TDS) let out the condensate in the steam line (22). There are 6 steam traps installed in the steam pipelines for 6 machines in the skin and hide section. The Features and advantages of a floating ball steam Trap (FBS) over a TDS trap are detailed in Table 9. Therefore, using FBS instead of TDS traps, about 1.5–2% of steam that goes out along with condensate can be saved. Hence, replacing all the TDS Traps with FBS traps is recommended in a phased manner. It would yield a noticeable cost save of $ 8,900 per year with an investment of $ 2,570, giving a payback period of just 4 months.

Table 9
Features and advantages of floating ball steam trap

No	Feature	Advantages
1	Single moving part	Easy maintenance and low spare part cost
2	Easily accessible cover	In-line maintenance
3	High surface quality float	Long service life
4	Easy access to discharge orifice	Great reaction to the changes in the steam load
5	Float departs from the orifice as a rotating	Constant condensate discharge
6	Float and orifice	Not affected by back pressure
7	The orifice is well placed underwater level	No steam leakage
8	Contains thermostatic venting equipment	Quick service without steam lock
9	Built-in strainer	Prevents dirt
10	Prevents steam locking	Preferred where the steam lock is possible and increases the system efficiency

Installation of VFD to the Dust Extraction Blower. A Variable Frequency Drive (VFD) converts standards 3 ϕ Alternate Current (AC) power input at 415 V, 50 Hz into an adjusted voltage and frequency output that controls the speed of an AC motor. VFDs were designed to ensure efficiency improvements even under part loads by reducing speed. Generally, power consumption is proportional to cubic speed [$P \alpha N^3$] (Ganguly et al., 2016). In the Sheba factory, the dust extraction Induced Draft (ID) fan is installed on the skin buffing floor with a rating of 45 kW. It sucks dust from the buffed leather in the buffing machines and discharges it to the collector. There are 9 buffing machines, and one de-dusting machine operates according to the production schedule. During the study, the power consumption of this blower was observed to be 17 kW against a rated power of 45 kW. The fan's power consumption differs daily depending on the customer's requirements. It is quite obvious that this fan would be operating on a varying load (35–85%) directly influenced by the dust accumulation. Regardless of machine operation, the dust extraction fan operates continuously.

It is therefore recommended to install a VFD to this ID Fan and make it operate at a higher efficiency level by adjusting the fan power requirement according to the dust loading in the machines. An investment of about $ 2,900 may result in annual savings of approximately $ 740. This results in a payback time that is no longer than 47 months.

Installation of VFD for Fume Extraction Unit. In the hide and skin of the section to provide a good quality chemical spray over the hide and skin in both sections, the chemicals are sprayed by the Forced Draft (FD) fan over the layers of leather as well as heated by steam to a temperature of 100–110°C. These processes are carried out by spraying various pre-mixed chemicals continuously through multi-hole nozzles in the closed cabin. This results in the emission of dense fumes from the closed spray cabin. These fumes are exited from the tanks through headers provided on the sides of the cabin. A blower arrangement sucks the fumes out and lets them into the atmosphere. Since the spray process is intermittent, it was observed that fumes generation is also intermittent. However, while spraying chemicals, the blower keeps exiting the fumes to atmospheric air during non-spraying) continuously. The loading of the motor varies from 45 to 65%.

It is recommended to install a Variable Frequency Drive (VFD) for the blowers of the fume extraction units of the skin and hide spray machine. The VFD can be put in a closed loop with a pressure sensor control at a point near the hollow hood (A chemical sensor that senses the inlet of the fume can also be used). The sensor would sense the fume's presence and signal the VFD. The VFD would actuate the motor and vary the speed of the blower based on the quantum of fume emitted. Upon installation of VFD, it is anticipated that about 30% of present energy consumption can be saved. It could save nearly $ 5,400 per year with an investment of around $ 5,830. It brings to a payback period of a maximum of 13 months.

CONCLUSION

An energy conservation study was carried out in the Sheba leather factory in Mekelle in northern Ethiopia. The plant has all types of utilities and technologies at work, suggesting that it is operating fairly efficiently. However, the management still looks for avenues to reduce energy consumption to a lesser value. Hence, the management has requested the help of the Centre for Energy, Mekelle University, Ethiopia, to conduct a detailed energy audit and suggest ways to reduce energy consumption. The following are the recommendations as summarised below:

a. 19 proposals have been identified for possible energy savings
b. An energy-saving potential of about $ 29,900 / year can be realised by implementing these proposals
c. The implementation would require a one-time investment of about $15,900 to reap the benefits and be paid back in about 7 months.
d. Of the total savings identified, $14,000 can be realised without significant investment.
e. CO_2 Reduction is possible by implementing energy-saving proposals around 52.70 tons of CO_2/y

The list of conservation suggestions and their technological and economic viability are provided in Table 10.

Table 10
A summary of recommendations for energy conservation

No	Energy Saving Proposal	Investment Required ($)	Annual Savings ($)	Payback Period months
Nil Investment Proposals—4				
1	Optimisation of the operating steam pressure	Nil	370	0
2	Operating pressure reduction for screw-type air compressors	Nil	3150	0
3	Reduction of compressed air leakages in the system	Constant Maintenance	10334	0
4	Reduction of compressor air intake temperature	Negligible	140	0
	Total	**0**	**13994**	**0**
Small Investment Proposals—4				
1	Proper Insulation of Steam Lines	145	200	10
2	Proper Insulation of Hot Water Storage Tank	150	285	06

Table 10 *(Continue)*

No	Energy Saving Proposal	Investment Required ($)	Annual Savings ($)	Payback Period months
3	Utilisation of a blow gun for cleaning purposes	185	2150	01
4	Replacement of the existing cast aluminium blades with FRP blades	300	150	24
	Total	**780**	**2785**	**0.28**
Medium Investment Proposals—5				
1	Arresting of steam leakages	570	5925	01
2	Installation of temperature Indicator Cum controller (TIC) in cooling tower	430	385	14
3	Installation of automatic star-delta-star starter in the part-loaded motor	640	2090	04
4	Installation of servo stabiliser in the lighting feeder	715	2090	03
5	Waste heat recovery from the boiler flue gas	1430	715	24
	Total	**3785**	**12095**	**04**
Large Investment Proposals—3				
1	Replacement of thermodynamic steam traps with floating ball steam traps	2570	8900	04
2	Installation of VFD to the Dust Extraction Blower	2900	740	47
3	Installation of VFD for fume extraction unit	5830	5400	13
	Total	**11300**	**15040**	**09**

ACKNOWLEDGEMENTS

The authors appreciate the German Agency for International Cooperation (GIZ) for the financial support to conduct this research in the Sheba leather industry, Wukro at Tigray region, Ethiopia. Also, the authors extend their thanks to the Management of Sheba leather industry, Wukro in Tigray region for their guidance in making this Energy Assessment Assignment a success.

REFERENCES

Al-Ghandoor, A., Al-Hinti, I., Jaber, J. O., & Sawalha, S. A. (2008). Electricity consumption and associated GHG emissions of the Jordanian industrial sector: Empirical analysis and future projection. *Energy Policy*, *36*(1), 258-267. https://doi.org/10.1016/j.enpol.2007.09.020

Benhelal, E., Zahedi, G., Shamsaei, E., & Bahadori, A. (2013). Global strategies and potentials to curb CO2 emissions in cement industry. *Journal of Cleaner Production*, *51*, 142-161. https://doi.org/10.1016/j.jclepro.2012.10.049

Berry, J., Griffin, M., & Wright, A. L. (2006). *Steam pressure reduction, opportunities, and issues*. Oak Ridge National Lab. (ORNL).

Bhukya, P., & Basak, D. (2014). Energy saving technologies in industries-an overview. *International Journal of Scientific and Research Publications*, *4*(4), 499-504.

Bureau of Energy Efficiency. (2018). *Energy conservation guidelines for industries.* Bureau of Energy Efficiency.

Da Cunha, F. (2007). Compressed air: Energy efficient reference guide, CEA Technology Inc. (*CEATI*) *Customer Energy Solution Interest Group* (*CESIG*). https://natural-resources.canada.ca/sites/nrcan/files/energy/pdf/energystar/compressed-air-ref-eng.pdf

Edenhofer, O., Pichs-Madruga, R., & Sokona, Y. (Eds.). (2012). *Renewable energy sources and climate change mitigation.* Climate Change.

Fawkes, S., Oung, K., Thorpe, D., Zhu, X., & Farrell, T. C. (2016). *Best practices and case studies for industrial energy efficiency improvement: An introduction for policy makers*. UNEP DTU Partnership.

Ganguly, S., Raje, S., Kumar, S., Sartor, D., & Greenberg, S. (2016). *Accelerating energy efficiency in Indian data centers: Final report for phase I activities.* Berkeley National Laboratory.

Gebreslassie, M. G., Kalamegam, M. N., Gebrelibanos, K. G., Mebrahtu, A. H., Bahta, S. T., Nurhussien, F. F., &Yohannes, K. G. (2022). Evidence-based energy conservation potentials and policy implications in the textile and garment industries of Ethiopia. *Energy Efficiency*, *15*(6), 39. https://doi.org/10.1007/s12053-022-10047-8

IEA. (2020). *Energy technology perspectives (2020).* International Energy Agency. https://iea.blob.core.windows.net/assets/7f8aed40-89af-4348-be19 c8a67df0b9ea/Energy_Technology_Perspectives_2020_PDF.pdf

Kingston, R., & Baghzouz, Y. (1994, May 1-5). *Power factor and harmonic compensation in industrial power systems with nonlinear loads* [Paper presentation]. Proceedings of Industrial and Commercial Power Systems Conference, Irvine, Canada. https://doi.org/10.1109/ICPS.1994.303580

Mulatu, D., Habte, L., & Ahn, J. W. (2018). The cement industry in Ethiopia. *Journal of Energy Engineering*, *27*(3), 68-73. https://doi.org/10.5855/ENERGY.2018.27.3.068

Önüt, S., & Soner, S. (2007). Analysis of energy use and efficiency in Turkish manufacturing sector SMEs. *Energy Conversion and Management*, *48*(2), 384-394. https://doi.org/10.1016/j.enconman.2006.07.009

Ramakrishna, G. (2014). Energy consumption and economic growth: The Ethiopian experience. *Journal of Economic and Financial Modelling*, *2*(2), 35-47.

Rossiter, A. P., & Jones, B. P. (Eds.). (2015). *Energy management and efficiency for the process industries*. John Wiley & Sons.

Singh, P., Ansu, A. K., Sharma, R. K., Kumari, P., Kumar, A., & Kumar, R. (2023). Development, thermal properties, and reliability testing of eutectic polyethylene glycol as phase change materials for thermal energy storage applications. *International Journal of Thermophysics*, *44*(3), Article 39. https://doi.org/10.1007/s10765-022-03146-2

Sony, M., & Mekoth, N. (2018). A qualitative study on electricity energy-saving behaviour. *Management of Environmental Quality: An International Journal*, *29*(5), 961-977. https://doi.org/10.1108/MEQ-02-2018-0031

Tesema, G., & Worrell, E. (2015). Energy efficiency improvement potentials for the cement industry in Ethiopia. *Energy*, *93*(Part 2), 2042-2052. https://doi.org/10.1016/j.energy.2015.10.057

Zeitz, R. A. (Ed.). (1997). *Council of Industrial Boiler Owners (CIBO): Energy efficiency handbook.* CIBO.

Pertanika J. Sci. & Technol. 32 (S1): 55 - 68 (2024)

PERTANIKA JOURNALS

SCIENCE & TECHNOLOGY

Journal homepage: http://www.pertanika.upm.edu.my/

Energy Utilization and Production Assessment in a Cement Industry

Tsegay Gebru[1], Narayanan Kalamegam Millerjothi[2]*, Nagarajan Mohan Raj[3] and Soundararajan Seenivasan[4]

[1]Department of Mechanical Engineering, Ethiopian Institute of Technology, Mekelle University, Mekele, Po. Box No.231, Ethiopia
[2]Department of Mechanical Engineering, Sri Eshwar College of Engineering, Coimbatore - 641 202, Tamil Nadu, India
[3]Department of Mechanical Engineering, Sri Krishna College of Technology, Coimbatore - 641 042, India
[4]Department of Mechanical Engineering, Rathinam Technical Campus, Coimbatore - 641 021, India

ABSTRACT

Cement industries are one of the fastest-growing economic sectors in developing nations like Ethiopia. It provides direct and indirect employment opportunities to a huge number of persons and contributes a major part to the nation's gross domestic product. Thus, the main objective of this study was to analyze the usage of power consumption and rate of production in the particular cement industry. For this purpose, a comprehensive study was conducted in the Messebo cement factory in northern Ethiopia, one of Ethiopia's key industries, which has unlimitedly contributed to Ethiopian economic development. It was achieved through primary and secondary data from the Messebo cement factory for the last seven years and compared with an actual and designed production rate and power consumption usage value. Besides money lost, profit and efficiency were analyzed based on the values of excess power used and production rate. From the results, the average usage of actual power and rated power has been observed to be 40.43 million kWh per year and 27.72 million kWh per year, respectively. In an average of seven years, the money lost due to excess power consumption and reduced production was estimated at roughly 4.4 million birr per year and 15 million birr per year, respectively.

Keywords: Cement factory, economic analysis, efficiency, power usage, production rate

ARTICLE INFO

Article history:
Received: 27 July 2023
Accepted: 17 October 2023
Published: 19 January 2024

DOI: https://doi.org/10.47836/pjst.32.S1.04

E-mail addresses:
tsegay.gebru@mu.edu.et (Tsegay Gebru)
millerjothi@gmail.com (Narayanan Kalamegam Millerjothi)
n.mohanraj@skct.edu.in (Nagarajan Mohan Raj)
seenikct@gmail.com (Soundararajan Seenivasan)
* Corresponding author

ISSN: 0128-7680
e-ISSN: 2231-8526

INTRODUCTION

Ethiopia's cement industries have developed substantially in the past two decades. Moreover, challenges and barriers associated with the Ethiopian government's regulations and investment policy could erode these profits. A world highway reveals around 16.8 million tons of cement, an average of 10% growth in yearly consumption. Ethiopia is the topmost cement manufacturer in sub-Saharan Africa (Mulatu et al., 2018).

Energy is one of the important needs of human beings and is essential for the world's growth and will persist in developing to at least 1/3 by 2035 (Fedeler et al., 2021; Gebreslassie et al., 2022). Ethiopia is well placed to become the cement production hub of Africa because of the natural resources of surplus raw material for cement, lower labor cost, and accessibility of world market opportunity through agreement to avail free trading **(**Tesema & Worrell, 2015).

Messebo Cement Company is one of the biggest East African cement industries in the Tigray region in southern Ethiopia. Its products are used by many of the grand projects constructed by the government of Ethiopia and domestic and international contractors. In most housing development projects in the country, hydropower dams such as Tana Beles, Tis- Abay, Tekeze, Gilgel Gibe I, II & III, and heavy bridges were constructed with cement from Messebo. Even now, the supply and demand of the factory are not balanced; there has been very high demand, starting from the embellishment of the factory up to now (Messebo Cement Factory, 2015).

Cement production is performed through a series of activities, such as extraction of raw material, material preparation through ball mill, clinker burning, and cement milling and packing (Figure 1). In some cases, the raw material obtained from the resources is quite hard, and then it undergoes several stages for the dry cement process. Crushing is the first step, and the materials are broken into minute sizes that vary based on the requirements. Then, the pulverized powders are placed in kilns and dried by heating at a preferred high temperature. The dried powders are transferred to heavy ball mills and tube mills to make the finest powder.

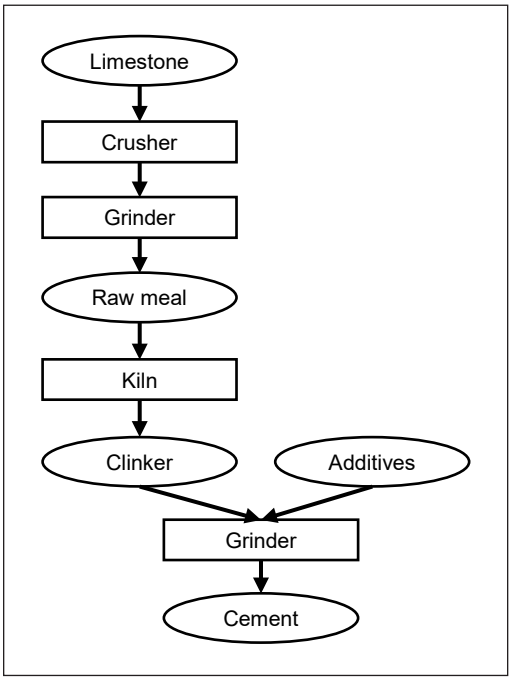

Figure 1. Process flow diagram for dry cement production

Finely dried materials are mixed in appropriate proportions mechanically or

pneumatically **(**Gomes, 1990**)**. The simplified production flow process for dry cement is shown in Figure 2.

Generally, the energy share compared to the production cost in the industries is in the range of 20 to 60% of operational costs (Galitsky & Worrell, 2008; Wang et al., 2009). It indicates that special attention is required to improve plant performance in the cement industry. As the various studies indicate, energy consumption varies with the processes involved in each part of the operation (Khajeh et al., 2014). The specific energy consumption for making powder is expected to range from 0.5 to 0.9 kWh/ton of materials (Bhatty, 2011).

Another important process is clinker production, where most of the energy is consumed, and over 90% of the total energy used by the industry is consumed. Clinker is prepared by pyro-processing in lengthy large rotary kilns consisting of up to eight meters tube diameter and laid at an angle of 3°C–4°C degrees that rotates two or three times per minute (World Business Council for Sustainable Development, 2014). The heat is required for the dry kilns at an average use of 4.7 MJ per ton of clinker. Typically, cement production is considered an energy-intensive stage process for both wet and dry, and consumption of energy accounts for 20%–40% of production cost (Hasanbeigi et al., 2012). Power consumption varies depending on the nature of the process involved. Power consumption for raw material preparation requires about 20–35 kWh /ton. Energy use for the operation of auxiliary machinery is expected to be roughly 10 kWh / ton of clinker. The process flow diagram for the cement production is shown in Figure 3.

Energy needs for grinding based on the requirement of surface area and energy required for heavy-duty ball mills may consume ranges from 32 to 37 kWh/ton (Schorcht et al., 2013; Seebach et al., 1996). Subject to high-temperature treatment, clinker is produced through a kiln, and its temperature is reduced drastically to change its properties **(**Gebreslassie et al., 2018**)**. As reported by the European Cement Research Academy (ECRA), 2009, in a dry kiln cement industry, the usage of electricity is typically broken down as follows: 38% cement grinding, 24% raw material grinding, 22% clinker formation and grinding,

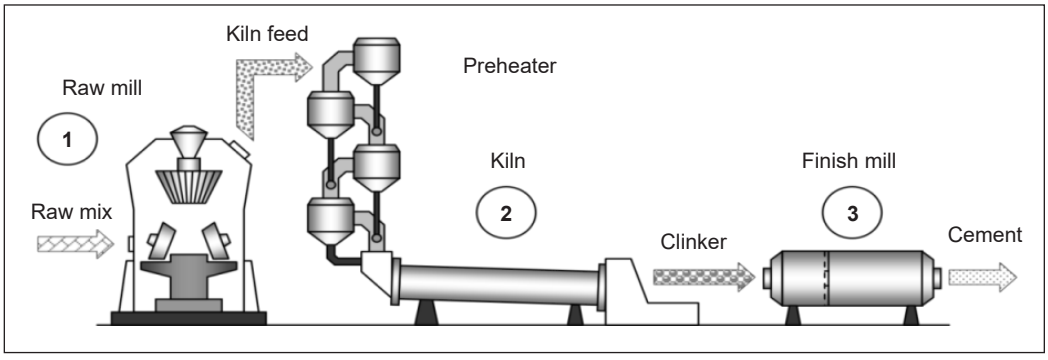

Figure 2. Simplified Schematic of the dry cement production process

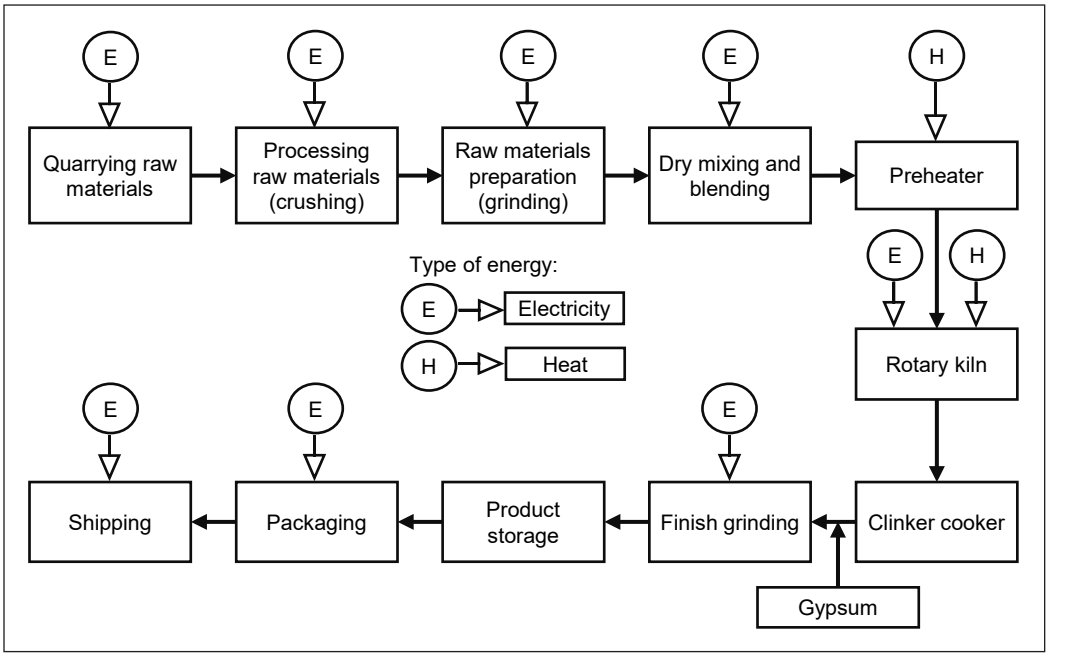

Figure 3. Process flow diagram for the cement production

6% homogenization of raw material, 5% raw material extraction and 5% for transportation and packaging (Schneider, 2017).

The objective of this article was to study the utilization of energy consumption and rate of production by considering various aspects. The energy bills and production rate were collected for the last seven consecutive years between 2012 and 2018. The expected scope of this study period would be valid up to 2024, associated with the production rate, specific energy consumption, raw material cost, and economic analysis.

MATERIALS AND METHODS

Cement production in the Messebo plant is processed through Lines 1 and 2. The performance study was carried out in Line 2, where two cement plants are operated, and each mill consists of a ball-type unit for crushing materials into minute fragments that vary in size. In this study, physical data collection, such as electricity bills, solid and liquid fuels, cement production rate, power consumption, and load factor, has been carried out. In addition to that, some of the physical measurements were taken from the machinery where major energy was consumed in the factory.

The physical measurements of actual production Pr_a (Ton/hr) for the 7 years from 2012 to 2018 were recorded from the register maintained in the company. Similarly, the actual specific power consumption, P_a (kWh/ton), for the 7 years from 2012 to 2018 was recorded from the register maintained in the log sheet.

Production and power consumption in the Messebo cement factory vary uncertain each year, and this has fluctuated year by year. However, as indicated in the technical specification, the designed rate of cement production (Pr_s) and rated energy consumption (P_s) of the plant were constant, recorded as 150 tons per hour and 33kWh per ton, respectively. The Messebo cement factory was designed to operate 8400 hours per year, and the designed production cost was found to be 356 birr per ton. Table 1 indicates the production rate and power consumption value for the Messebo plant in Line 2 (Messebo Cement Factory, 2019).

Table 1
Production rate and power consumption values of the cement plant in Line 2

Year	2012	2013	2014	2015	2016	2017	2018
Actual production Pr_a (Ton/hr)	135	77	67	98	99	120	104
Actual power consumption, P_a (kWh/ton)	46.49	52.58	57.78	52.31	45.27	41.48	47.24

Power Consumption

Generally, the specific energy consumption is expressed in kWh per ton of clinker. The excess power consumption by machinery of each process can be calculated by applying the Equations 1 and 2:

$$P_{e,i} = P_{a,i} - P_{s,i}\,\frac{kWh}{ton} \tag{1}$$

$$P_e = \sum_{i=1}^{n} P_{e,i} \quad \left(\frac{kWh}{ton}\right) \tag{2}$$

Excess power consumed during the operation of the cement mill for a specific year is calculated using two methods. One method is by multiplying an excess power per ton with an actual production rate per ton per year, and the second one is by subtracting actual power consumed per year and designing power consumption per year by applying the following relation:

$$P_{e,i}\ \frac{kWh}{year} = P_{e,i}\left(\frac{kWh}{year}\right) \times Pr_{a,i}\left(\frac{Ton}{year}\right) \quad = P_{a,i}\left(\frac{kWh}{year}\right) - P_{s,i}\left(\frac{kWh}{year}\right) \tag{3}$$

On the other hand, the actual power and designed power usage for specific years can be determined from Equations 4 and 5. A power quality analyzer measured the actual power consumption. Generally, power quality can be used to measure kW, kVAh, kWh, PF, kVARh, and Harmonics.

$$P_{a,i}\left(\frac{kWh}{year}\right) = P_{a,i}\left(\frac{kWh}{ton}\right) \times Pr_{a,i}\left(\frac{Ton}{year}\right) \tag{4}$$

$$P_{s,i}\left(\frac{kWh}{year}\right) = P_{s,i}\left(\frac{kWh}{ton}\right) \times Pr_{a,i}\left(\frac{Ton}{year}\right) \tag{5}$$

Production Rate

The production rate was synthesized and interpreted with data collected from the factory's monitor sheet. Generally, the actual production rate is different from the designed production rate of the cement mill. It is directly related to the plant efficiency of the cement factory. In order to analyze the total actual production of cement per ton per year, Equation 6 can be used (Madlool et al., 2013).

$$Pr_{a,i}\left(\frac{Ton}{year}\right) = Pr_{a,i}\left(\frac{Ton}{hr}\right) \times \left(\frac{hrs}{day}\right) \times \left(\frac{days}{year}\right) \quad (6)$$

The difference between the actual rate of production and the designed rate of production calculates the reduced production rate. The reduced production rate of cement for the specific year is determined by Equations 7 to 9 (Ayu et al., 2015):

$$Pr_{d,i} = Pr_{a,i} - Pr_{s,i}\left(\frac{Ton}{hr}\right) \quad (7)$$

$$Pr_{d} = \sum_{i=1}^{n} Pr_{d,i}\left(\frac{Ton}{hr}\right) \quad (8)$$

$$Pr_{d,i}\left(\frac{Ton}{year}\right) = Pr_{d,i}\left(\frac{Ton}{hr}\right) \times \left(\frac{hrs}{day}\right) \times \left(\frac{days}{year}\right) \quad (9)$$

Economic Analysis

Using excess power against a reduction in production rate can also be expressed in profit losses. The electricity tariff for high-voltage industries given by the Ethiopian electric power corporation is detailed in Table 2 (Messebo Cement Factory, 2019).

Table 2
Electricity tariff for high voltage industries

Particulars	Unit cost (birr/ kWh)
Equivalent flat rate	0.3904
Peak	0.4626
Off-peak	0.3544
Service charge	54.01

The total money loss of excess power consumption for the specific year can be determined by Equation 10:

$$P_{e,i}\left(\frac{birr}{year}\right) = \sum_{i=1}^{7}\left(\overbrace{P_{e,i}\left(\frac{kWh}{year}\right) \times \frac{birr}{kWh}}^{Excess\ electric\ power} + \overbrace{P_{e,i}\left(\frac{kWh}{year}\right) \times \frac{birr}{kWh}}^{for\ service\ charge}\right) \quad (10)$$

Money lost due to reduced production from the designed production rate is determined by multiplying the reduced production rate ($Pr_{d,i}$) and the expected profit per ton of the factory. Therefore, the total money lost due to the reduced production rate in all seven years is the sum lost each year, as expressed in Equation 11.

$$Pr_{d,i}\left(\frac{birr}{Year}\right) = \sum_{i=1}^{7}\left(Pr_{d,i}\left(\frac{Ton}{year}\right) \times Pr_{d,s}(\frac{birr}{Ton}\right) \quad (11)$$

Total money loss from the cement plant in Line 2 due to improper electric power usage and an effective production rate in all seven years is calculated by adding some excess energy and reduced production. The cash profit of the factory varies from year to year, depending on the variation in production rate. As we have discussed, the designed production rate was about 150 tons per hour, which amounted to 1,260,000 tons per year. The designed value of anticipated production cost was to be 356 birr per ton. So, the expected and actual profit can be obtained from Equations 12 and 13.

$$\text{Expected profit per year (birr)} = \text{Pr}_{\text{s,i}}\left(\frac{\text{Ton}}{\text{year}}\right) \times \left(356\ \frac{\text{birr}}{\text{Ton}}\right) \tag{12}$$

$$\text{Actual profit per year (birr)} = \text{Pr}_{\text{a,i}}\left(\frac{\text{Ton}}{\text{year}}\right) \times \left(356\ \frac{\text{birr}}{\text{Ton}}\right) \tag{13}$$

Plant Efficiency

Cement plant efficiency (Equation 14) is determined by the ratio of standard power usage to the actual power usage of the plant (Worrell et al., 2013).

$$\eta_{P_i} = \frac{P_{s,i}}{P_{a,i}} \tag{14}$$

Also, production rate efficiency (Equation 15) is determined by the ratio of the actual production rate to the standard production rate.

$$\eta_{Pr_i} = \frac{Pr_{a,i}}{Pr_{s,i}} \tag{15}$$

RESULTS AND DISCUSSION

The comprehensive study was conducted in the Messebo cement factory in the Tigray region in the northern part of Ethiopia, which is one of the key industries of Ethiopia. For this purpose, the last seven consecutive years between 2012 and 2018 were considered.

Power Consumption

Figure 4 shows the variation in power consumption usage for the last seven consecutive years between 2012 and 2018 and compares it with actual and designed power consumption. Generally, the efficient plant indicates that the actual power consumption should be approximately equal to the designed power consumption. Depending on the plant design system, power usage should be constant every year. It can be observed that the actual power usage was more than the rated power consumption for all seven consecutive years. From the figure, the average value of actual and rated power usage is 40.43 million kWh per year and 27.72 million kWh per year, respectively. It can also be observed that the horizontal line indicates an excess power lost during the cement plant operation, amounting to an average value of 12.71 million kWh per year.

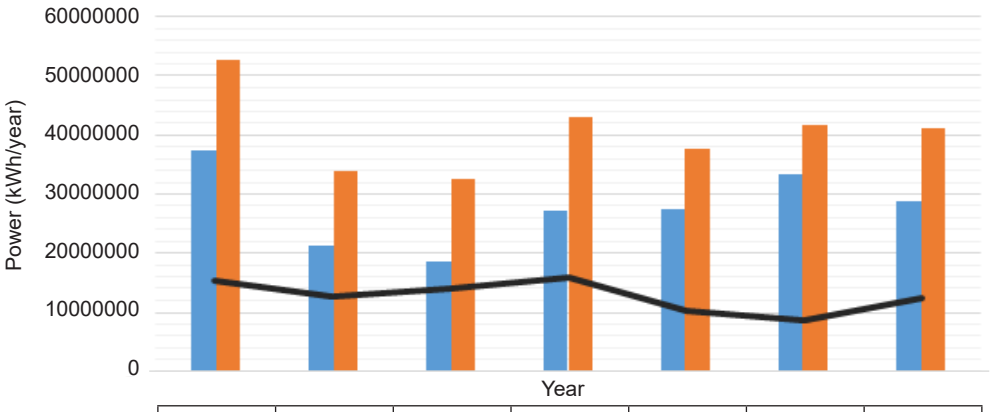

	2012	2013	2014	2015	2016	2017	2018
Ps,i	37422000	21344400	18572400	27165600	27442800	33264000	28828800
Pa,i	52719660	34008744	32518584	43061592	37646532	41811840	41268864
Pe,i	15297660	12664344	13946184	15895992	10100664	8547840	12440064

Figure 4. Power consumption details of cement plant for seven consecutive years

Production Rate

The actual and designed production rates are plotted for the last seven consecutive years (Figure 5). The designed production rate is constant, almost 150 tons per hour, equivalent to 1.2 million tons per year. The percentage shown in the vertical axis indicates the quantity of cement production related to the expected value. In 2012, the reduced production rate was almost 10%, which seems to be 90% of the designed production rate achieved by the plant. However, the actual production rate has gradually been reduced for the other six consecutive years, as shown in the figure. In 2014, the reduced production rate was almost

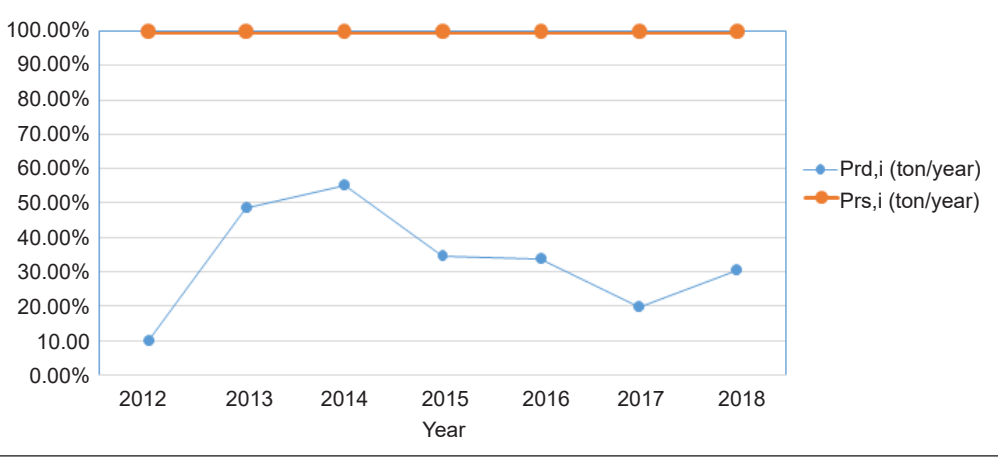

Figure 5. The production rate for seven consecutive years

56% of the designed rate, indicating that the actual production rate is 46% of the designed rate. It implies that the cement plant's performance was quite low, thereby increasing profit loss due to a lower production rate.

Money Lost

Figure 6 compares money lost between excess power and reduction in production for the last seven consecutive years. Figure 5 shows a similar trend: the money lost due to both parameters was very high in 2014. On average, in the seven years, the money lost due to excess power consumption was estimated at roughly 4.4 million birr per year, whereas in the case of reduced production rate, it was around 15 million birr per year. Hence, the money lost due to the lower production rate was 3.5 times higher than that lost due to excess power usage.

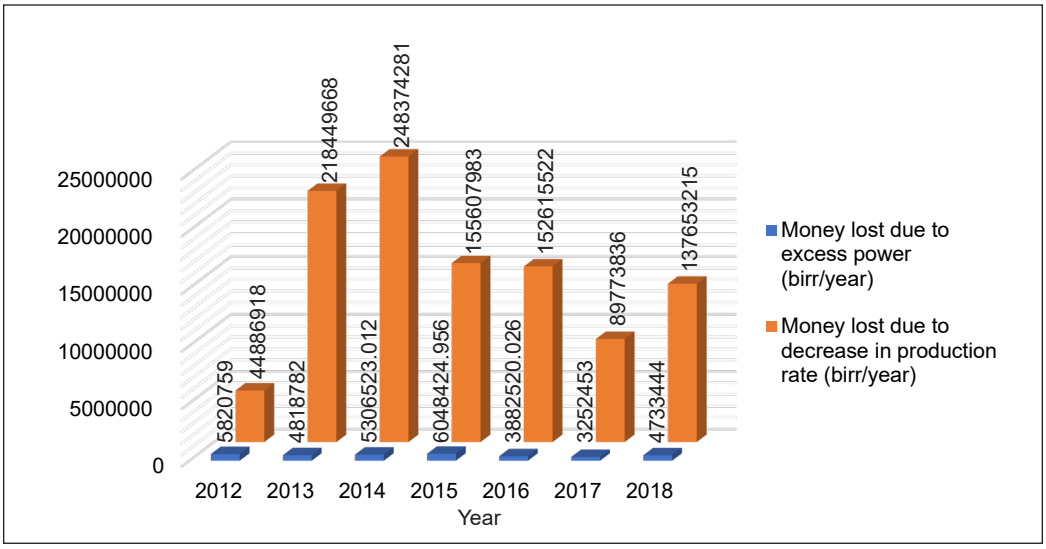

Figure 6. Variation of money lost for seven consecutive years

Profit Analysis

Figure 7 portrays the expected profit, actual profit, and money lost every seven consecutive years for the Messebo plant. The factory's cash profit depends on the cement factory's performance and may be affected by other factors. The expected profit is always constant at about 0.44 million birr per year, but the actual profit is always less than the expected profit, and it varies from year to year, as shown in the chart. On average, the actual profit was calculated to be around 0.29 million birr per year, whereas in the case of money lost, it was estimated to be 0.15 million birr per year. The maximum reduction in actual profit is observed to be about 33.3% compared to that of expected profit.

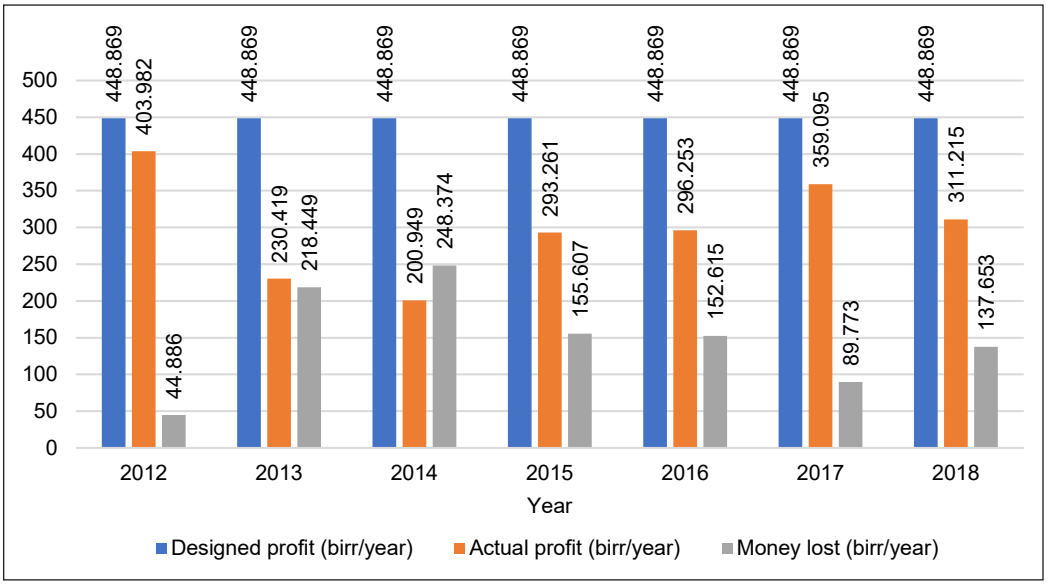

Figure 7. Profit description chart for seven consecutive years

Efficiency Analysis

Figure 8 represents the power usage and production rate efficiency for the last seven consecutive years. The rated specific power consumption was recorded as 33 kWh per ton, as taken from the Messebo plant manual. Power usage is the ratio of actual power usage to designed power usage. Similarly, production efficiency describes the ratio of the actual production rate to the designed production rate. In 2012, there was a significant improvement of about 90% compared with other consecutive years, whereas p usage was

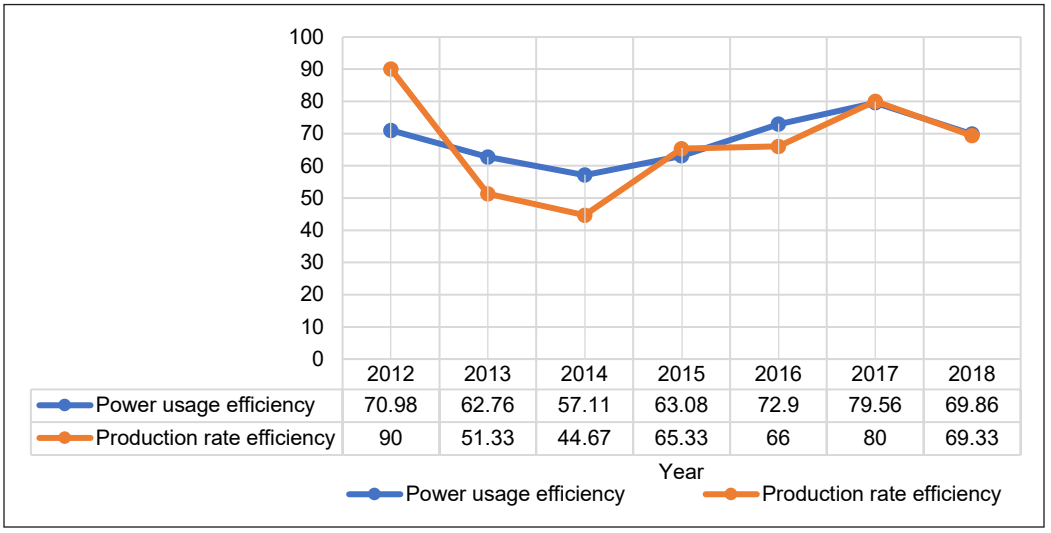

Figure 8. Power usage and production rate efficiency of cement factory

less than 0%. In 2014, there was a substantial reduction in production rate and power usage, about 45% and 57%, respectively.

CONCLUSION

Messebo cement factory has two production lines: Lines 1 and 2. However, in Line 2, there are two cement plants in operation condition, and this analysis was carried out for one mill only. Since both mills have been designed similarly, the power usage and production rate should be the same. This study evaluates the last seven successive years of the actual and designed value of production rate and power consumption usage. Some of the significant conclusions and the results of the present investigations are presented below:

- As we have seen in the power consumption analysis part, the average value of actual and rated power usage in the cement plant is 40.43 million kWh per year and 27.72 million kWh per year, respectively.
- The utilization of power consumption was less, around 32%, compared to rated power usage. It can be increased by proper scheduling to minimize the maintenance period.
- Money lost due to excess power consumption was estimated at roughly 4.4 million birr per year due to improper use of power in the plant. However, on the other side, a reduction in the production rate was determined to be around 15 million birr per year, 3.5 times higher than the money lost due to excess power usage.
- The actual profit was around 0.29 million birr per year, whereas in the case of money lost, it was estimated at 0.15 million birr per year.
- A significant improvement of about 90% can be seen in 2012, and for power usage, it is found to be less than 70%. There is a substantial reduction in production rate and power usage, about 45% and 57%, respectively.
- In 2014, the production rate was drastically reduced by almost 56%. It may be due to more showdowns happening in the plant. In order to improve the production rate, periodic maintenance shall be carried out in Lines 1 and 2.

ACKNOWLEDGEMENT

The authors acknowledged Mr. Gebrehiwet Gebremedhin, who was heading the center of excellence in the Messebo cement factory, permitted the research and supported us in using the facilities throughout the study period.

REFERENCES

Ayu, T. T., Hailu, M. H., Hagos, F. Y., & Atnaw, S. M. (2015). Energy audit and waste heat recovery system design for a cement rotary kiln in Ethiopia: A case study. *International Journal of Automotive and Mechanical Engineering, 12*, 2983-3002. https://doi.org/10.15282/ijame.12.2015.14.0249

Bhatty, J. I., Miller, F. M., & Bohan, R. P. (2011). *Innovations in Portland cement manufacturing* (2nd ed.). Portland cement Association.

Fedeler, K. (2021). *Reshaped rivers, ruins, and Renaissance: the politics of hydro-developmentalism in the case of Tana-Beles, Ethiopia* [Doctoral dissertation, The University of Edinburgh]. The University of Edinburgh. http://dx.doi.org/10.7488/era/1756

Galitsky, C., & Worrell, E. (2008). *Energy efficiency improvement and cost saving opportunities for the vehicle assembly industry: An energy star guide for energy and plant managers (No. LBNL-50939-Revision).* Lawrence Berkeley National Lab. (LBNL). https://doi.org/10.2172/927881

Gebreslassie, M. G., Gebrelibanos, K. G., & Belay, S. (2018). Energy consumption and saving potential in cement factory: thermal energy auditing. *AFRREV STECH: An International Journal of Science and Technology*, *7*(2), 92-106. https://doi.org/10.4314/stech.v7i2.9

Gebreslassie, M. G., Kalamegam, M. N., Gebrelibanos, K. G., Mebrahtu, A. H., Bahta, S. T., Nurhussien, F. F., & Yohannes, K. G. (2022). Evidence-based energy conservation potentials and policy implications in the textile and garment industries of Ethiopia. *Energy Efficiency*, *15*(6), 39. https://doi.org/10.1007/s12053-022-10047-8

Gomes, A. S. (1990). Energy saving and environmental impact in the cement industry. In J. Sirchis (Ed.) *Energy efficiency in the cement industry* (pp. 16-19). Elsevier Applied Science.

Hasanbeigi, A., Lu, H., Williams, C., & Price, L. (2012). *International best practices for pre-processing and co-processing municipal solid waste and sewage sludge in the cement industry* (Report No. LBNL-5581E). Lawrence Berkeley National Laboratory (LBNL). https://doi.org/10.2172/1213537

Khajeh, M. G., Iranmanesh, M., & Keynia, F. (2014). Energy auditing in cement industry: A case study. *Energy Equipment and Systems*, *2*(2), 171-184. https://doi.org/10.22059/EES.2014.9894

Madlool, N. A., Saidur, R., Rahim, N. A., & Kamalisarvestani, M. (2013). An overview of energy savings measures for cement industries. *Renewable and Sustainable Energy Reviews, 19*, 18–29. https://doi.org/10.1016/j.rser.2012.10.046

Messebo Cement Factory. (2015). *Manual for operation and maintenance: Mekelle, Ethiopia Messebo.* Messebo Cement Factory.

Messebo Cement Factory. (2019). *Annual performance report: Mekelle, Ethiopia.* Messebo Cement Factory.

Mulatu, D., Habte, L., & Ahn, J. W. (2018). The cement industry in Ethiopia. *Journal of Energy Engineering*, *27*(3), 68-73. https://doi.org/10.5855/ENERGY.2018.27.3.068

Schneider, M. (2017). Development of State of the Art-Techniques in Cement Manufacturing:

Trying to Look Ahead (ECRA), Revision 2017, WBCSD, Maison de la Paix, Chemin Eugène-Rigot 2B CP 2075, 1211 Geneva 1, Switzerland.

Schorcht, F., Kourt, I., Scalet, B. M., Roudier, S., & Sancho, L. D. (2013). *Best available techniques (BAT) reference document for the production of cement, lime and magnesium oxide: Industrial emissions directive 2010/75/eu integrated pollution prevention and control*. European Commission. https://eippcb.jrc.ec.europa.eu/sites/default/files/2019-11/CLM_Published_def_0.pdf

Seebach, V. H. M., Neumann, E., & Lohnherr, L. (1996). State-of-the-art of energy-efficient grinding systems. *ZKG international*, *49*(2), 62-67.

Tesema, G., & Worrell, E. (2015). Energy efficiency improvement potentials for the cement industry in Ethiopia. *Energy*, *93*(Part 2), 2042-2052. https://doi.org/10.1016/j.energy.2015.10.057

Trying to Look Ahead (ECRA), Revision 2017, WBCSD, Maison de la Paix, Chemin Eugène-Rigot 2B CP 2075, 1211 Geneva 1, Switzerland, https://ecra online.org/fileadmin/redaktion/files/pdf/CSI_ECRA_Technology_Papers_2017.pdf

Wang, J., Dai, Y., & Gao, L. (2009). Exergy analyses and parametric optimizations for different cogeneration power plants in cement industry. *Applied Energy*, *86*(6), 941-948. https://doi.org/10.1016/j.apenergy.2008.09.001

World Business Council for Sustainable Development. (2014). *Guidelines for co-processing fuels and raw materials in cement manufacturing*. World Business Council for Sustainable Development. https://docs.wbcsd.org/2015/10/CSI_Co-Processing_Fuels_and_Raw_Materials.pdf

Worrell, E., Kermeli, K., & Galitsky, C. (2013). *Energy efficiency improvement and cost saving opportunities for cement making an ENERGY STAR®Guide for energy and plant managers* (Report No. 430-R-13-009). EPA-United States Environmental Protection Agency. https://dspace.library.uu.nl/handle/1874/321366

Nomenclature

P_a	actual power consumed
P_e	excess power consumed
P_s	designed power consumption
Pr_a	actual production rate
Pr_d	reduced production rate
Pr_s	designed production rate
$ɳp$	power usage efficiency
$ɳpr$	production rate efficiency
i	indicates for specific year
n	total number of year

Pertanika J. Sci. & Technol. 32 (S1): 69 - 92 (2024)

PERTANIKA JOURNALS

SCIENCE & TECHNOLOGY

Journal homepage: http://www.pertanika.upm.edu.my/

Solar Energy Prediction Based on Intelligent Predictive Controller Algorithm

Linnet Jaya Savarimuthu[1], Kirubakaran Victor[1]*, Preethi Davaraj[2], Ganeshan Pushpanathan[3], Raja Kandasamy[4], Ramshankar Pushpanathan[5], Mohanavel Vinayagam[6], Sachuthananthan Barathy[7] and Vivek Sivakumar[8]

[1]Centre for Rural Energy, The Gandhigram Rural Institute - Deemed to be University, Gandhigram - 624302, Tamil Nadu, India

[2]Department of Computer Science and Engineering, PSNA College of Engineering & Technology, Dindigul -624622, Tamil Nadu, India

[3]Department of Mechanical Engineering, Sri Eshwar College of Engineering, Coimbatore - 641202, Tamil Nadu, India

[4]Department of Mechanical Engineering, Anna University Regional Campus - Coimbatore, Coimbatore - 641046, Tamil Nadu, India

[5]Department of Civil Engineering, College of Engineering Guindy, Anna University, Chennai – 600 025, Tamil Nadu, India

[6]Centre for Materials Engineering and Regenerative Medicine, Bharath Institute of Higher Education and Research, Chennai, 600073, Tamil Nadu, India

[7]Department of Mechanical Engineering, Sree Vidyanikethan Engineering College, Tirupati - 517102, Andhra Pradesh, India

[8]Department of Civil Engineering, GMR Institute of Technology, Razam, Andra Pradesh - 532127, India

ABSTRACT

The technological advancement in all countries leads to massive energy demand. The energy trading companies struggle daily to meet their customers' power demands. For a good quality, disturbance-free, and reliable power supply, one must balance electricity generation and consumption at the grid level. There is a profound change in distribution networks due to the intervention of renewable energy generation and grid interactions. Renewable energy sources like solar and wind depend on environmental factors and are subject to unpredictable variations. Earlier, energy distribution companies faced a significant challenge in demand forecasting since it is often unpredictable. With the prediction of the ever-varying power from renewable sources, the power

ARTICLE INFO

Article history:
Received: 27 July 2023
Accepted: 17 October 2023
Published: 19 January 2024

DOI: https://doi.org/10.47836/pjst.32.S1.05

E-mail addresses:
linnetjaya@gmail.com (Linnet Jaya Savarimuthu)
kirbakaran@yahoo.com (Kirubakaran Victor)
dmdpreeth@gmail.com (Preethi Davaraj)
ganeshan.p@sece.ac.in (Ganeshan Pushpanathan)
rajagce@gmail.com (Raja Kandasamy)
ramshankar1991@gmail.com (Ramshankar Pushpanathan)
mohanavel2k16@gmail.com (Mohanavel Vinayagam)
bsachu7@yahoo.co.in (Sachuthananthan Barathy)
1717vivek@gmail.com (Vivek Sivakumar)
* Corresponding author

ISSN: 0128-7680
e-ISSN: 2231-8526

generation and distribution agencies are facing a challenge in supply-side predictions. Several forecasting techniques have evolved, and machine learning techniques like the model predictive controller are suitable for arduous tasks like predicting weather-dependent power generation in advance. This paper employs a Model Predictive Controller (MPC) to predict the solar array's power. The proposed method also includes a system identification algorithm, which helps acquire, format, validate, and identify the pattern based on the raw data obtained from a PV system. Autocorrelation and cross-correlation value between input and predicted output 0.02 and 0.15. The model predictive controller helps to recognize the future response of the corresponding PV plant over a specific prediction horizon. The error variation of the predicted values from the actual values for the proposed system is 0.8. The performance analysis of the developed model is compared with the former existing techniques, and the role and aptness of the proposed system in smart grid digitization is also discussed.

Keywords: Energy demand, future response, model predictive control, performance analysis, prediction, renewable energy, smart grid, system identification

INTRODUCTION

The growing awareness of green energy is moving the global power sector towards renewables. The variability in renewable-based power generation with respect to time needs to be predicted in advance to plan the power distribution properly. This universal transformation headed for renewable energy sources (RES) has motivated the progress of photovoltaic (PV) panels. As per the prediction by (Khalil, 1981), the opportunities for solar photovoltaic applications are growing exponentially. For instance, the production costs of generating electricity from solar PV panels have dropped drastically, but the energy conversion efficiency is increasing. In particular, between 2010 and 2017, the electricity cost of large-scale PV panels decreased by 73%, as described by (IRENA, 2018). The industries also seek carbon-neutral energy purchase plans (Jin et al., 2018). The increasing efficiency and decreasing cost have made PV panels a competitive alternative for non-renewable energy sources in many countries (Andrade & Bessa, 2017). Energy footprints have become essential in manufacturing systems (Jeon et al., 2015).

The energy output from the PV panel ultimately depends on weather conditions like cloud envelopes and solar radiation. It makes the energy output produced by the PV panels unpredictable and uneven (Suresh et al., 2013). So, forecasting the power output of solar power plants has become crucial for energy traders, who get attracted to long-time horizons, typically day-ahead forecasting, since most electric power is traded on the day-ahead marketplace (Marimuthu & Kirubakaran, 2014). As a result, the profitability of these operations depends on the capability of forecasting the fluctuated solar PV panel

energy output precisely. Though the demand for accurate and well-organized solar PV panel output power prediction is evident, the consequence is far from trivial. There are many technical hitches in the existing research. One apparent trouble is the inherited deviation of weather, making accurate weather forecasting challenging (Sassi & Oulamara, 2017). Many technologies are available for forecasting, including mathematical calculations based on weather data, artificial intelligence-based techniques, and a combination of both methods (Gopinath et al., 2014). This paper has attempted to employ a controller to predict power output. The primary objectives of this paper are to design an intelligent predictive control technique for solar power generators and simulate and conduct performance analysis for the same.

Literature Review

Power forecasting has become a crucial component of the electricity sector. It helps load scheduling, electricity price-fixing, and other related decision-making processes. Solar energy, a predominant source in tropical countries like India, is of more importance. Hence, the time ahead prediction is very vital. This process of prediction can be done either directly or indirectly. The direct method involves systems that predict the power for a given solar thermal or photovoltaic system (Accenture, 2016). The indirect process involves predicting solar irradiance or insolation, which is the necessary input to the power generating systems (Khosravi et al., 2018; Ozoegwu, 2019; Zendehboudi et al., 2018). These systems predict the global horizontal irradiance and diffuse horizontal irradiance falling on the earth at a particulate latitude and longitude (Guermoui et al., 2018). The electrical power can be predicted based on the pre-predicted solar irradiance.

Also, the parameters involved in power prediction for solar thermal-based power generation systems differ from those of the photovoltaic system (Prabhu et al., 2015). In a solar thermal system, heat is of prime importance because the system generates heat from sunlight, which is then applied to the heat engine to generate power (Rodat et al., 2016). Whereas in photovoltaic-based power generation, sunlight is directly converted into electricity. Different methods are in practice to predict the output power of a solar photovoltaic system, and they can be classified as numerical methods based on regression, correlation, and other mathematical calculations, intelligent methods like neural networks, fuzzy logic, model predictive controller, and hybrid methods which are the combination of the two mentioned above (Moon & Park, 2014).

Firstly, the numerical calculation methods are found to be in use widely. The regression-based systems use the relationship between atmospheric parameters like weather, temperature, irradiance, and output power to manipulate the prediction (Kuhe et al., 2021). Multiple linear regression is applied to predict power by fitting the variables into the linear equation derived from the historical data (Abuella & Chowdhury, 2015). Wavelet transform

is a mathematical function that analyzes time series categorization and pattern recognition in machine learning. It significantly impacts solving the non-linearity of solar photovoltaic systems and predicts the output power based on time series analysis (Mandal et al., 2012).

Secondly, intelligent systems are emerging at a rapid pace due to the advantages they offer. Artificial neural networks simulate the functions of the human brain to perform a task. ANN-based prediction models work by studying the input-output relationship (Zafarani et al., 2018). The network automatically adjusts its weights and biases in line with the input and output parameter relationships. This method involves a vast amount of historical statistics for better training the network. They can be designed efficiently in MATLAB through codes or built-in applications (Ehsan et al., 2014; Mandal et al., 2012). Fuzzy logic-based prediction works on IF-THEN rules designed by manipulating how the system works (Ncane & Saha, 2019). The system requires translating the input variables into fuzzy, understandable form and retranslating the output again. So, the power prediction in this model needed precise rule database design (Chugh et al., 2015).

Thirdly, the models can be combined to fit the needs of the required system. Hybrid models used for solar power prediction combine one or more methods or technology to do the task (Das et al., 2023). The combination can be intelligent—hybrid or numerical intelligent hybrid (Aliberti et al., 2018). The first case of combining two or more intelligent techniques is discussed below. The artificial neuro-fuzzy inference system groups artificial neural networks and fuzzy controllers (Raja et al., 2023). In this hybrid, the artificial neural networks determine the fuzzy controller's rules, making the design process less complicated. The forecasting system with ANFIS has combined advantages of both Artificial Neural Networks (ANN) and fuzzy logic (Frei, 2008).

However, the Adaptive Network-based Fuzzy Inference System (ANFIS) can be integrated with previous soft computing techniques such as particle swarm optimization or genetic algorithm for forecasting (Guermoui et al., 2018). The particle swarm optimization method is a population-based optimization algorithm stimulated by nature. It works by computing the movement of particles in a given space at a time and velocity (Yadav et al., 2019b). A genetic algorithm is an evolutionary algorithm that produces or determines high-quality outputs and works like human gene selection strategies like selection, mutation, and crossover (Padmanathan et al., 2019). This technology can be combined with ANFIS predictors to optimize the data sets for ANFIS training (Yadav et al., 2019a). Also, the three techniques can be combined for predicting solar photovoltaic power (Semero et al., 2018).

The numerical-intelligent hybrids are the one that combines one or more mathematical and intelligent techniques for task completion. A Binary Genetic Algorithm (GA) through the Gaussian process regression model-based suitability function can also determine a predictor's high-impact input parameters (Kenning, 2016). An integrated hybrid methodology uniting Particle Swarm Optimization (PSO) and GA can optimize an

ANFIS and will contribute more towards the performance enhancement of the predictor (Viswavandya & Mohanty, 2018).

Another numerical-intelligent hybrid forecasting model connects the wavelet transform (WT), adaptive neuro-fuzzy inference system (ANFIS), and also with hybrid firefly and particle swarm optimization algorithm (HFPSO) (Abdullah et al., 2019; Karan, 2019; Lund et al., 2019; Taki et al., 2019), where the wavelet transform reduces noise in both the meteorological and solar power data. ANFIS is the predictor, whereas the HFPSO is the combination of the firefly (FF) and particle swarm optimization (PSO) algorithm, which is engaged in optimizing the input parameters of the ANFIS to enhance the accuracy (Oldewurtel et al., 2012). Season-based models with self-evolving algorithms can be designed by integrating evolutionary seasonal decomposition least-square support vector regression (ESDLS-SVR) (Lin & Pai, 2016). This method combines three technologies: empirical mode decomposition, least square method, and support vector machine. Empirical Mode Decomposition (EMD) processes non-linear series through time-space analysis, and the support vector machine is a discriminative classifier trained by the supervised learning process (Vinayagar et al., 2022).

Finally, this paper proposes a solar output power predictor based on model predictive controllers. Model predictive controllers are widely employed because it is an optimization-based strategy that identifies the control inputs that affect the outputs over a given time frame (Mikhaylidi et al., 2015). The forecasts can be obtained by applying the Model Predictive Controller (MPC) to the solar photovoltaic system (Arnold & Andersson, 2011). The MPCs are extensively employed to control predicted energy demand and supply in-home and micro-grid management systems (Hernández-hernández et al., 2017). A receding horizon MPC Scheme solves the comfort tracking problem by considering solar outputs and thermal inertia as a second-order state-space model designed for a generic building studied and employed in Spain (Enríquez et al., 2016). The other applications of MPCs in the Energy Management System (EMS) include optimal operation schemes, forecasting, cost minimization, and energy optimization (Lee et al., 2018). MPC-enabled EMSs can help in optimal scheduling for end-user smart appliances, heating or cooling devices, local power generation devices for residential needs, weather-dependent generation and demand forecasts, electric pricing, and technical and operative constraints (Parisio et al., 2015). Unlike the methods discussed above, The papers aim to simplify the predictor design and establish an input-output relationship-based prediction model. The comparison of different strategies employed and their findings are reported in Table 1.

Role of Forecasting in Digitization of Smart Grid. Society today depends on a wide range of digital technologies that consume more power. So, the heavily industrialized nations accommodate renewable energy to meet the growing power needs, infrastructure security,

Table 1
The comparison of different methods employed and their findings

Reference	Method	Findings
Yadav et al., 2019b	PSO ANFIS	PSO is employed to optimize the parameters and rules for ANFIS
Ehsan et al., 2014	ANN	ANN is trained with the back-propagation algorithm.
Semero et al., 2018	GA- PSO-ANFIS	The design involves three soft computing techniques, adding to the computational complexity.
Viswavandya and Mohanty, 2018	Fuzzy Logic & ANFIS	Fuzzy shows better performance than ANN in the case proposed.
Abdullah et al., 2019	HFPSO – WT ANFIS	The HFPSO is used to optimize the training data, and the WT is availed to optimize the ANFIS parameters.
Chugh et al., 2015	Fuzzy Logic	The predictive system has less design complexity and better performance.
Yadav et al., 2019b	PSO -ANFIS	Particle swarm optimization is applied to optimize the performance of ANFIS.
Abuella and Chowdhury, 2015	MLRA	Multiple linear regression analysis involves complex calculations, and the performance is low compared to intelligent techniques.
Mandal et al., 2012	WT-BPNN & WT-RBFNN	Two ANN-based models are compared, and the wavelet transform is used for data set optimization.
Ncane and Saha, 2019	Fuzzy & ANN	Fuzzy logic and neural network-based models are compared.
Yadav et al., 2019a	GA-ANFIS	A genetic algorithm is used to enhance the performance of the ANFIS predictor.
Lin and Pai 2016	ESDLS-SVR	The method evolves according to seasonal variations and performs better in forthcoming years.

and balancing climate problems. However, this integration process has more challenges in the control paradigm of the grid and transmission activities (Yaniktepe et al., 2017). It demands a robust and automated grid technology with a bidirectional flow of electricity and information. Many countries are on the verge of modernizing their existing grids into smart grids and deploying micro-grids for decentralized power generation and distribution (Taticchi et al., 2015). The need of the hour requires a sound policy for deploying smart grids. These policies shall include regulations for power generation and finance models, such as regulatory targets, and address the data requirements, renewable energy credits, and different interconnection tariffs and utility subsidies (Brown & Zhou, 2013; NEP, 2017).

The smart grid is an ‘‘electricity network that can intelligently include the behavior and actions of all consumers connected to it—generators, customers and those that do both—that efficiently distribute sustainable, economical and secure electricity supplies’’ stated by the European Union for smart grids (India Smart Grid Forum, 2019). Customers are the active players in an electricity system, and forecasting the power generation can help them contribute more towards power savings and peak demands (Vassiliadis, 2000).

Hybridizing renewable energy and energy storage facilities with an existing grid would boost the grid's potential, but control strategies are required (Vigneshwari et al., 2016). The above data includes the forecasted data, which is highly crucial for developing state-of-the-art energy management systems.

The role played by different countries in digitizing the energy sector was reported in 2017. According to it, the USA prefers policies based on environmental implications; China focuses on strengthening policies on the supply side. European Union aims to install smart meters in 80% of houses by 2020, while Japan strives to reduce GHG emissions by 30% by 2030. In contrast, Denmark has demonstrated the advantages of a smart grid for the country's prosperity (Zame et al., 2018).

An extensive study on the Indian perspective of solar photovoltaic (PV) systems has been done to find the acceptability of solar PV systems among the citizens of the nation and the hurdles in retrofitting new energy technologies in the country (Padmanathan et al., 2019). The smart grid within the Indian context and the factors influencing the micro-grid costs, such as distributed generation assets, grid automation, micro-grid optimization software, development and installation charges, and energy storage, were discussed by Kumari (2017). The author also suggests that microgrids will help in decreasing power costs. India's first micro-grid was at UpariBabhan, Rajasthan, with a generation capacity 15.78kW and consumption rates of 10.43kW (Gupta, 2018). The industries to deploy microgrids in the next five years based on Zpryme and IEEE surveys are given in Table 2.

Different Smart grid topologies are discussed by Singh et al. (2015), which include radial grid, mesh grid, and ring grid. The authors have also presented a smart micro-grid model with 300W to 1 KW SPVS, an intellectual bidirectional converter turn out Sinusoidal Pulse Width Modulation (SPWM) AC power of 230 Volt, 50 Hz, and 1800Wh battery storage unit which depicts power savings up to 50% or more. Lampropoulos et al. (2010) discuss how load and generation forecasting could help develop small, decentralized power generation units through data availability, defining user groups, and data process.

Table 2
The industries to deploy micro-grids in the next five years based on Zpryme and IEEE survey

Industry	Possibility
Health Care	44%
Military	43%
Government (non-military)	40%
Utilities	39%
Manufacturing	37%
Residential	34%
Agriculture	31%
Education	27%
Transportation	23%
Mining	19%
Construction	14%
Retail	11%
Other	4%

Forecasting is now becoming a mandatory power management component as the grids are digitized. It is evident that smart grids make power management easy, transparent, hassle-free, and economical

(Sivaneasan et al., 2017). These advantages of the smart grids can be made possible only with the forecast data of the power generation units. Hence, energy forecasting contributes more towards the electricity value chain presumably. Though numerous technologies are available for power forecasting, not all technologies always hold good for all grids (Ramachandra et al., 2005). The model predictive controller discussed here has a good adaptability range and can be reprogrammed easily for different grid specifications at low computation cost and complexity. Hence, this work applies it to forecasting the solar photovoltaic power generation.

MATERIALS AND METHODS

The day ahead forecast model reported in this research is designed for a 1 kW grid-connected solar power plant at Gandhigram Rural Institute (Latitude: 10.277565^{o}, Longitude: 77.936200^{o}), an educational institute in India. The 1 KW plant is designed with 4 Rene Sola JC255m-24/Bb modules connected in series with a conversion efficiency of 15.7% and an area of 6.1 m^2. The system data acquisition has been done by ZeverCom acquisition systems and stored in the cloud.

Solar energy prediction is becoming a significant problem in the framework of renewable energy sources (RES), so Machine Learning Algorithms are employed more for this process. This paper proposed a consequential methodology based on machine learning algorithms to accomplish realistic and perfect results, which includes system identification and model predictive control techniques. The block diagram of the proposed system is represented in Figure 1.

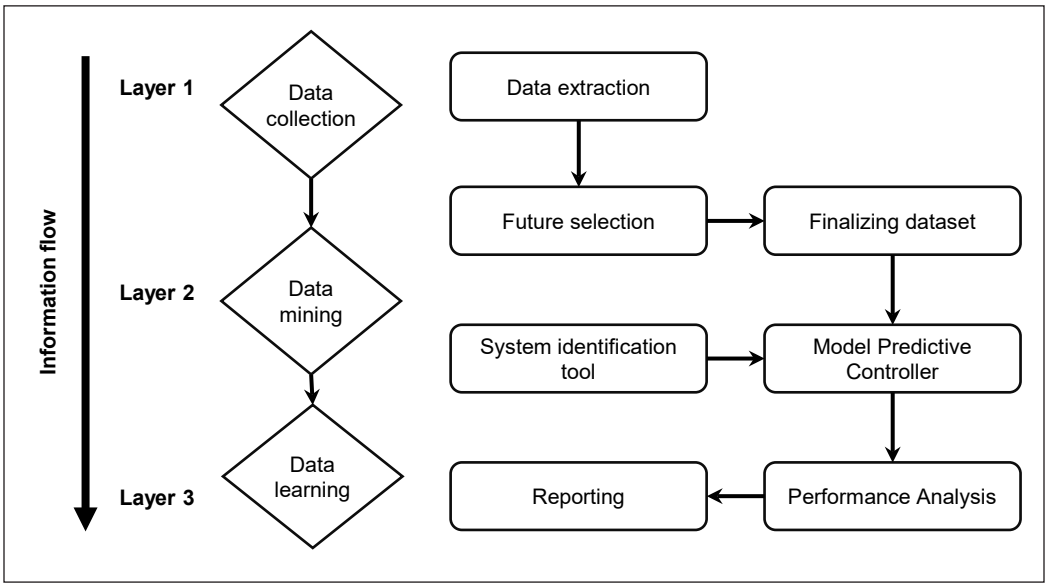

Figure 1. Block diagram of the proposed system

The first step in the process is data collection, which includes recording the raw weather data and the power production at the Gandhigram Rural Institute (GRI) 1 kW grid-connected solar power plant to get significant numeric values. The power data is predicted from the weather data. The second step in the process is data mining. The collected data is processed to fix redundancy errors missing data issues, and remove outcasts. It performs correlation analysis among the weather features and the energy output to get rid of hopeless features.

The third step is to apply the data to the MPC controller. The MPC Controller predicts and analyses the performances of the proposed system with the aid of soft computing algorithms. The system identification tool and model predictive controller (MPC) approach are used to recognize the pattern of collected data and envisage future potential and fluctuations. Hence, the specific features are imported as the input source for MPC, which is to be adjusted and controlled for solar radiation prediction problems.

The final step is to analyze the performance of the designed MPC controller. A steady-state error evaluation determines the performance of the proposed system. The steady-state error is the deviation of the control system's output from the input response in the limit while time goes to infinity (i.e.) once the response has reached a steady state. The steady-state error for the proposed control system is given by Equation 1 (Ramedani et al., 2013).

$$E(\infty) = \lim_{s \to 0} s\, E(s) = \lim_{s \to 0} \frac{s\, R(s)}{1 + G(s)} \quad (1)$$

Where R(s) is the Laplace transform of the reference input signal, E(s) is the error signal, G(s) is the plant of the system, and Y(s) is the Laplace transform of the output signal.

PROPOSED PREDICTION METHOD

System Identification Algorithm

Identifying a system is required to obtain corrective measures to improve the overall system performance. System identification is an approach that provides valuable techniques for analyzing the system properties, performing simulations, understanding the experimental phenomena (machine learning process), predicting events in the future (time series analysis), and obtaining a system model of signal in filter design (signal processing techniques). The ultimate purpose of the system identification process is to build a UPA model from a system's offered input and output data.

Therefore, the procedure is to pick a particular input u, apply it to the system, and then measure the system response y. From this input/output data (u and y), a model, a differential/difference equation, or transfer functions can be obtained. A transfer function correlates a control system's input and output signal for all possible input values. The second-order transfer functions are commonly used in convention for a dynamic system to exhibit oscillations and are usually represented as Equation 2 (Liu et al., 2018).

$$G(s) = \frac{b_0}{s^2 + a_1 s + a_0} \quad (2)$$

where G(s) is the transfer function of the system.

Also, the transfer function obtained from the real-time data utilized for the design of the solar power predictor is given by Equation 3.

$$G(s) = \frac{0.5495\, s^2 + 1.8\, s + 5.766}{s^3 + 2.078\, s^2 + 11.31\, s + 7.769} \quad (3)$$

This transfer function was obtained from physical modeling and data collection. The data from the controller was taken as an output, and the input was taken from the panel simulation. In a modeling task, the following steps are employed in sequence: (1) collection of prior information of the system, (2) selection of the model set and model structure, (3) experimental design and collection of data, and (4) model parameter estimation and model validation process. The phases of the system identification procedure are shown in Figure 2.

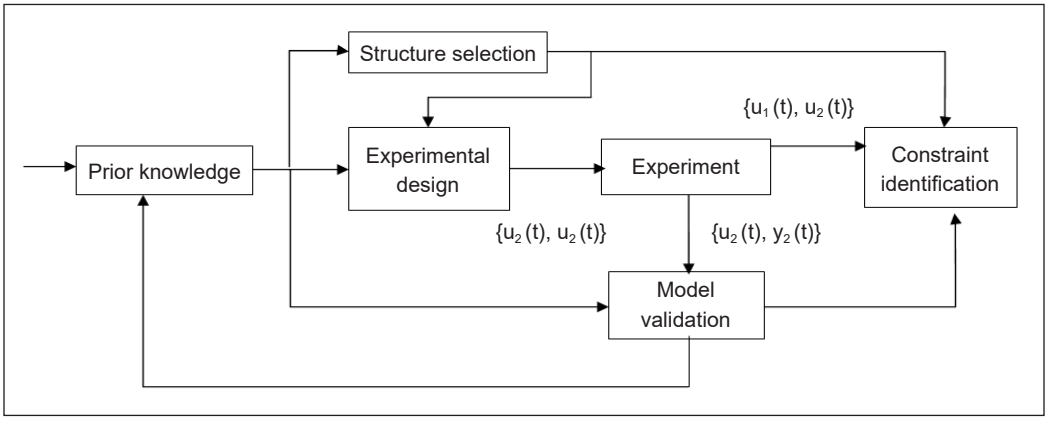

Figure 2. Stages of the system identification procedure

Model Predictive Control (MPC)

A model of process control is available to predict the future progress of the system for optimization of the control signal. The main aim of the MPC is to develop a model of the process to forecast the future response of the system as well as to compute control actions if necessary. The control objective is correlated with an error function based on the deviation between the desired and the actual responses. This objective function is called the cost function J, and the optimal control action is established while minimizing the cost function within the optimization window (Kazem et al., 2016). The MPC structure is shown in Figure 3.

In MPC, future values from the output variables are predicted based on a dynamic model of the system process and with the current measurements. In order to minimize an

objective function, J, the manipulated variables, $u(k)$, at the k-th sampling instant, must be considered. Equality and inequality constraints with the measured disturbances were integrated into the control calculations (Jeon et al., 2015). The designed manipulated variables are realized as a reference value or a set point for lower-level control loop processes.

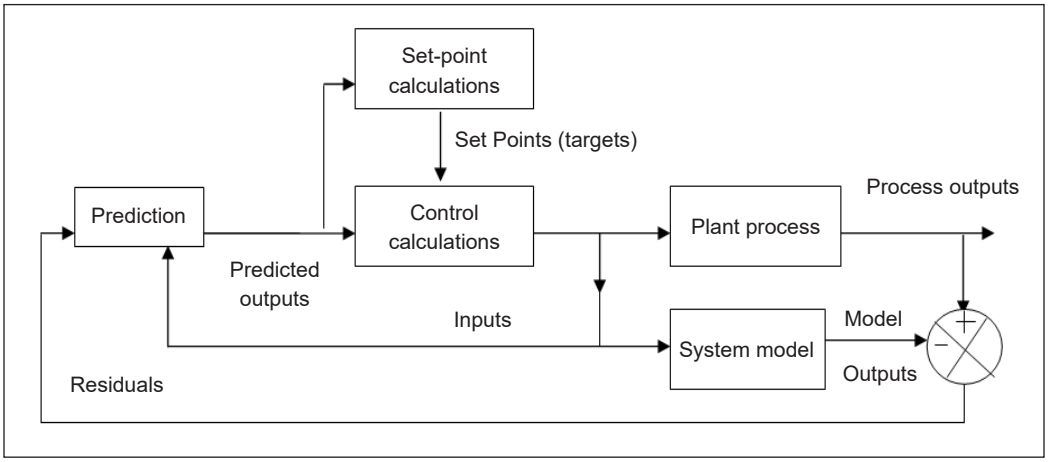

Figure 3. Model Predictive Controller (MPC) structure

Receding Horizon Control (RHC)

MPC is formed with an iterative and finite-horizon optimization of a respective plant model. At time interval t, the state of the existing plant is sampled, and cost-minimizing control strategies are worked out for a sensibly short time horizon in the future behavior [t, t + h]. An online method or on-the-fly calculation can also investigate the state trajectories derived from the current state and find a cost-minimizing control strategy until the time t + h (Kazantzidis et al., 2018). The block diagram for the receding horizon and the concept showing the optimization problem are represented in Figures 4 and 5.

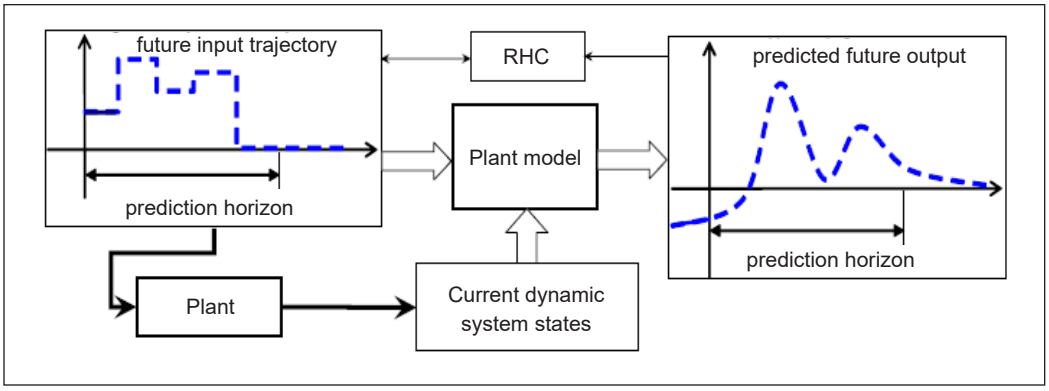

Figure 4. Block diagram for the receding horizon (Gorinevsky, 2005)

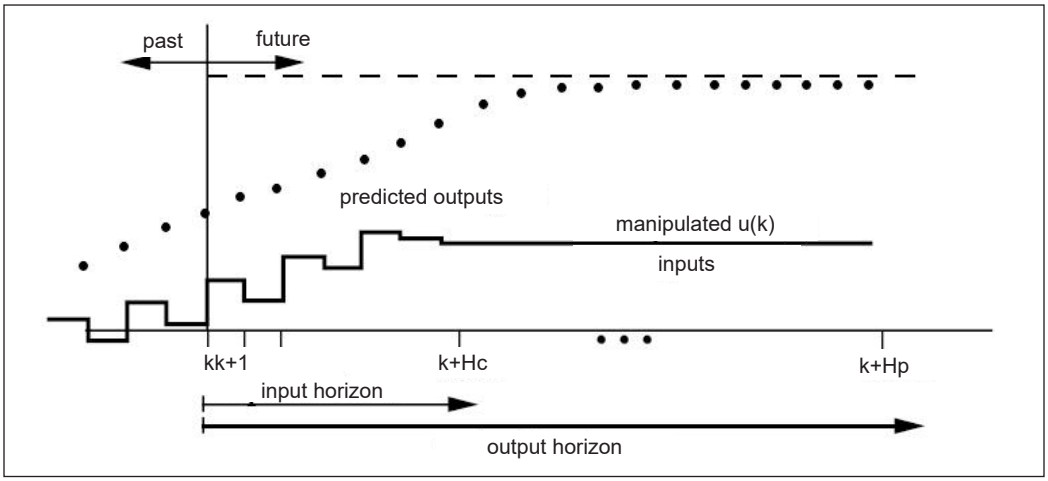

Figure 5. The receding horizon concept shows an optimization problem (Shahriar et al., 2013)

The sampling-based MPC systems keep the control signal constant over the interval [t,t+h]. The value of h can then be considered as the sampling interval, and the prediction horizon can be a small number of sampling intervals. It can reduce the computational power required to employ a model predictive controller (Halvgaard et al., 2012).

Only the initial measure of the process control system strategy is executed. The state of the plant is tested again, and the calculations are repeated starting from the new current state, which in turn yields a new control and a new predicted state path (Gonela et al., 2019). The prediction horizon that remains being shifted forward and meant for this re-computation technique, the Model Predictive Controller (MPC), is also known as Receding Horizon Control (RHC) (Alqahtani et al., 2016).

RESULTS AND DISCUSSION

System Identification Fitness

The real-time sample data have been collected from the solar power plant system under various conditions through Zever Solar Data logging systems for linear system fitness, and the data have been taken for estimation and validation. Figure 6 shows the simulated result of the selected model with the measured output obtained from the MATLAB platform. The system identification tool preferred showing the residual analysis results for every chosen model. The validation data set computed the prediction errors or the residuals (Arnold & Andersson, 2011). The correlation functions are shown in Figure 7. Graphical User Interface in the system identification tool allows us to view and analyze the linear/non-linear system responses. The transient response of the system obtained from the MATLAB software is represented in Figure 8. Correlation analysis identifies the fascinating relationships in data and helps us realize the relevance of attributes concerning

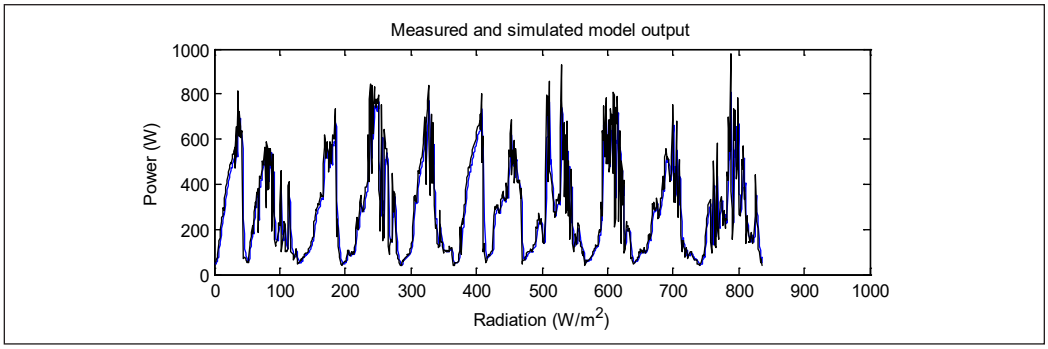

Figure 6. Model validation output

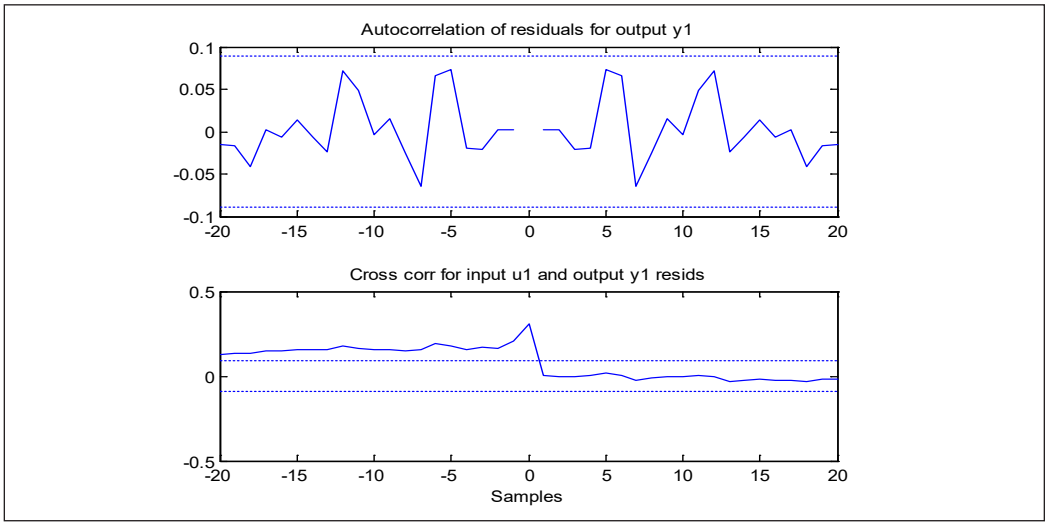

Figure 7. Residual analysis of the system

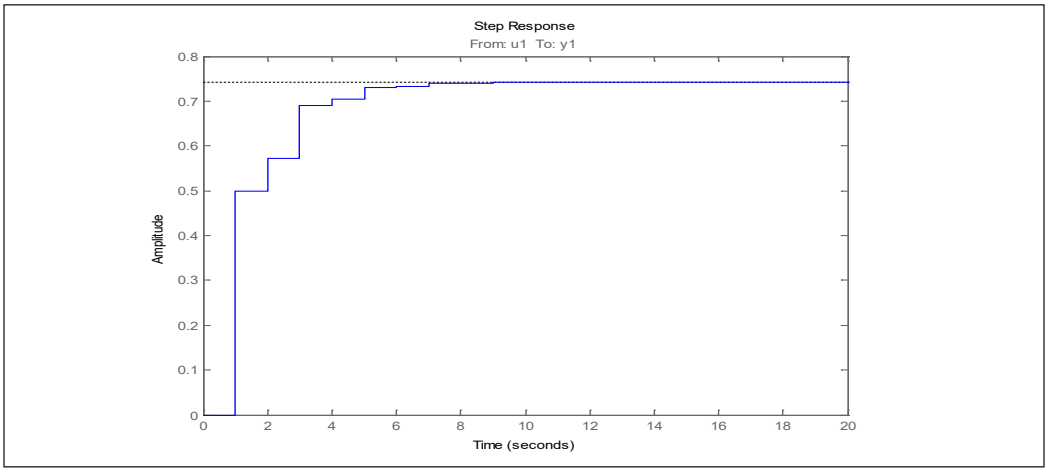

Figure 8. Power response of a system with a system identification tool

the objectives. It helps optimize the input variables and the data size, which will help in memory reduction. Autocorrelation and cross-correlation values between input and predicted output are 0.02 and 0.15 (Enríquez et al., 2016).

Model Predictive Control (MPC)

The transfer function obtained from the system identification tool is imported into the MPC tool. MPC offers a better understanding of the experimental phenomena (machine learning process), is excellent in predicting events in the future (time series analysis), and makes it easy to obtain a system model of signal in filter design (signal processing techniques) (Basallo et al., 2017).

The control actions of providing values for horizon, constraints, and adjusting the weights were done accordingly in the MPC tool based on our required control action. Figure 9 shows the MPC structure for a solar power plant system. By importing a plant model (or controller) in the MATLAB MPC tool, the graphic shows the count for the five possible signal types (Godina et al., 2018). The overall result for the solar power plant System design by MPC in MATLAB/Simulink is shown in Figure 10.

As the simulation runs, the plant output and the reference signal are displayed, and the MPC response is shown in Figure 11 and Figure 12, representing the step response of a dynamic system model to a step input of unit amplitude.

The performance index is a steady-state error, defined as the error between the power response and the predicted power response, with a value of 0.8. Hence, Figure 12 gives a solution for an optimization problem to find the optimal control action that drives the response of predicted plant output to the desired set-point as close as possible. The system identification process contributes to the proper functioning of the MPC controller, which performs the prediction. The System Identification Process (SIP) and MPC complement each other for better efficiency.

The performance of the proposed predictor model can be well understood from the results. The error variation of the predicted values from the actual values for the proposed system is 0.8. Achieving the error of such a low value with very few datasets describes the efficiency of the model design. The results of the proposed model are compared with the other models discussed in the literature review. Table 3 compares the methods employed, indices used for performance evaluation, and the actual error value obtained through simulation. This comparison is not exhaustive since the compared models are designed for different specifications, sizes, and locations. Also, the metrics used for comparison vary widely; no standard error metrics are used in all literature. From Table 3, the numerical methods show good performance only in some instances, and the intelligent techniques-based models like artificial neural networks, fuzzy logic, and ANFIS demonstrate better performance in almost all cases. However, the hybrids remain competitive with intelligent

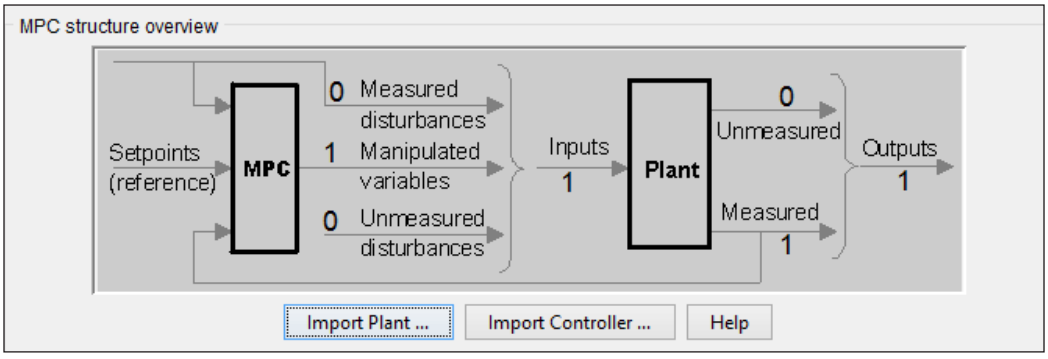

Figure 9. MPC structure

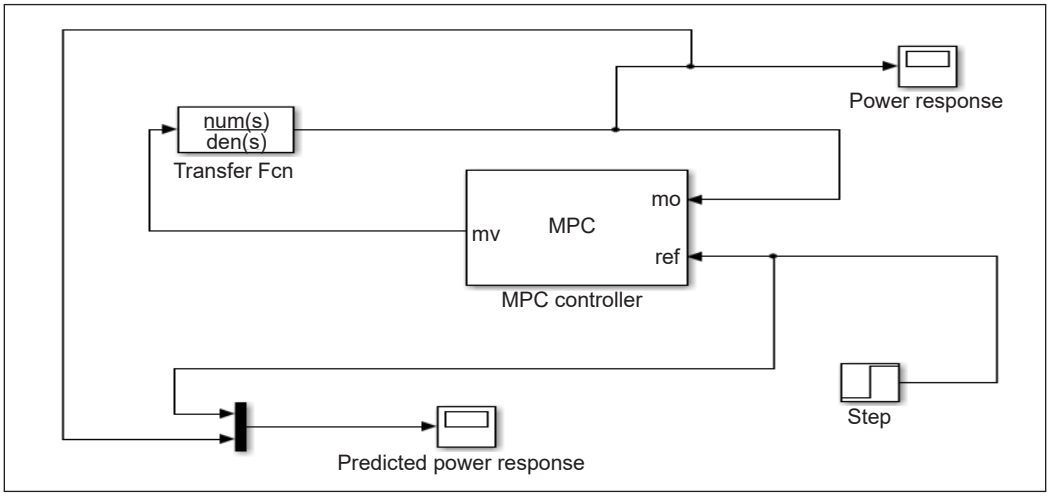

Figure 10. Simulation block diagram

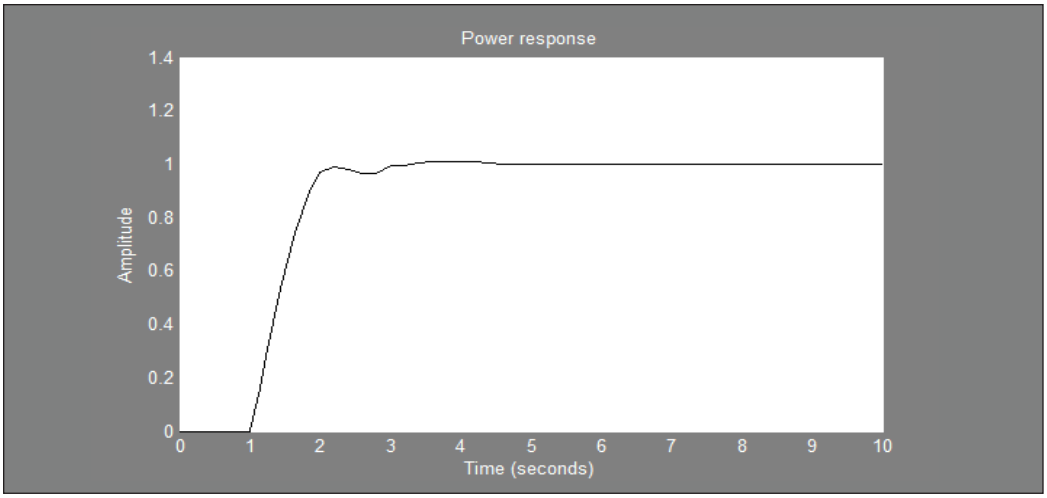

Figure 11. Power response in Model Predictive Controller

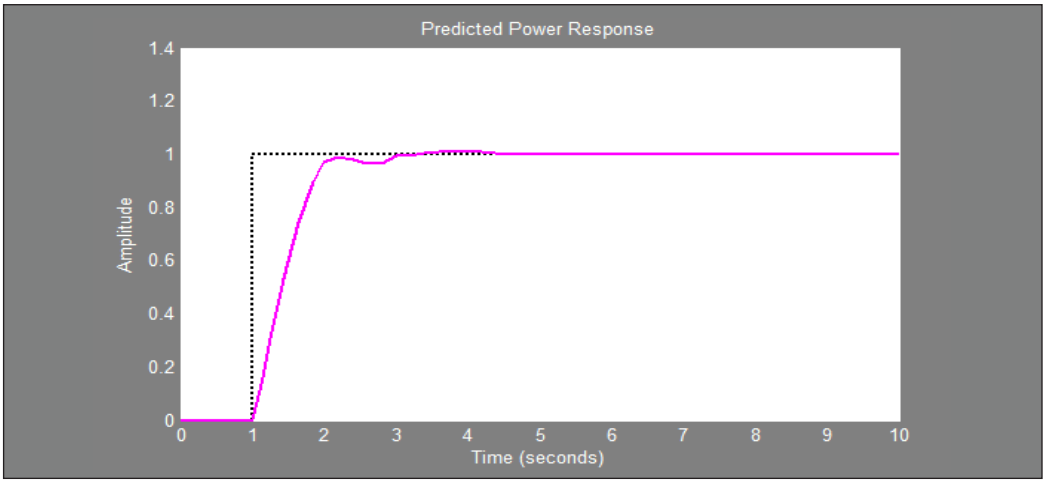

Figure 12. Predicted power response in Model Predictive Controller

Table 3
Comparison of methods employed, indices used for performance evaluation, and the actual error value obtained through simulation

Reference	Method	Performance Index	Error Value
Yadav et al., 2019b	PSO ANFIS	MAPE	BPNN – 11.5852 ANFIS – 10.7300 PSO-ANFIS – 3.5196
Ehsan et al., 2014	ANN	MSE	0.0198 to 0.025.
Semero et al., 2018	GA- PSO-ANFIS	NMAE	5.31
Viswavandya and Mohanty, 2018	Fuzzy logic & ANFIS	MAE	ANFIS – 0.067 Fuzzy – 0.187
Abdullah et al., 2019	HFPSO – WT ANFIS	MAE	25.6249 to 44.8471
Chugh et al., 2015	Fuzzy Logic	MAPE	1.052
Abuella and Chowdhury, 2015	MLRA	RMSE	0.0736
Mandal et al., 2012	WT-BPNN & WT-RBFNN	RMSE	WT+BPNN 0.55 to 2.05 WT+RBFNN 0.32 to 1.57
Ncane and Saha, 2019	Fuzzy & ANN	MAE	Fuzzy – 1.924 ANN – 2.626
Yadav et al., 2019a	GA-ANFIS	RMSE	0.023 TO 0.316
Lin and Pai, 2016	ESDLS-SVR	RMSE	0.1618 to 0.5502
Our proposed Model	MPC	SSE	0.8

performance, speed, and accuracy techniques. However, the design complexity makes it a challenge to be implemented widely (Clastres, 2011). Another factor to be discussed is how good the predictor is in solar power plant capacity scaling. Since the proposed controller is a closed-loop system, carrying the scaling even resolves for unstable controllers if the closed-loop system is stable.

The Novelty of the Model

The unique features include a built-in error feedback system for the predictive controller and the correlation analysis between the output and input variables performed in the system identification block of MATLAB. Correlation analysis identifies the fascinating relationships in data and helps us realize the relevance of attributes concerning the objectives. It helps optimize the input variables and the data size, which will help in memory reduction. Moreover, the proposed model suits building-integrated photovoltaic (BIPV) and building-attached photovoltaic (BAPV). If the energy produced and consumed by the building are equal, it is called a net-zero energy building. Data availability on power generation helps schedule power usage and storage; hence, energy prediction has become integral to such buildings. The prediction results can also help in handling overload conditions. Furthermore, an additional unit called an automatic overload alert system can be integrated with the proposed model. This feature will send a text to the residence owner once overload conditions are reached prior to the event. It will allow the residence owners to think of future overload prevention strategies. Specifically, this feature could be a significant component of smart homes, which are increasing at 15%–18% in metropolitan cities and 5%–10 % in other cities of India (Jain, 2016).

The other advantage includes the ease of tuning and replicating the proposed method, making it appropriate for industrial and residential units. Tuning is an easy chore in MPC, unlike other machine learning methods, which require an entirely new set of data for the changed condition of the SPVS. The numerical methods will require the designers to recalculate from the initial stage. The intelligent methods will require tuning, which retrains the model with new data sets. However, in the case of hybrids, most models need a complete redesign, while the self-evolving models will adapt to the new capacity. In the proposed case, tuning is unnecessary since the feedback system in the controller automatically upgrades itself for the new capacity even though many control parameters are involved in this model predictive controller.

CONCLUSION

In this study, the primary focus was on the critical importance of accurate solar power prediction, a key factor for solar energy suppliers and grid operators aiming to maintain a balanced supply-demand equilibrium within an electrical grid, ultimately impacting their profitability. The study harnessed the synergy of enhanced data availability and the computational prowess of machine learning algorithms to bolster the optimization and overall performance of prediction systems.

The System Identification process and the application of a Model Predictive Controller (MPC) were leveraged as potent tools for forecasting renewable energy, specifically in the context of solar energy. Real-time sample data from a solar power plant was gathered,

forming the basis for accurate predictions. Meteorological data played a pivotal role in predicting fluctuations in solar power generation. Data was utilized for system estimation and validation using a system identification toolbox, culminating in deriving a transfer function that exhibited optimal fitness. The obtained transfer function was incorporated into MATLAB's Model Predictive Controller (MPC) toolbox, where a controller was meticulously designed. The designed controller demonstrated exceptional accuracy in predicting the output power response for a solar power plant system with the R square value of 0.8 and MSE of 0.12.

This research underscores the significance of advanced techniques, such as System Identification and Model Predictive Control, in achieving highly precise solar power predictions. These findings directly affect the efficient management of solar energy resources and their integration into the electrical grid, with potential benefits for suppliers and grid operators.

The future scope of this research includes conducting comparative analyses with benchmark models, assessing seasonal variations in solar energy prediction, and broadening the range of case studies across diverse geographic locations and climates, emphasizing in-depth Analysis and sensitivity testing to enhance the manuscript's quality and applicability.

ACKNOWLEDGEMENT

The author acknowledges the financial support received from the AICTE - MODROBS scheme.

REFERENCES

Abdullah, N. A., Abd Rahim, N., Gan, C. K., & Nor Adzman, N. (2019). Forecasting solar power using hybrid firefly and particle swarm optimization (HFPSO) for optimizing the parameters in a wavelet transform-adaptive neuro fuzzy inference system (WT-ANFIS). *Applied Sciences*, *9*(16), 3214. https://doi.org/10.3390/app9163214

Abuella, M., & Chowdhury, B. (2015, October 4-6). *Solar power forecasting using Artificial Neural Networks* [Paper presentation]. North American Power Symposium (NAPS), Charlotte, USA. https://doi.org/10.1109/NAPS.2015.7335176

Accenture. (2016). Recommendations for Updating India Smart Grid Roadmap: 2016.

Aliberti, A., Bottaccioli, L., Cirrincione, G., Macii, E., Acquaviva, A., & Patti, E. (2018). ForecastingShort-term Solar Radiation for Photovoltaic Energy Predictions. *International Conference on Smart Cities and Green ICT Systems*. 44–53. https://doi.org/ 10.5220/0006683600440053

Alqahtani, A., Marafi, S., Musallam, B., El, N., Abd., & D., Khalek, E., (2016). Photovoltaic power forecasting model based on nonlinear system identification. *Canadian Journal of Electrical and Computer Engineering*, *39*(3). https://doi.org/ 10.1109/CJECE.2016.2584081

Andrade, J. R., & Bessa, R. J. (2017). Improving renewable energy forecasting with a grid of numerical weather predictions. *IEEE Transactions on Sustainable Energy*, *8*(4), 1571-1580. https://doi.org/10.1109/TSTE.2017.2694340

Arnold, M., & Andersson, G. (2011, August 22-26). *Model predictive control of energy storage including uncertain forecasts* [Paper presentation]. Power Systems Computation Conference (PSCC), Stockholm, Sweden.

Basallo-Triana, M. J., Rodríguez-Sarasty, J. A., & Benitez-Restrepo, H. D. (2017). Analogue-based demand forecasting of short life-cycle products: a regression approach and a comprehensive assessment. *International Journal of Production Research*, *55*(8), 2336-2350. https://doi.org/10.1080/00207543.2016.1241443

Brown, M. A., & Zhou, S. (2013). Smart-grid policies: An international review. In P. D. Lund, J. Byrne, R. Haas & S. Flynn (Eds.) *Advances in Energy Systems: The Large-scale renewable energy integration challenge* (pp.127-147). Wiley. https://doi.org/10.1002/9781119508311.ch8

Chugh, A., Chaudhary, P., & Rizwan, M. (2015, December 17-20). *Fuzzy logic approach for short term solar energy forecasting* [Paper presentation]. Annual IEEE India Conference (INDICON), New Delhi, India. https://doi.org/10.1109/INDICON.2015.7443206

Clastres, C. (2011). Smart grids: Another step towards competition, energy security and climate change objectives. *Energy policy*, *39*(9), 5399-5408. https://doi.org/10.1016/j.enpol.2011.05.024

Das, R. K., Nayak, B., Ganeshan, P., Gautam, S. S., & Mandal, K. K. (2023) Dynamic mechanical behavior of a nano sized alumina fiber reinforced epoxy hybrid composites. *Materials Today: Proceedings, 76*(Part 3), 524-527. https://doi.org/10.1016/j.matpr.2022.11.158.

Ehsan, R. M., Simon, S. P., & Venkateswaran, P. R. (2014, December 17-18). *Artificial neural network predictor for grid-connected solar photovoltaic installations at atmospheric temperature* [Paper presentation]. International Conference on Advances in Green Energy (ICAGE), Thiruvananthapuram, India. https://doi.org/10.1109/ICAGE.2014.7050142

Enríquez, R., Jiménez, M. J., & del Rosario Heras, M. (2016). Solar forecasting requirements for buildings MPC. *Energy Procedia*, *91*, 1024-1032. https://doi.org/10.1016/j.egypro.2016.06.271

Frei, C. W. (2008). What if…? Utility vision 2020. *Energy Policy*, *36*(10), 3640-3645. https://doi.org/10.1016/j.enpol.2008.07.016

Godina, R., Rodrigues, E. M., Pouresmaeil, E., Matias, J. C., & Catalão, J. P. (2018). Model predictive control home energy management and optimization strategy with demand response. *Applied Sciences*, *8*(3), 408. https://doi.org/10.3390/app8030408

Gonela, V., Salazar, D., Zhang, J., Osmani, A., Awudu, I., & Altman, B. (2019). Designing a sustainable stochastic electricity generation network with hybrid production strategies. *International Journal of Production Research*, *57*(8), 2304-2326. https://doi.org/10.1080/00207543.2018.1516900

Gopinath, M. S., Balaji, R., & Kirubakaran, V. (2014, March 13-15). *Cost effective methods to improve the power output of a solar panel: An experimental investigation* [Paper presentation]. Power and Energy Systems Conference: Towards Sustainable Energy, Bangalore, India. https://doi.org/10.1109/PESTSE.2014.6805282

Gorinevsky, D. (2005). Lecture 14 - Model predictive control part 1: The concept. In *EE392m: Control engineering in industry* (pp.14-26). Sandford University. https://web.stanford.edu/class/archive/ee/ee392m/ee392m.1056/Lecture14_MPC.pdf

Guermoui, M., Melgani, F., & Danilo, C. (2018). Multi-step ahead forecasting of daily global and direct solar radiation: a review and case study of Ghardaia region. *Journal of Cleaner Production*, *201*, 716-734. https://doi.org/10.1016/j.jclepro.2018.08.006

Gupta, A. (2018, July 25). Overview- Forecasting and scheduling regulations in the Indian States. *Renewables Now*. https://renewablesnow.com/news/overview-forecasting-scheduling-regulations-in-indian-states-621216/

Halvgaard, R., Bacher, P., Perers, B., Andersen, E., Furbo, S., Jørgensen, J. B., Poulsen, N. K., & Madsen, H. (2012). Model predictive control for a smart solar tank based on weather and consumption forecasts. *Energy Procedia*, *30*, 270-278. https://doi.org/10.1016/j.egypro.2012.11.032

Hernández-Hernández, C., Rodríguez, F., Moreno, J. C., da Costa Mendes, P. R., Normey-Rico, J. E., & Guzmán, J. L. (2017). The comparison study of short-term prediction methods to enhance the model predictive controller applied to microgrid energy management. *Energies*, *10*(7), 884. https://doi.org/10.3390/en10070884

IRENA. (2018). *Renewable power generation costs in 2017* (Technical report). The International Renewable Energy Agency. chrome-extension://efaidnbmnnnibpcajpcglclefindmkaj/https://www.irena.org/-/media/Files/IRENA/Agency/Publication/2018/Jan/IRENA_2017_Power_Costs_2018_summary.pdf

India Smart Grid Forum. (2019). *Smart Grid Bulletin*. https://indiasmartgrid.org/isgf/public/bulletin/168205 7744wX5jhWnzL1u1maXAPbFyEv9AWng722hLtN1pWXQQ.pdf

Jain. A. (2016, September 16). Why smart homes are popular. *The Hindu*. https://www.thehindu.com/features/homes-and-gardens/Why-smart-homes-are-popular/article14384601.ece

Jeon, H. W., Taisch, M., & Prabhu, V. V. (2015). Modelling and analysis of energy footprint of manufacturing systems. *International Journal of Production Research*, *53*(23), 7049-7059. https://doi.org/10.1080/00207543.2014.961208

Jin, T., Shi, T., & Park, T. (2018). The quest for carbon-neutral industrial operations: Renewable power purchase versus distributed generation. *International Journal of Production Research*, *56*(17), 5723-5735. https://doi.org/10.1080/00207543.2017.1394593

Karan, M. (2019, July 22). How India in a short period of time has become the cheapest producer of solar power. *Economic Times*. https://economictimes.indiatimes.com/small-biz/productline/power-generation/how-india-in-a-short-period-of-time-has-become-the-cheapest-producer-of-solar-power/articleshow/70325301.cms

Kazantzidis, A., Nikitidou, E., Salamalikis, V., Tzoumanikas, P., & Zagouras, A. (2018). New challenges in solar energy resource and forecasting in Greece. *International Journal of Sustainable Energy*, *37*(5), 428-435. https://doi.org/10.1080/14786451.2017.1280495

Kazem, H. A., Yousif, J. H., & Chaichan, M. T. (2016). Modeling of daily solar energy system prediction using support vector machine for Oman. *International Journal of Applied Engineering Research*, *11*(20), 10166-10172. https://doi.org/10.19026/rjaset.13.2936

Kenning, T. (2016, Feb 15). *Lack of skilled workforce for India's rapidly growing solar sector*. PV Tech.

Khalil, T. M. (1981). Comparative analysis of energy resources. *The International Journal of Production Research*, *19*(4), 401-409. https://doi.org/10.1080/00207548108956668

Khosravi, A., Nunes, R. O., Assad, M. E. H., & Machado, L. (2018). Comparison of artificial intelligence methods in estimation of daily global solar radiation. *Journal of Cleaner Production*, *194*, 342-358. https://doi.org/10.1016/j.jclepro.2018.05.147

Kuhe, A., Achirgbenda, V. T., & Agada, M. (2021). Global solar radiation prediction for Makurdi, Nigeria, using neural networks ensemble. *Energy Sources, Part A: Recovery, Utilization, and Environmental Effects*, *43*(11), 1373-1385. https://doi.org/10.1080/15567036.2019.1637481

Kumari, V., (2017). Future of microgrids in India. *International Journal of Research in Engineering and Technology*. 6 (2), 70-73. https://doi.org/10.15623/ijret.2017.0602011

Lampropoulos, I., Vanalme, G. M., & Kling, W. L. (2010, October 11-13). *A methodology for modeling the behavior of electricity prosumers within the smart grid* [Paper presentation]. IEEE PES Innovative Smart Grid Technologies Conference Europe (ISGT Europe), Gothenburg, Sweden. https://doi.org/10.1109/ISGTEUROPE.2010.5638967

Lee, J., Zhang, P., Gan, L. K., Howey, D. A., Osborne, M. A., Tosi, A., & Duncan, S. (2018). Optimal operation of an energy management system using model predictive control and Gaussian process time-series modeling. *IEEE Journal of Emerging and Selected Topics in Power Electronics*, *6*(4), 1783-1795. https://doi.org/10.1109/JESTPE.2018.2820071

Lin, K. P., & Pai, P. F. (2016). Solar power output forecasting using evolutionary seasonal decomposition least-square support vector regression. *Journal of Cleaner Production*, *134*(Part B), 456-462. https://doi.org/10.1016/j.jclepro.2015.08.099

Liu, X., Paritosh, P., Awalgaonkar, N. M., Bilionis, I., & Karava, P. (2018). Model predictive control under forecast uncertainty for optimal operation of buildings with integrated solar systems. *Solar Energy*, *171*, 953-970. https://doi.org/10.1016/j.solener.2018.06.038

Lund, P. D., Byrne, J., Haas, R., & Flynn, D. (Eds.). (2019). *Advances in Energy Systems: The Large-scale renewable energy integration challenge*. Wiley. https://doi.org/10.1002/9781119508311.ch8

Mandal, P., Madhira, S. T. S., Meng, J., & Pineda, R. L. (2012). Forecasting power output of solar photovoltaic system using wavelet transform and artificial intelligence techniques. *Procedia Computer Science*, *12*, 332-337. https://doi.org/10.1016/j.procs.2012.09.080

Marimuthu, C., & Kirubakaran, V. (2014). A critical review of factors affecting wind turbine and solar cell system power production. *International Journal of Advance Engineering Research Studies 3*(2), 143-147.

Mikhaylidi, Y., Naseraldin, H., & Yedidsion, L. (2015). Operations scheduling under electricity time-varying prices. *International Journal of Production Research*, *53*(23), 7136-7157. https://doi.org/10.1080/00207543.2015.1058981

Moon, J. Y., & Park, J. (2014). Smart production scheduling with time-dependent and machine-dependent electricity cost by considering distributed energy resources and energy storage. *International Journal of Production Research*, *52*(13), 3922-3939. https://doi.org/10.1080/00207543.2013.860251

National Energy Policy. (2017). NITI Aayog, Government of India. https://niti.gov.in/writereaddata/files/new_initiatives/NEP-ID_27.06.2017.pdf

Ncane, Z. P., & Saha, A. K. (2019, January 28-30). *Forecasting solar power generation using fuzzy logic and artificial neural network* [Paper presentation]. Southern African Universities Power Engineering Conference/Robotics and Mechatronics/Pattern Recognition Association of South Africa (SAUPEC/RobMech/PRASA), Bloemfontein, South Africa. https://doi.org/10.1109/RoboMech.2019.8704737

Oldewurtel, F., Parisio, A., Jones, C. N., Gyalistras, D., Gwerder, M., Stauch, V., Lehmann, B., & Morari, M. (2012). Use of model predictive control and weather forecasts for energy efficient building climate control. *Energy and buildings*, *45*, 15-27. https://doi.org/10.1016/j.enbuild.2011.09.022

Ozoegwu, C. G. (2019). Artificial neural network forecast of monthly mean daily global solar radiation of selected locations based on time series and month number. *Journal of Cleaner Production*, *216*, 1-13. https://doi.org/10.1016/j.jclepro.2019.01.096

Padmanathan, K., Govindarajan, U., Ramachandaramurthy, V. K., Rajagopalan, A., Pachaivannan, N., Sowmmiya, U., Padmanaban, S., Holm-Nielsen, J. B., Xavier, S., & Periasamy, S. K. (2019). A sociocultural study on solar photovoltaic energy system in India: Stratification and policy implication. *Journal of cleaner production*, *216*, 461-481.https://doi.org/10.1016/j.jclepro.2018.12.225

Parisio, A., Wiezorek, C., Kyntäjä, T., Elo, J., & Johansson, K. H. (2015, August 24-28). *An MPC-based energy management system for multiple residential microgrids* [Paper presentation]. IEEE International Conference on Automation Science and Engineering (CASE), Gothenburg, Sweden. https://ieeexplore.ieee.org/servlet/opac?punumber=7279855

Prabhu, V. V., Trentesaux, D., & Taisch, M. (2015). Energy-aware manufacturing operations. *International Journal of Production Research*, *53*(23), 6994-7004. https://doi.org/10.1080/00207543.2015.1100766

Raja, K., Ganeshan, P., Singh, B. K., Upadhyay, R. K., Ramshankar, P., & Mohanavel, V. (2023). Effect of mol.% of Yttria in Zirconia matrix alongside a comparative study among YSZ, alumina & ZTA ceramics in terms of mechanical and functional properties. *Sādhanā*, *48*(2), 72. https://doi.org/10.1007/s12046-023-02136-w

Ramachandra, T. V., Jha, R. K., Krishna, S. V., & Shruthi, B. V. (2005). Solar energy decision support system. *International Journal of Sustainable Energy*, *24*(4), 207-224. https://doi.org/10.1080/14786450500292105

Ramedani, Z., Omid, M., & Keyhani, A. (2013). Modeling solar energy potential in a Tehran province using artificial neural networks. *International Journal of Green Energy*, *10*(4), 427-441. https://doi.org/10.1080/15435075.2011.647172

Renewables Now. (July 25). https://renewablesnow.com/news/overview-forecasting-scheduling-regulations-in-indian-states-621216/

Rodat, S., Tantolin, C., Le Pivert, X., & Lespinats, S. (2016). Daily forecast of solar thermal energy production for heat storage management. *Journal of Cleaner Production*, *139*, 86-98. https://doi.org/10.1016/j.jclepro.2016.08.019

Sassi, O., & Oulamara, A. (2017). Electric vehicle scheduling and optimal charging problem: complexity, exact and heuristic approaches. *International Journal of Production Research*, *55*(2), 519-535. https://doi.org/10.1080/00207543.2016.1192695

Semero, Y. K., Zhang, J., & Zheng, D. (2018). PV power forecasting using an integrated GA-PSO-ANFIS approach and Gaussian process regression based feature selection strategy. *CSEE Journal of Power and Energy Systems*, *4*(2), 210-218. https://doi.org/10.17775/CSEEJPES.2016.01920

Shahriar, M. S., Ahmed, M. A., Rahman, M. I., & Khan, A. I. (2013, December 19-21). *Comparison of MPC and conventional control methods for the stability enhancement of UPFC connected SMIB system* [Paper presentation]. 2nd International Conference on Advances in Electrical Engineering (ICAEE), Dkaka, Bangladesh. https://doi.org/10.1109/ICAEE.2013.6750337

Singh, S. N., Prathiba, V. S., & Katiki, N. (2015, August 7-8). *Smart micro grid model for rural India* [Paper presentation]. 2nd International conference on Innovative Engineering Technologies (ICIET), Bangkok, Thailand. https://doi.org/10.15242/iie.e0815022

Sivaneasan, B., Yu, C. Y., & Goh, K. P. (2017). Solar forecasting using ANN with fuzzy logic pre-processing. *Energy procedia*, *143*, 727-732. https://doi.org/10.1016/j.egypro.2017.12.753

Suresh, V., Naviynkumar, S., & Kirubakaran, V. (2013, December). Improved power output of PV system by low cost evaporative cooling technology. In *2013 International Conference on Green Computing, Communication and Conservation of Energy (ICGCE)* (pp. 640-643). IEEE. https://doi.org/10.1109/ICGCE.2013.6823514

Taki, M., Rohani, A., Yildizhan, H., & Farhadi, R. (2019). Energy-exergy modeling of solar radiation with most influencing input parameters. *Energy Sources, Part A: Recovery, Utilization, and Environmental Effects*, *41*(17), 2128-2144. https://doi.org/10.1080/15567036.2018.1550126

Taticchi, P., Garengo, P., Nudurupati, S. S., Tonelli, F., & Pasqualino, R. (2015). A review of decision-support tools and performance measurement and sustainable supply chain management. *International Journal of Production Research*, *53*(21), 6473-6494.https://doi.org/10.1080/00207543.2014.939239

Vassiliadis, D. (2000). System identification, modeling, and prediction for space weather environments. *IEEE Transactions on Plasma Science*, *28*(6), 1944-1955. https://doi.org/10.1109/27.902223

Vigneshwari, C. A., Velan, S. S. S., Venkateshwaran, M., Mydeen, M. A., & Kirubakaran, V. (2016, April). Performance and economic study of on-grid and off-grid solar photovoltaic system. In *2016 international conference on energy efficient technologies for sustainability (ICEETS)* (pp. 239-244). IEEE. https://doi.org/10.1109/ICEETS.2016.7582933

Vinayagar, K., Ganeshan, P., Raja, P. N., Hussain, M. S. Z., Kumar, P. V., Ramshankar, P., Mohanavel, V., Mathankumar, N., Raja, K., & Bezabih, T. T. (2022). Optimization of crashworthiness parameters of thin-walled conoidal structures. *Advances in Materials Science and Engineering*, *2022,* 4475605. https://doi.org/10.1155/2022/4475605

Viswavandya, M., & Mohanty, A. (2018). Fuzzy logic and ANFIS based short term solar energy forecasting. *International Journal on Future Revolution in Computer Science & Communication Engineering*, *4*, 631-636.

Yadav, H. K., Pal, Y., & Tripathi, M. M. (2019a). A novel GA-ANFIS hybrid model for short-term solar PV power forecasting in Indian electricity market. *Journal of Information and Optimization Sciences*, *40*(2), 377-395. https://doi.org/10.1080/02522667.2019.1580880

Yadav, H. K., Pal, Y., & Tripathi, M. M. (2019b). PSO tuned ANFIS model for short term photovoltaic power forecasting. *International Journal of Recent Technology and Engineering*, *7*(6), 937-942.

Yaniktepe, B., Kara, O., & Ozalp, C. (2017). The global solar radiation estimation and analysis of solar energy: Case study for Osmaniye, Turkey. *International Journal of Green Energy*, *14*(9), 765-773. https://doi.org/10.1080/15435075.2017.1329148

Zafarani, R., Eftekharnejad, S., & Patel, U. (2018). Assessing the utility of weather data for photovoltaic power prediction. *arXiv preprint arXiv:1802.03913*. https://doi.org/10.48550/arXiv.1802.03913

Zame, K. K., Brehm, C. A., Nitica, A. T., Richard, C. L., & Schweitzer, G. D. (2018). Smart grid and energy storage: Policy recommendations. *Renewable and Sustainable Energy Reviews*, *82*(Part 1), 1646-1654. https://doi.org/10.1016/j.rser.2017.07.011

Zendehboudi, A., Baseer, M. A., & Saidur, R. (2018). Application of support vector machine models for forecasting solar and wind energy resources: A review. *Journal of Cleaner Production*, *199*, 272-285. https://doi.org/10.1016/j.jclepro.2018.07.164

Pertanika J. Sci. & Technol. 32 (S1): 93 - 110 (2024)

PERTANIKA JOURNALS

SCIENCE & TECHNOLOGY

Journal homepage: http://www.pertanika.upm.edu.my/

Fuzzy Logic-based Power Optimizer for Solar Photovoltaic Power Systems

Revathy Subbiah Rajaram[1]*, Padaga Kumar Babu[2], Kirubakaran Victor[1], Raja Kandasamy[3], Ganeshan Pushpanathan[4], Vivek Sivakumar[5], Ramshankar Pushpanathan[6], Mohanavel Vinayagam[7] and Sachuthananthan Barathy[8]

[1]Centre for Rural Energy, The Gandhigram Rural Institute - Deemed to be University, Gandhigram - 624302, Tamil Nadu, India
[2]Department of Mechanical Engineering, Geethanjali Institute of Science and Technology, Nellore - 524316, Andhra Pradesh, India
[3]Department of Mechanical Engineering, Anna University Regional Campus - Coimbatore, Coimbatore - 641046, Tamil Nadu, India
[4]Center for Augmented Intelligence and Design, Department of Mechanical Engineering, Sri Eshwar College of Engineering, Coimbatore - 641202, Tamil Nadu, India
[5]Department of Civil Engineering, GMR Institute of Technology, Razam, Andra Pradesh - 532127, India
[6]Department of Civil Engineering, College of Engineering Guindy, Anna University, Chennai - 600 025, Tamil Nadu, India
[7]Centre for Materials Engineering and Regenerative Medicine, Bharath Institute of Higher Education and Research, Chennai, 600073, Tamil Nadu, India
[8]Department of Mechanical Engineering, Sree Vidyanikethan Engineering College, Tirupati - 517102, Andhra Pradesh, India

ABSTRACT

Solar photovoltaics has become the most popular renewable energy source due to its simplicity in installation and maintenance. However, the dependence on the availability of solar energy at the instant makes its operation non-linear. Various optimizing solutions are proposed to rule out this disadvantage. This paper dwells on a machine language approach to solve this problem. A maximal tracker for power points relies on fuzzy logic control. An embedded power optimizer is designed and tested under different environmental conditions through simulation. The results presented allow researchers to test various artificial intelligence techniques for renewable energy extraction processes.

Keywords: Fuzzy logic, machine language, MATLAB, photovoltaics, solar energy

ARTICLE INFO

Article history:
Received: 27 July 2023
Accepted: 17 October 2023
Published: 19 January 2024

DOI: https://doi.org/10.47836/pjst.32.S1.06

E-mail addresses:
revathysrajaram@gmail.com (Revathy Subbiah Rajaram)
kumarbabudrp@gmail.com (Padaga Kumar Babu)
kirbakaran@yahoo.com (Kirubakaran Victor)
rajagce@gmail.com (Raja Kandasamy)
ganeshan.p@sece.ac.in (Ganeshan Pushpanathan)
1717vivek@gmail.com (Vivek Sivakumar)
ramshankar1991@gmail.com (Ramshankar Pushpanathan)
mohanavel2k16@gmail.com (Mohanavel Vinayagam)
bsachu7@yahoo.co.in (Sachuthananthan Barathy)
* Corresponding author

ISSN: 0128-7680
e-ISSN: 2231-8526

INTRODUCTION

The solar photovoltaic technology has gained more importance in the recent years. The advantages of solar energy are manifold. The energy benefits include low or no transmission and distribution losses and high penetration levels (Raja et al., 2023). A short payback period and low electricity cost per watt-hour come under the economic profits (Yamunadevi et al., 2021). The benefits of solar energy in the environment are low carbon emission, reduced usage of land and water, improvement in public health, and a higher lifetime of about 25 years (Kaygusuz, 2009). The recent survey data from the Ministry of New and Renewable Energy, Government of India, shows a rapid increase in the installation of rooftop-based solar photovoltaic systems (Das et al., 2023). India, being a tropical country, is blessed with abundant solar potential. The government has set an ambitious target of having 175 GW of renewable energy capacity by 2022, including 98,298 MW of solar, 59,400MW of wind, 4385 MW of small hydropower, and 9880 MW from biomass (Padmanathan et al., 2019). Though the initiative received a warm welcome, the associated challenges in integrating renewable power into the existing grid are tricky (Azaharahmed et al., 2021). However, today's solar cells, like monocrystalline or polycrystalline, have a limited power conversion efficiency (Vinayagar et al., 2022).

The power produced by solar photovoltaic systems is affected by factors like mismatch losses caused by various factors like manufacturing differences, thermal variations, partial shading conditions, non-uniform degradation, and aging of the solar cells or modules (Rajeshwaran et al., 2018). The unidentical electrical characteristics of the PV cells/modules, inconsistency in the semiconductor materials used, and lack of precision cause manufacturing mismatch losses. Partial shading has been identified as a significant driving factor for mismatch losses (Saravanan et al., 2021). If only a fraction of cells is shaded, a problem arises as the exact amount of current must flow through cells connected in series. This reduction in current production by the non-shaded cells becomes an issue (Saravanan et al., 2021). Shading of only one cell in a module could reduce the module's power output by 86%, although the irradiance loss is only 3%.

The solar modules usually come with a lifetime warranty of about 20 years and are reported with a 1% yearly degradation. The aging process accelerates due to mechanical damages, hotspots, and uneven degradation (Radhaboy et al., 2019). Fractional power loss of up to 12% happens due to premature aging. The degradation rate due to aging in thin-film cells is 0.5%–0.7% per year, and the crystalline cells are 0.8% per year. There can be significant variations in temperature between modules depending on the differences in airflow over the modules (Raja et al., 2020). Modules centered in the array are generally not as affected by airflow as modules at the edge, which causes the centered modules to be hotter (Islam et al., 2018). Furthermore, the erratic weather patterns caused by global warming also affect the performance of solar modules, leading to inconsistent and unreliable

power outputs (Revathy & Kirubakaran, 2020). Hence, including optimization components in the balance of the system is unavoidable.

Most optimization systems comprise a maximum power point tracker and other power electronics controllers like buck converters, boost converters, or buck-boost converters (Noman et al., 2017). The maximum power point tracker (MPPT) monitors the output generated by the solar array at a particular instant and makes optimization decisions (Vignesh Kumar et al., 2019). Usually, the power electronic controllers are used to maximize or minimize the solar array output voltage according to the load requirements. However, this maximum power point tracker makes the major decisions—does the optimization require a boost or reduction in voltage values? If so, at what rate? These questions are very crucial in the process of optimization, and this decides the system's overall performance and directly influences the profit made out of the power generation (Vignesh Kumar et al., 2019).

The highly effective maximum power point trackers measure and monitor the current and voltage outputs of the solar photovoltaic array to calculate the total power delivered at that instant. It then compares this estimated power value to the other power values at different operating points. By incessantly adjusting the operating parameters, it arrives at the best possible optimized value of power that can be delivered instantly. It also created a signal code based on the power electronics circuit's operation to provide the optimal output. The abovementioned process requires consistent operation at high speeds so the system supplies reliable power. Most earlier algorithms, like voltage-based control, current-based control, and hill-climbing algorithms, work fine under normal circumstances. Still, in case of frequent weather changes, they oscillate and fail at most operating points (Motahhir et al., 2018). Traditional MPPT algorithms, such as Perturb and Observe (P&O) and Incremental Conductance (IncCond), suffer from drawbacks like oscillations and slow convergence in dynamic conditions (Smith et al., 2023). Fuzzy logic controllers have emerged as a viable alternative due to their ability to adapt to changing needs and handle imprecise data (Lee et al., 2007). Hence, this process requires a method that can offer accuracy at high speeds and automatically adapt to the frequent changes in operating conditions.

The advantages of the fuzzy logic-based maximum power point trackers are multifold. Fuzzy logic controllers excel in handling solar PV systems' non-linear and uncertain nature. They can effectively track the maximum power point (MPP) even in partial shading, temperature fluctuations, and rapid irradiance changes (Gonzalez et al., 2023).

Fuzzy logic controllers adapt to varying operating conditions without requiring extensive parameter tuning. This adaptability is particularly useful in real-world applications where environmental factors constantly change (Smith et al., 2023). Fuzzy logic controllers exhibit smoother tracking than traditional algorithms, reducing oscillations around the MPP and minimizing stress on the PV system (Lee et al., 2007).

Despite their advantages, fuzzy logic-based MPPT controllers face specific challenges and areas for improvement. Implementing fuzzy logic controllers can be computationally intensive, which may limit their use in low-power embedded systems. Researchers are exploring optimizing their computational efficiency (Gonzalez et al., 2023). Some studies have proposed hybrid MPPT approaches combining fuzzy logic with other techniques like neural networks or genetic algorithms to improve tracking accuracy and speed (Lee et al., 2007). Investigating methods for automatically tuning the fuzzy logic controller's parameters in real-time is to enhance adaptability and performance in rapidly changing environments (Smith et al., 2023).

Recent research in the field of fuzzy logic-based MPPT controllers for solar PV systems has yielded promising results. Fuzzy logic controllers have been applied in multi-objective optimization scenarios, simultaneously considering factors like efficiency, tracking speed, and system stability (Lee et al., 2007). Integrating machine learning techniques with fuzzy logic controllers improves prediction accuracy and enhances the controller's adaptability (Smith et al., 2023). As researchers continue to address challenges and explore innovative approaches, the future of fuzzy logic-based MPPT controllers holds promise for further improving the efficiency and reliability of solar PV systems (Gonzalez et al., 2023; Lee et al., 2007).

Several machine language techniques are gaining popularity for their problem-solving skills, especially when there is a high level of non-linearity (Mlakić et al., 2018). Fuzzy logic, a popular machine language-based technique, combines human reasoning skills with the thinking process to resolve intricate non-linear problems (Patan et al., 2021). A fuzzy logic controller works in three steps: (1) fuzzification, (2) inference, and (3) defuzzification, as shown in Figure 1 (Karthika et al., 2014).

Fuzzification is the procedure of encoding the user-specified inputs into the machine-interpretable format, usually called fuzzy subsets (NG- -ve, ZE- 0, PE- +ve). The controller can only understand and handle these subsets (Bouselham et al., 2017).

The subsets thus arrived at are branded by membership functions; the choice of MFs and their respective ranges for preferred inlet and outlet variables influences the better

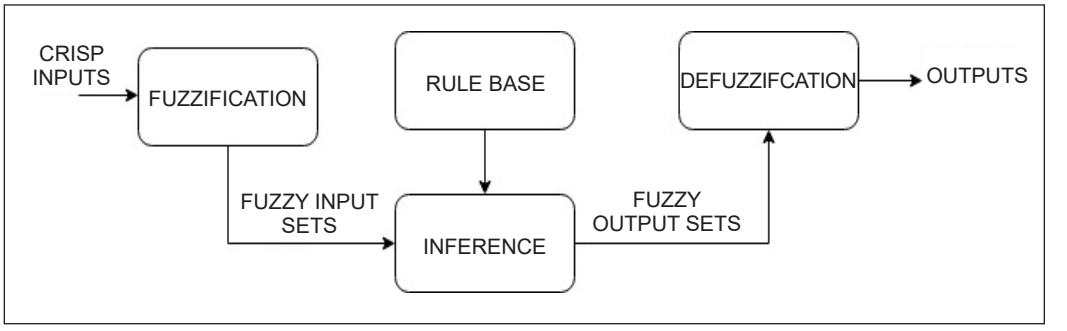

Figure1. Fuzzy controller block

performance of the controller. Defuzzification: The final step is where the fuzzy subsets are decoded to actual interpretable output variables (Saravana et al., 2014).

This paper discusses such a technique, which integrates machine learning with power electronics to optimize the performance of solar photovoltaic systems. The work involves designing a maximum power point tracker using a fuzzy logic-based controller. The output of this controller is applied to a conventional boost converter for better optimization.

MATERIALS AND METHODS

The proposed optimization technique involves the design of a solar photovoltaic array, a fuzzy logic controller, and a boost converter. All the scenarios are simulated using MATLAB/SIMULINK, and the performance is tested under different operating conditions.

Solar photovoltaic array with DC-DC converter: A solar photovoltaic array is designed in MATLAB SIMULINK and comprises 5 Canadian Solar CS5C -80M modules connected as a string. Under standard testing conditions, the array characteristics are a maximum array voltage of 110 V, a maximum array current of 4.97 A, and a maximum power of around 550 W.

Boost Converter: The (DC-DC converter) is designed for an optimum value of 100 V and 1 kHz (Revathy et al., 2022).

Fuzzy Logic Controller: The design of the fuzzy logic controller should align with the specific goals and requirements of the MPPT system and consider the characteristics of the PV system being controlled. It often involves balancing simplicity and accuracy to maximize energy harvesting from solar PV panels. The various stages involved in the design are explained below.

Input Selection: The design of a fuzzy controller involves many steps, where the first step consists of identifying the inputs. There are several choices in the case of inputs; weather parameters like irradiance and temperature can be considered if the required historical data is available. However, in most cases, the solar photovoltaic systems output current and voltage are preferred for more straightforward calculations (Kumar et al., 2019).

Output Selection: The primary output variable is the duty cycle or control signal for the DC-DC converter or inverter, which regulates the power flow between the PV panels and the load or battery.

Membership Function Selection: The next stage is the determination of membership functions for the fuzzy controller. Since the fuzzy controller does not interpret the real-time data, we convert them into fuzzy sets using a specific linguistic label called membership functions. Membership functions define how each input is mapped to fuzzy sets (e.g., power at an instant, change of power at another moment). The choice of membership functions should reflect the characteristics of the input data. Standard membership functions include triangular, trapezoidal, or Gaussian (Padmanathan et al., 2019).

Fuzzy Set Determination: Dedicated fuzzy sets or linguistic variables are selected for each input chosen. The fuzzy sets classify the input into different ranges for decision-making (for instance, negative, zero, and positive).

Fuzzy Rules Generation: The next stage involves creating a set of rules based on which the controller operates. Most of these rules are usually If-then-based conditions executed using basic Boolean operators like AND, OR, and NOT.

Rule Base Design: This stage involves designing a fuzzy inference system that utilizes the membership functions and the rules to arrive at optimal duty signal value in its machine language. This stage includes defining inference methods, such as Mamdani or Sugeno, to determine how the rules interact.

Defuzzification: The outputs of the inference system need to be translated into control signals understandable by the electronic circuits through defuzzification. Defuzzification is the opposite of fuzzification (Balasubramanian & Singaravelu, 2012)

Parameter Tuning: The membership functions and the rule weights must be fine-tuned to achieve the desired duty cycle through simulations in MATLAB.

Validation and Testing: To validate its efficiency, the FLC-based MPPT is tested with real-time data through simulation in the MATLAB platform, the solar PV system, and the DC-DC converter.

Figure 2 depicts the design aspects of the fuzzy controller.

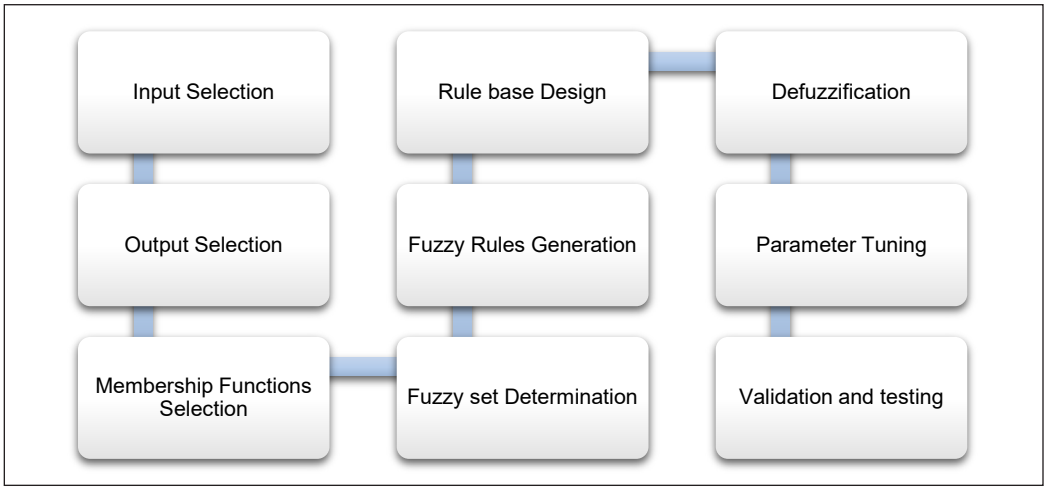

Figure 2. Fuzzy logic controller design

FUZZY LOGIC CONTROLLER DESIGN

A fuzzy controller works based on a distinctive rule base usually depicted in table form. The output parameters of the solar photovoltaic system, such as the voltage and current values, are considered input for the proposed controller. These values after acquisition

are multiplied to calculate the power values at respective timestamps. The power error is calculated by subtracting the power at a particular instant from the power at the previous moment. Similarly, the change in error is calculated by subtracting the error in power at an instant k and the error at the last instant (k-1). Two factors, the error in Power E(k) (Equation 1) and the change in error CE(k) (Equation 2), are chosen as inlet factors for the fuzzy controller.

$$E(k) = P_{pv}(k) - P_{pv}(k-1) \quad (1)$$

$$CE(k) = E(k) - E(k-1) \quad (2)$$

The change in power from kth instant to k-1th instant is considered an error (Equation 1). The error and the change in error are considered the inlets of the fuzzy controller, and the duty cycle value D is regarded as the output value (Saravana et al., 2014). During fuzzification, the inlet and the outlet are broken into five fuzzy sets. The fuzzy sets are NS, NB, Z, PS, and PB. NS refers to Negative Small, NB to Negative Big, Z to zero, PS to Positive Small, and PB to Positive Big (Saravanan et al., 2022). Triangular membership functions are employed in both inlets and outlets for better results. The membership functions (MFs)for error, change of error, and duty ratio are given in Figures 3 to 5, respectively.

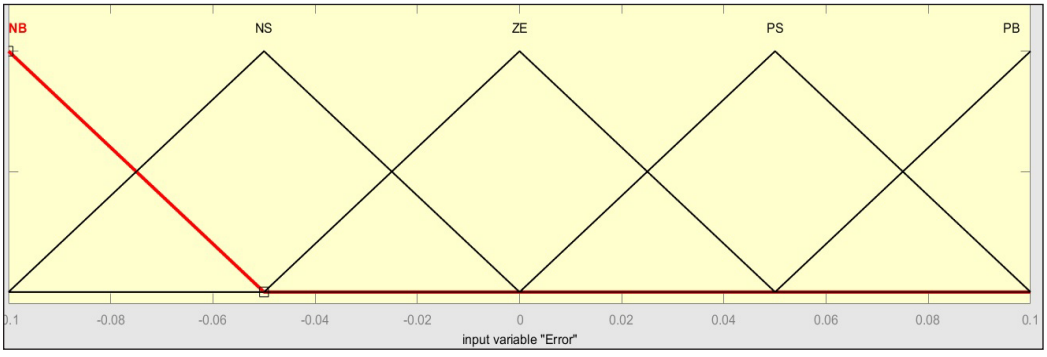

Figure 3. MF representing E(k)

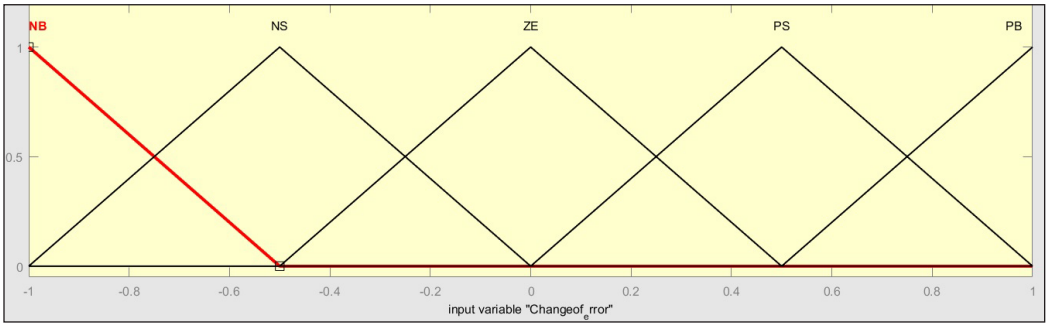

Figure 4. MF representing CE(k)

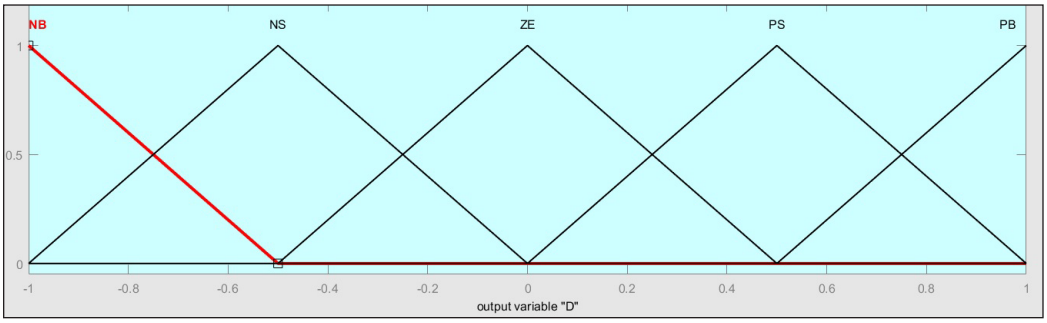

Figure 5. MF of the duty - D

The rules are framed with the fuzzy sets of the inputs and outputs. There are 25 rule sets for the FLC designed, and they are given in Table 1, which is easy to interpret. The first rule is interpreted as if the error and its change are NB; the duty ratio is NB.

The boost converter is controlled using these principles for the maximal power point. The rules in Table 1 are represented in a three-dimensional graph shown in Figure 6

The proposed fuzzy controller uses a Max-Min combination of the inference system called Mamdani. Mamdani Inference Systems are used in various applications, including control systems, decision support systems, and expert systems, where precise control and reasoning are required in uncertain or non-linear environments. The defuzzification is carried out through the

Table 1
Rules of fuzzy controller

CE \ E	NB	NS	Z	PS	PB
NB	NB	NB	NS	NS	Z
NS	NB	NS	NS	Z	PS
Z	NS	NS	Z	PS	PS
PS	NS	Z	PS	PS	PB
PB	Z	PS	PS	PB	PB

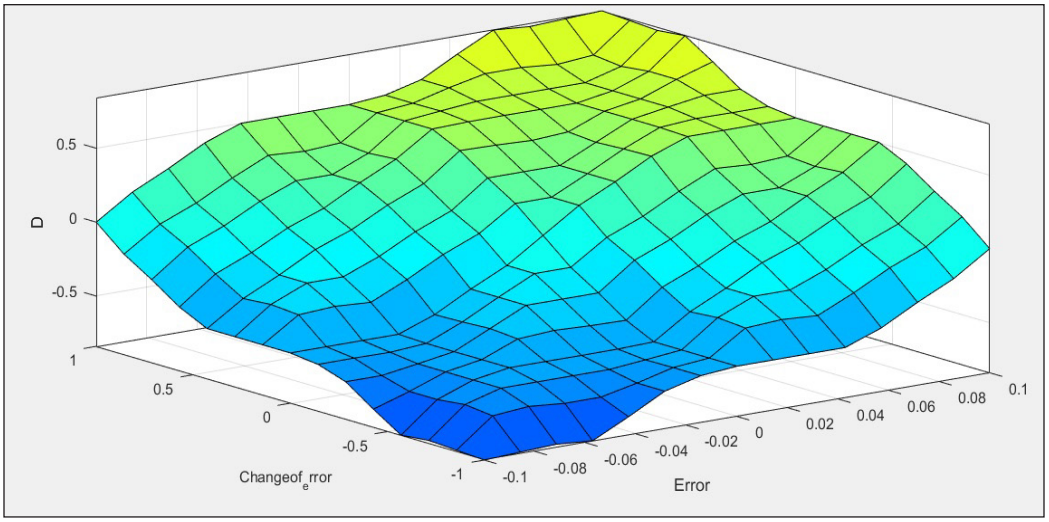

Figure 6. FLC rules

Centre of Arc method (COA), which involves the calculation of the center of gravity of the output variable Duty ratio, which is given by Equation 3 (Bendib et al., 2014).

$$\Delta D = \frac{\sum_{i=1}^{n} \mu(\Delta D_i) * \Delta D_i}{\sum_{i=1}^{n} \mu(\Delta D_i)} \quad (3)$$

The actual output D(k) is calculated by defuzzifying the change in duty ratio ΔD(k) and scaling it by a gain $S_{\Delta D}$ as in Equation 4 (Bendib et al., 2014).

$$D(k) = D(k-1) + S_{\Delta D} * \Delta D(k) \quad (4)$$

This duty ratio is input for the pulse width modulating generator, which generates the pulse D and regulates the boost converter's operation for optimized output power. The power optimization circuit driven by the fuzzy logic controller to extract maximum power is analyzed in MATLAB/SIMULINK for the proposed SPV array. The composition of the array includes 5 Canadian Solar CS5C -80M modules, all connected in series and to a DC-DC converter to optimize power. The proposed SIMULINK model is shown in Figure 7.

The fuzzy controller proposed involves current and voltage sensors at the initial level to derive the error and change in error values. The controller achieves good response time and reduced voltage fluctuations during the tracking process. Hence, the operational accuracy and speed of the fuzzy logic controller are undebatable. However, the only disadvantage is the design phase, where the designer must have exclusive knowledge of the detailed photo voltaic system.

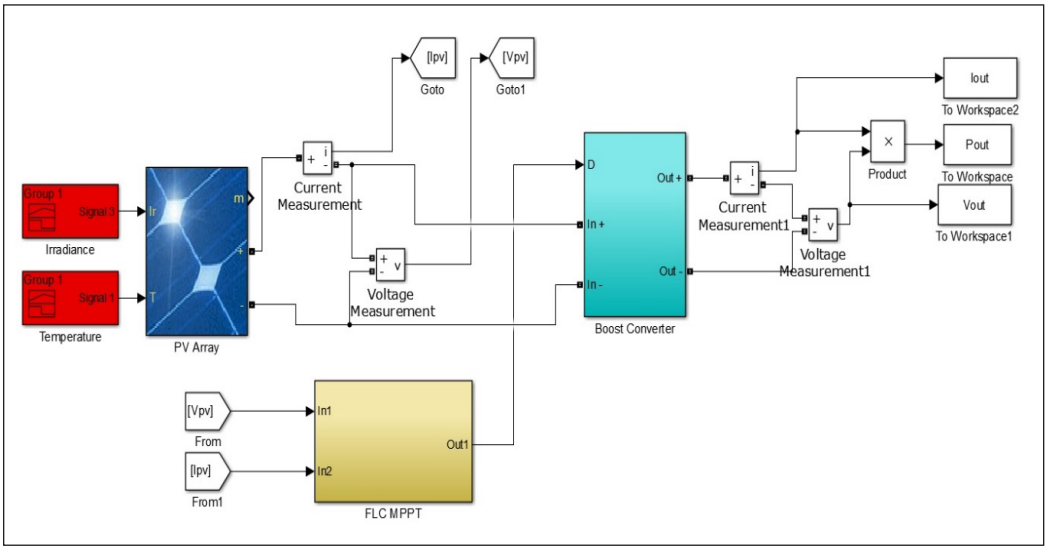

Figure 7. Power optimization of an SPV array with proposed MPPT in MATLAB/ SIMULINK

RESULTS AND DISCUSSION

The proposed maximum power point techniques are tested under various conditions. Testing Maximum Power Point Tracking (MPPT) techniques under multiple conditions is crucial for several reasons such as:

- Environmental conditions like varying solar irradiance (G) and module temperatures (T) reflect real-world scenarios. Testing under these conditions ensures that the MPPT algorithms perform optimally in the varying sunlight and temperature levels experienced by solar panels in different locations and climates.
- Solar panels are often installed in diverse environments with fluctuating weather patterns. MPPT algorithms need to adapt to these changes to ensure maximum energy harvesting.
- MPPT algorithms must be robust and reliable. Testing under different conditions helps identify potential weaknesses or vulnerabilities in the algorithms.
- Testing under standard conditions (i.e., STC) provides a baseline for validation, ensuring that the MPPT algorithms meet the expected performance levels.
- Understanding how MPPT algorithms behave under different conditions is essential since it aids in developing new algorithms or improving existing ones, fostering innovation in renewable energy technology.
- Understanding how MPPT functions under various conditions helps optimize the entire energy system in larger solar power installations.

The conditions and their description are given in Table 2.

According to the standard testing condition variables, the given solar photo voltaic array works at an irradiance level of 1000W/m^2 and an average temperature of 25^{o}C. The output power measured under different conditions is shown in Figures 7 to 10. The output at STC is used as a reference with other test conditions for better understanding. The maximum deliverable power the optimizers generate with the fuzzy controller under standard testing conditions is 0.488 kW.

The graph in Figure 9 depicts the dynamic performance of a photovoltaic array under rapidly changing weather conditions, simulated using SIMULINK. During a 50-second duration, the irradiance and temperature levels were intentionally varied three times,

Table 2
Test conditions

Test Conditions	Description
STC	Standard Testing Condition (G= 1000 W/m^2& T = 25^{o}C)
VWC	Rapidly varying weather condition G (W/m^2) = [700, 800, 900]; T(^{o}C) = [25, 30, 35]
PSC I	One module of the array is shaded partially
PSC II	Two modules are shaded partially.
PSC III	Three modules are shaded partially.

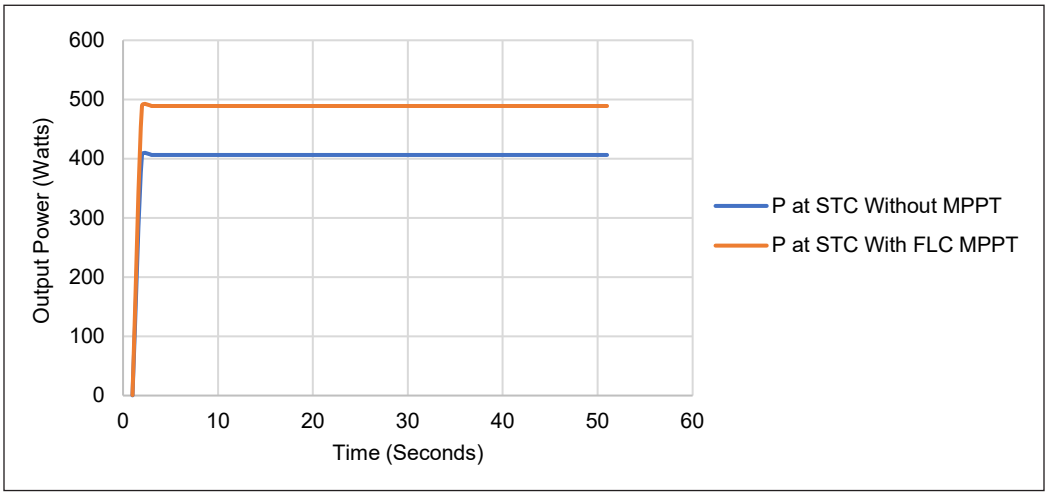

Figure 8. Output power of the power optimizer at STC

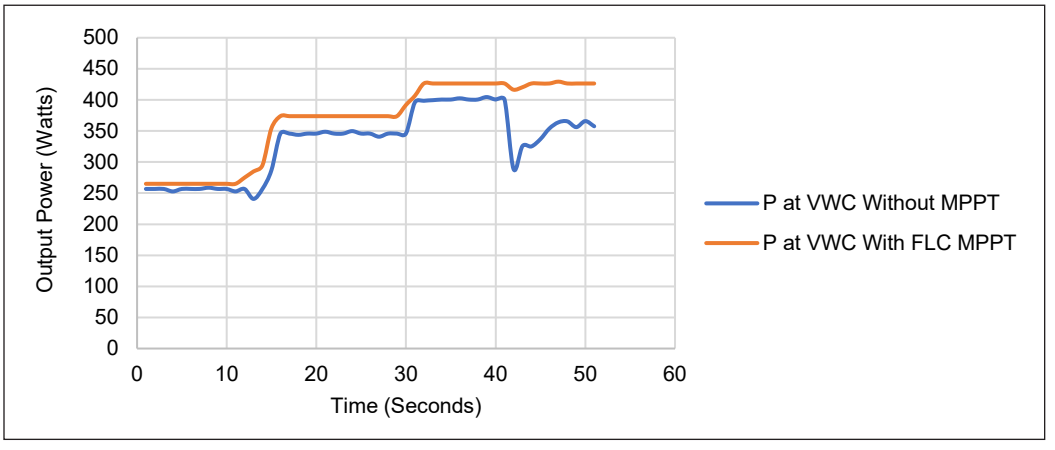

Figure 9. Output power of the power optimizers at VWC

showcasing the array's real-time response to these fluctuations. The graph illustrates a direct relationship between increased irradiance and higher power output, indicating the array's sensitivity to sunlight intensity. A Fuzzy Logic Control (FLC) Maximum Power Point Tracking (MPPT) system is in place, ensuring optimal power output. Even during sudden dips in irradiation, around the 40-second mark, the FLC MPPT system swiftly adapts, maintaining the array's power output at an optimal level. This graph provides valuable insights into the array's ability to efficiently harness solar energy under challenging and rapidly changing weather conditions, highlighting the effectiveness of the FLC MPPT system in maximizing energy harvest.

The graph in Figure 10 depicts a solar PV array's power-voltage (P-V) characteristics under both standard and partial shading conditions. Under standard conditions, the chart

exhibits a smooth curve with a single peak representing the array's maximum power point (MPP), where the power output is optimized at a specific voltage. However, the graph shows a more intricate pattern with multiple peaks under partial shading conditions, simulated by varying irradiance levels on different modules. These peaks indicate local maximum power points, posing a challenge for most MPPT algorithms in correctly identifying the global MPP. Notably, the Fuzzy Logic Control (FLC) based MPPT algorithm stands out by accurately pinpointing the highest peak, representing the actual maximum power point of the solar PV array under partial shading conditions.

Figure 11 directly compares the output power of a solar array employing Fuzzy Logic Control (FLC) Maximum Power Point Tracking (MPPT) and the same array without MPPT. The maximum power point (MPP) is identified at 320 W. The FLC MPPT algorithm

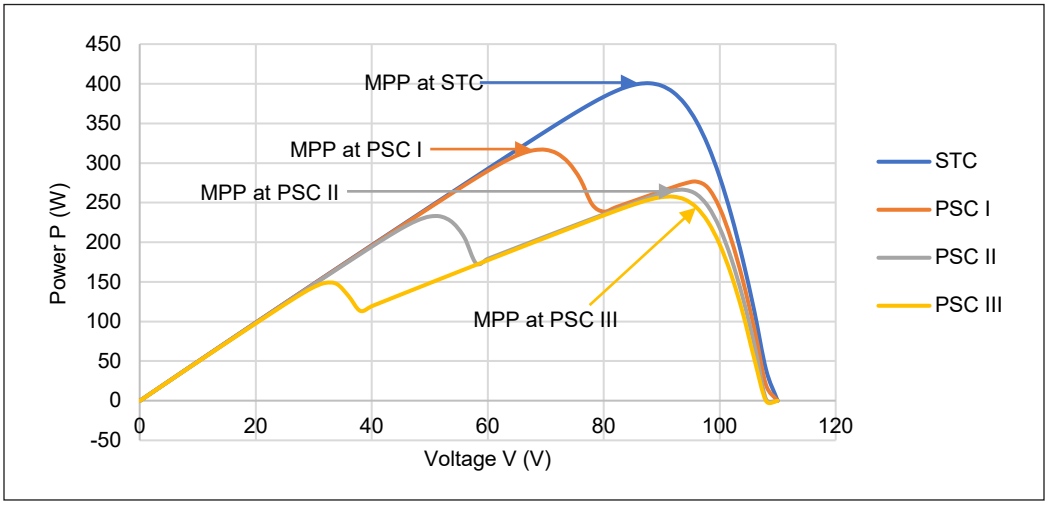

Figure 10. PV Curve under PSCs without optimization

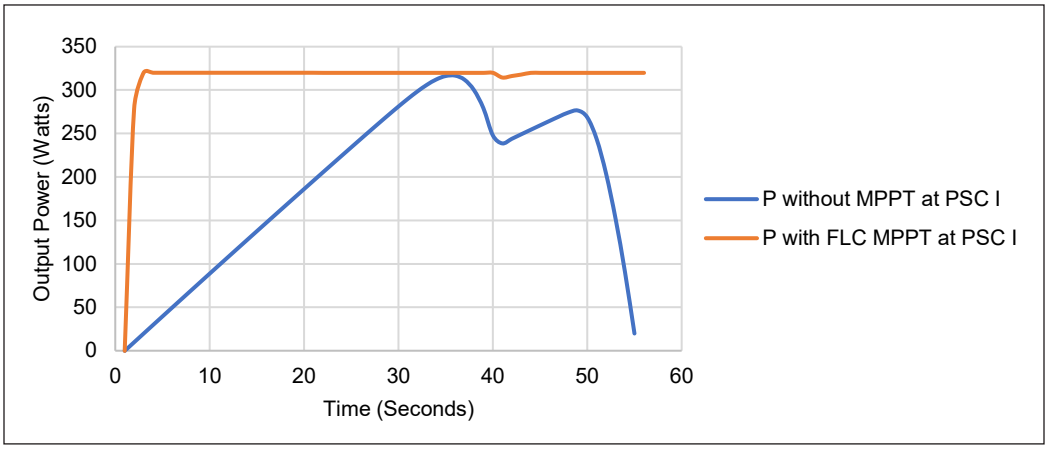

Figure 11. Output power of the optimizers under PSC I

optimizes the solar array's output to this value, ensuring efficient energy conversion. In contrast, the PV output without MPPT exhibits a less refined behavior, displaying two distinct peaks at 320 W and 275 W. This disparity illustrates the FLC MPPT's ability to pinpoint and maintain the MPP accurately, enhancing the solar array's performance and maximizing its power output.

Figure 12 displays the power characteristics of a solar array, revealing two distinct Maximum Power Points (MPPs) at 233 W and 266 W. Initially, the MPP is at 233 W, but with increased irradiance levels, it shifts to 266 W. The Fuzzy Logic Control (FLC) Maximum Power Point Tracking (MPPT) system efficiently optimizes the array's output to match this higher MPP, demonstrating its ability to adapt and maximize energy generation in response to changing light conditions.

In PSC III (Figure 13), initially, the MPP is identified at 150 W under specific irradiance conditions. As irradiance levels rise, the MPP significantly increases to 257 W. The Fuzzy Logic Control (FLC) Maximum Power Point Tracking (MPPT) system

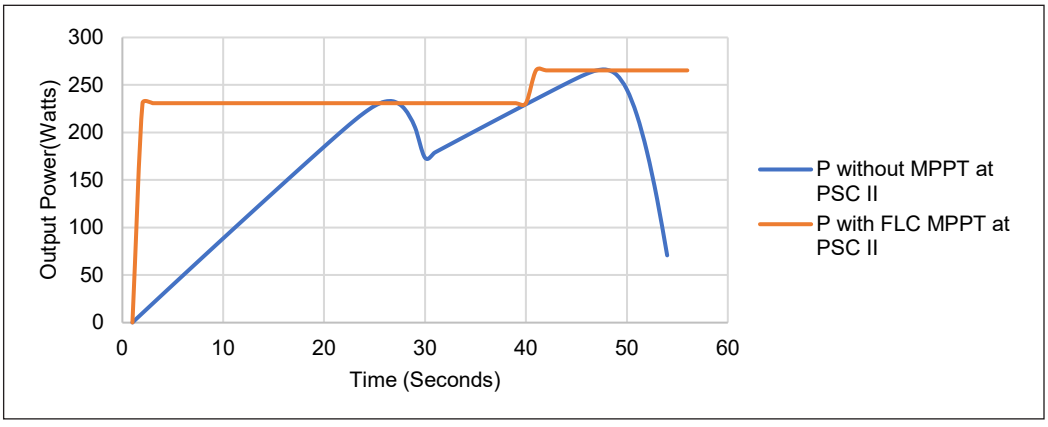

Figure 12. Output power of the optimizers under PSC II

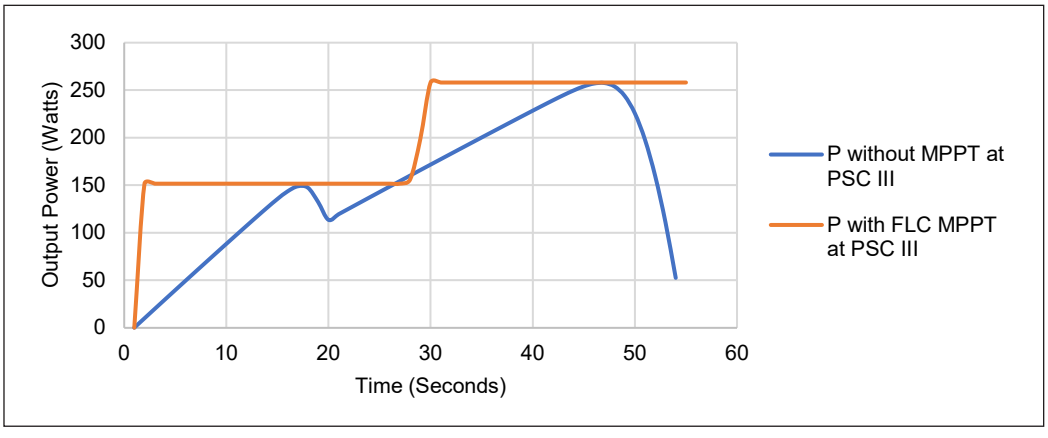

Figure 13. Output power of the optimizers under PSC III

is crucial in optimizing the array's output precisely to this higher MPP, showcasing its adaptability to changing light intensities and effectiveness in maximizing energy generation.

Table 3 displays the maximum power the Fuzzy Logic Control (FLC) MPPT optimizer achieves across different testing conditions. While the power values decrease under specific conditions, the proposed MPPT demonstrates superior adaptability, ensuring better optimization in the given scenarios.

Table 3
Maximum power obtained through the proposed MPPT

Test Condition	Power (Watts)
STC	500
VWC	430
PSC I	320
PSC II	266
PSC III	257

The power conversion efficiency of the photovoltaic array is given by Equation 5. P_{max} is the maximum power produced in Watts (W), G represents the irradiance levels in $W/m^{2,}$ and A refers to the array area of the total array, which is 1.6864 m^2.

$$\eta = \frac{P_{max}}{GA} \times 100 \quad (5)$$

The response time T_r of a Maximum Power Point Tracking (MPPT) system refers to the time it takes for the MPPT algorithm to detect a change in the operating conditions (such as variations in irradiance levels or temperature) and adjust the photovoltaic (PV) system to operate at the new maximum power point (MPP). In other words, it measures how quickly the MPPT algorithm can track and adapt to the optimal operating point as environmental conditions fluctuate. The response time for the proposed FLC-based MPPT can be observed in Figure 14.

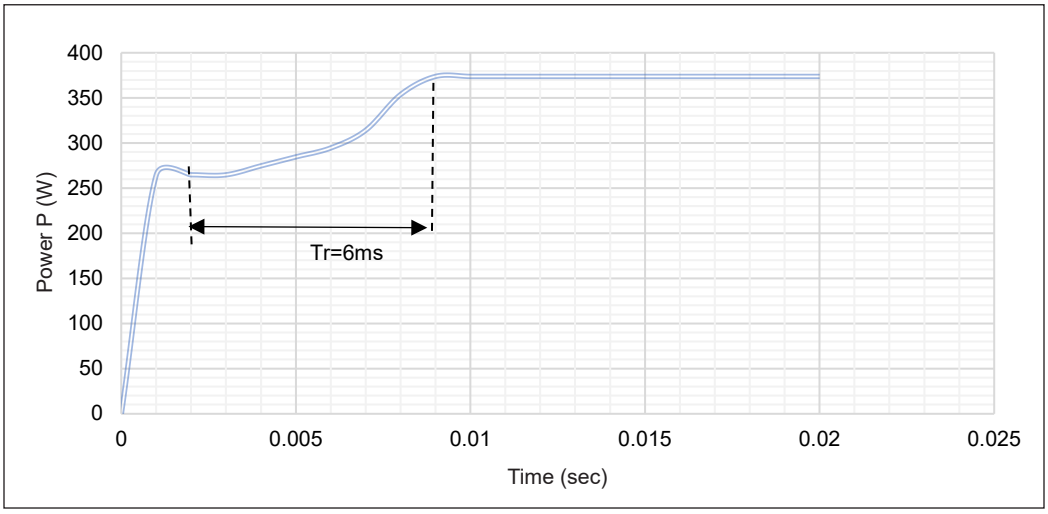

Figure 14. Response time, T_r

Table 4 provides a comprehensive summary of the proposed MPPT system's performance metrics, including maximum power output, response time, efficiency, stability in avoiding oscillations around multiple peaks, and sensor requirements. Oscillations occur when an MPPT cannot identify the MPP under multiple peak conditions. The results of the FLC MPPT (Figures 8 to 13) do not display any oscillations in the power curve.

Table 4
Evaluation of FLC-based optimizer

Evaluation Parameters	Pmax (kW)	T_r(ms)	Ƞ (%)	Oscillations	Sensors
FLC	0.488	6	28	Nil	V, I

The techno-economic analysis of the proposed controller is determined to appraise the financial profitability of the controller using the capital expenditure (CAPEX) method. The parameters involved in the process include the initial capital cost and the energy yield obtained through simulation results. Net income is calculated based on the electricity tariff, which is INR (Indian Rupee) 5.25 per kWh for the purchase of solar photovoltaic power, assuming it increases by 2% yearly (Chandel et al., 2014). The operation expenditure (OPEX) is calculated as a maintenance charge, which is assumed to be 6% of the capital expenditure (Chandel et al., 2014). The payback period is usually mentioned in years to recover the capital investment from the net income. The proposed controller's payback period is estimated to be 36 months.

CONCLUSION

The design of Maximum Power Point Tracking (MPPT) systems involves a multitude of challenges, encompassing the intricacies of the photovoltaic system itself, the selection of converters, the choice of tracking algorithms, system aging, geographical and climatic conditions, and ongoing maintenance. This multifaceted nature of MPPT design complicates the evaluation of algorithms using a limited set of assessment parameters. Nonetheless, intelligent techniques, such as fuzzy controller-based optimization, offer a compelling solution for fine-tuning solar photovoltaic systems with minimal error compromises and an increased efficiency of 28%. The data unequivocally demonstrates that fuzzy controller-based optimization elevates performance by consistently enhancing maximum power values across various testing conditions with an overall response time of 6 ms, ensuring swift adaptation to changing environmental conditions. Fuzzy logic controllers, operating on degrees of truth rather than absolute truth, render them system-independent, albeit with a more intricate design involving membership functions and rules that demand substantial knowledge of PV parameters, making them suitable for multiple peak conditions encountered during partial shading. Despite this, the technology remains a commendable

choice due to its swiftness, precision, sensitivity to partial shading scenarios, and overall efficiency. Future developments in rule design for fuzzy controllers promise to make the optimizer more accessible to non-technical operators, further underscoring its potential as a valuable tool in optimizing solar energy systems.

ACKNOWLEDGEMENT

The authors gratefully acknowledge the funding received from the All India Council for Technical Education (AICTE) under the Modernization and Removal of Obsolescence (MODROBS) scheme (AICTE File No. 9-41/RIFD/MODROB/Policy-1/2017-18 Dt. 26.03.2019).

REFERENCES

Aldair, A. A., Obed, A. A., & Halihal, A. F. (2018). Design and implementation of ANFIS-reference model controller based MPPT using FPGA for photovoltaic system. *Renewable and Sustainable Energy Reviews*, *82*, 2202-2217. https://doi.org/10.1016/j.rser.2017.08.071

Azaharahmed, M., Raja, K., Patan, M. K., Prasad, C. D., & Ganeshan, P. (2021). Invasive weed optimized area centralized 2 degree of freedom combined PID controller scheme for automatic generation control. *Journal of Electrical Engineering & Technology*, *16*, 31-42. https://doi.org/10.1007/s42835-020-00565-9

Balasubramanian, G., & Singaravelu, S. (2012). Fuzzy logic controller for the maximum power point tracking in photovoltaic system. *International Journal of Computer Applications*, *41*(12), 22-28. https://doi.org/10.5120/5594-7840.

Bendib, B., Krim, F., Belmili, H., Almi, M. F., & Boulouma, S. (2014). Advanced Fuzzy MPPT Controller for a stand-alone PV system. *Energy Procedia*, *50*, 383-392. https://doi.org/10.1016/j.egypro.2014.06.046

Bouselham, L., Hajji, M., Hajji, B., & Bouali, H. (2017). A new MPPT-based ANN for photovoltaic system under partial shading conditions. *Energy Procedia*, *111*, 924-933. https://doi.org/10.1016/j.egypro.2017.03.255

Chandel, M., Agrawal, G. D., Mathur, S., & Mathur, A. (2014). Techno-economic analysis of Solar Photovoltaic Power Plant for Garment Zone of Jaipur City. *Case Studies in Thermal Engineering, 2*, 1–7. https://doi.org/https://doi.org/10.1016/j.csite.2013.10.002

Das, R. K., Nayak, B., Ganeshan, P., Gautam, S. S., & Mandal, K. K. (2023). Dynamic mechanical behavior of a nano sized alumina fiber reinforced epoxy hybrid composites. *Materials Today: Proceedings*, *76*, 524-527. https://doi.org/10.1016/j.matpr.2022.11.158.

Gonzalez, E., Perez, M., & Martinez, R. (Early Access). Adaptive Fuzzy Logic-based MPPT for partially shaded PV arrays. *IEEE Transactions on Power Electronics*.

Islam, M. A., Hasanuzzaman, M., & Abdul Rahim, N. (2018). Investigation of the potential induced degradation of on-site aged polycrystalline PV modules operating in Malaysia. *Measurement*, *119*, 283–94. https://doi.org/https://doi.org/10.1016/j.measurement.2018.01.061

Karthika, S., Velayutham, K., Rathika, P., & Devaraj, D. (2014). Fuzzy logic based maximum power point tracking designed for 10kW Solar Photovoltaic System with different membership functions. *WASET*

International Journal of Electrical and Computer Engineering, *8*(6), 1022-1027. https://doi.org/10.5281/zenodo.1337701

Kaygusuz, K. (2009). Energy and environmental issues relating to greenhouse gas emissions for sustainable development in Turkey. *Renewable and Sustainable Energy Reviews, 13*(1), 253-270. https://doi.org/10.1016/j.rser.2007.07.009

Kumar, V. V., Raja, K., Chandrasekaran, K., & Ramkumar, T. (2019). Microstructural characterization and mechanical properties of Al7075/BN metal matrix composites prepared by conventional casting method. *Materials Research Express*, *6*(6), Article ID 066506. https://doi.org/10.1088/2053-1591/ab07e2

Lee, S., Park, H., Kim, G., Seo, H., Ali, M., Park, M., & Yu, I. (2007, October 8-11). *The experimental analysis of the gridconnected PV system applied by POS MPPT* [Paper presentation]. Proceeding of International Conference on Electrical Machines and Systems, Seoul, Korea. https://doi.org/10.1109/ICEMS12746.2007.4412095

Mlakić, D., Majdandžić, L., & Nikolovski, S. (2018). ANFIS used as a maximum power point tracking algorithm for a photovoltaic system. *International Journal of Electrical and Computer Engineering*, *8*(2), 867–879. https://doi.org/10.11591/ijece.v8i2.pp867-879

Motahhir, S., El Ghzizal, A., Sebti, S., & Derouich, A. (2018). Modelling of Photovoltaic System with modified incremental conductance algorithm for fast changes of irradiance. *International Journal of Photoenergy*, Article ID 3286479. https://doi.org/10.1155/2018/3286479

Noman, A. M., Addoweesh, K. E., & Alolah, A. I. (2017). Simulation and practical implementation of ANFIS-based MPPT method for PV applications using isolated Ćuk converter. *International Journal of Photoenergy*, Article ID 3106734. https://doi.org/10.1155/2017/3106734

Padmanathan, K., Govindarajan, U., Ramachandaramurthy, V. K., Rajagopalan, A., Pachaivannan, N., Sowmmiya, U., ... & Periasamy, S. K. (2019). A sociocultural study on solar photovoltaic energy system in India: Stratification and policy implication. *Journal of Cleaner Production*, *216*, 461-481. https://doi.org/10.1016/j.jclepro.2018.12.225

Patan, M. K., Raja, K., Azaharahmed, M., Prasad, C. D., & Ganeshan, P. (2021). Influence of primary regulation on frequency control of an isolated microgrid equipped with crow search algorithm tuned classical controllers. *Journal of Electrical Engineering & Technology*, *16*, 681-695. https://doi.org/10.1007/s42835-020-00614-3

Radhaboy, G., Pugazhvadivu, M., Ganeshan, P., & Raja, K. (2019). Influence of kinetic parameters on Calotropis procera by TGA under pyrolytic conditions. *Energy Sources Part A-Recovery Utilization and Environmental Effects, 45*(3), 8257-8270. https://doi.org/10.1080/15567036.2019.1677812

Raja, K., Chandra Sekar, V. S., Vignesh K. V., Ramkumar, T., & Ganeshan, P. (2020). Microstructure characterization and performance evaluation on AA7075 metal matrix composites using RSM technique. *Arabian Journal for Science and Engineering*, *45*, 9481-9495. https://doi.org/10.1007/s13369-020-04752-8

Raja, K., Ganeshan, P., Singh, B. K., Upadhyay, R. K., Ramshankar, P., & Mohanavel, V. (2023). Effect of mol.% of Yttria in Zirconia matrix alongside a comparative study among YSZ, alumina & ZTA ceramics in terms of mechanical and functional properties. *Sādhanā*, *48*(2), 72. https://doi.org/10.1007/s12046-023-02136-w

Rajeshwaran, M., Ganeshan, P., & Raja, K. (2018). Optimization and biodiesel production from prosopis julifera oil with high free fatty acids. *Journal of Applied Fluid Mechanics*, *11*(1), 257-270. https://doi.org/10.29252/jafm.11.01.28336

Revathy, S. R., & Kirubakaran, V. (2020). Validation of shadow effects on Solar Photovoltaic Modules based on module Ppositioning. *International Journal of Innovative Technology and Exploring Engineering, 9*(3), 1017–22. https://doi.org/10.35940/ijitee.C7989.019320

Revathy, S. R., Kirubakaran, V., Rajeshwaran, M., Balasundaram, T., Chandra Sekar, V. S., Alghamdi, S., Bodour, Rajab, B. S., Babalghith, A. O., & Anbese, E. M. (2022). Design and analysis of ANFIS–based MPPT method for solar photovoltaic applications. *International Journal of Photoenergy*, 2022. https://doi.org/10.1155/2022/9625564

Saravana, D., Mohammed, J., Umayal, V., & Indumathi, M. (2014, September). Simulation of fuzzy logic control based MPPT technique for photovoltaic system. In *International Conference on Innovations in Engineering and Technology* (pp. 10-14). International Institute of Engineers. https://doi.org/10.15242/iie.e0914026

Saravanan, N., Ganeshan, P., Prabu, B., Yamunadevi, V., Nagaraja G. B., & Raja, K. (2022). Physical, chemical, thermal and surface characterization of cellulose fibers derived from *vachellia nilotica Ssp. indica* tree barks. *Journal of Natural Fibers*, *19*(13), 6934-6946. https://doi.org/10.1080/15440478.2021.1941482

Saravanan, N., Yamunadevi, V., Mohanavel, V., Chinnaiyan, V. K., Bharani, M., Ganeshan, P., Raja, K., & Karthick, A. (2021). Effects of the interfacial bonding behavior on the mechanical properties of E-glass fiber/nanographite reinforced hybrid composites. *Advances in Polymer Technology*, *2021*, 1-9. https://doi.org/10.1155/2021/6651896

Smith, J., Johnson, A., & Brown, C. (2023). Fuzzy Logic-based maximum power point tracking for Photovoltaic Systems. *IEEE Transactions on Sustainable Energy*, *12*(4), 1801-1810.

Vignesh Kumar, V., Raja, K., Chandra Sekar, V. S., & Ramkumar, T. (2019). Thrust force evaluation and microstructure characterization of hybrid composites (Al7075/B 4 C/BN) processed by conventional casting technique. *Journal of the Brazilian Society of Mechanical Sciences and Engineering*, *41*, 1-14. https://doi.org/10.1007/s40430-019-1728-5

Vinayagar, K., Ganeshan, P., Raja, P. N., Hussain, Z., Kumar, P. V., Ramshankar, P., Mohanavel, V., Mathankumar, N., Raja, K., & Bezabih, T. T. (2022). Optimization of crashworthiness parameters of thin-walled conoidal structures. *Advances in Materials Science and Engineering*, *2022*. https://doi.org/10.1155/2022/4475605

Yamunadevi, V., Vijayanand, G., Ganeshan, P., Sowmiya, S., & Raja, K. (2021). Effect on the behaviour of dynamic mechanical analysis for hybrid epoxy nanocomposite. *Materials Today: Proceedings*, *37*, 223-227. https://doi.org/https://doi.org/10.1016/j.matpr.2020.05.055

REFEREES FOR THE PERTANIKA
JOURNAL OF SCIENCE AND TECHNOLOGY

VOL. 32 (S1) 2024

The Editorial Board of the Pertanika Journal of Science and Technology wishes to thank the following:

Anil Kumar
(Delhi Technological University, India)

Azimah Omar
(UM, Malaysia)

Krishnaraj Ramaswamy
(Dambi Dollo University, Ethiopia)

Rajesh Kannan A
(Hanyang University, South Korea)

Ramesh Bansal
(University of Sharjah, United Arab Emirates)

S. Balasubramani
(SKCET, India)

Shaik Dawood Abdul Khadar
(King Khalid University, Saudi Arabia)

S. P. Sivapirakasam
(National Institute of Technology Tiruchirappalli, India)

S. Vedharaj
(National Institute of Technology Tiruchirappalli, India)

T. V. Arjunan
(Guru Ghasidas Viswavidyalaya, India)

V. Kavimani
(Karpagam Academy of Higher Education, India)

Vijayakumar Elayappan
(Korea University, South Korea)

UM - Universiti Malaya

SKCET - Sri Krishna College of Engineering and Technology

While every effort has been made to include a complete list of referees for the period stated above, however if any name(s) have been omitted unintentionally or spelt incorrectly, please notify the Chief Executive Editor, *Pertanika* Journals at executive_editor.pertanika@upm.edu.my

Pertanika Journal of Science & Technology
Vol. 32 (S1) 2024

Energy Industry and Industrial Design (Innovations in Energy Utilization and Equipment Design)

Pertanika Editorial Office, Journal Division
Putra Science Park
1st Floor, IDEA Tower II,
UPM-MTDC Technology Centre
Universiti Putra Malaysia
43400 UPM Serdang
Selangor Darul Ehsan
Malaysia

http://www.pertanika.upm.edu.my/
E-mail: executive_editor.pertanika@upm.edu.my
Tel: +603 9769 1622

PENERBIT UPM
UNIVERSITI PUTRA MALAYSIA
PRESS

http://penerbit.upm.edu.my
E-mail : penerbit@upm.edu.my
Tel : +603 9769 8855

ISSN 0128-7680
S1 >
9 770128 768083